2020

Optimization Study of a Combined Wind-Solar Farm for a Specified Demand

Venkat Siddhartha Rama
Wright State University

OPTIMIZATION STUDY OF A COMBINED WIND-SOLAR FARM FOR A SPECIFIED DEMAND

A thesis submitted in partial fulfillment
of the requirements for the degree of
Master of Science in Renewable and Clean Energy Engineering

By

VENKAT SIDDHARTHA RAMA
B.Tech., Jawaharlal Nehru Technological University Hyderabad, India, 2017

2020
Wright State University

WRIGHT STATE UNIVERSITY
GRADUATE SCHOOL

May 29, 2020

I HEREBY RECOMMEND THAT THE THESIS PREPARED UNDER MY SUPERVISION BY Venkat Siddhartha Rama ENTITLED Optimization Study of a Combined Wind-Solar Farm for a Specified Demand BE ACCEPTED IN PARTIAL FULFILLMENT OF THE REQUIREMENTS FOR THE DEGREE OF Master of Science in Renewable and Clean Energy Engineering.

_____
James Menart, Ph.D.
Thesis Director

_____
Raghavan Srinivasan, Ph.D., P.E.
Chair, Department of Mechanical
and Materials Engineering

Committee on Final Examination

_____
James Menart, Ph.D.

_____
Mitch Wolff, Ph.D.

_____
Rory Roberts, Ph.D.

_____
Barry Milligan, Ph.D.
Interim Dean of the Graduate School

Abstract

Rama Venkat Siddhartha M.S.R.C.E. Department of Mechanical and Materials Engineering, Wright State University, 2020. Optimization Study of a Combined Wind-Solar Farm for a Specified Demand.

At the present time, using wind and solar energy for producing electricity in the United States is becoming cost competitive. According to Lazard's 2019 [36] levelized cost of energy (LCOE) analysis of a number of energy sources used for producing electricity in the United States, wind and solar are cheaper than natural gas and coal. While capital, maintenance, operation, and fuel costs are included in LCOE numbers, energy source intermittency is not. Intermittency is an important issue with wind and solar energy sources, but not with natural gas or coal energy sources.

Combining wind and solar energy sources into one electrical generating station, is one means by which the intermittency of the electricity provided by wind alone and solar alone can be reduced. The combination of wind turbines and solar photovoltaic panels into a wind-solar farm can produce electricity over a greater fraction of the day or year than wind or solar alone. Predicting the energy output of different combinations of wind turbines and solar panels in a wind-solar farm is an objective of this work. While yearly electricity production rates are an important and necessary part of this work, this quantity does not provide a means to compare the wind-solar farms to each other, to a pure wind farm, to a pure solar farm, or to meeting a given electrical demand by purchasing all electricity from the local electrical grid. An economic analysis has to be performed to do this. This is the ultimate objective of this work.

The economic analysis done in this work determines the net present cost of providing a specified electricity demand by a wind-solar farm with grid backup. Including grid purchased electricity to meet demand that cannot be met by the wind-solar farm is essential in this economic analysis. This sets the net present cost of providing all the electricity demand by grid purchased electricity as the cost that must be beat by a wind-solar farm with grid backup. Using grid backup also ensures that all of the electrical demand is met. Doing the economic analysis this way, means the intermittency costs of wind and solar are included in the economic analysis.

The electrical output of many combinations of wind turbines and solar panels into one wind-solar farm are simulated in this work to see which combination provides the lowest net

present cost of electricity for a specified electrical demand. The net present cost analysis performed n this work is different than a LCOE analysis because all the electricity produced for the net present cost analysis does not have value. For most of the simulations in this work, excess generated electricity is given no value. Only one economic simulation, for a given location, performed in this work is allowed to sell excess electricity from the wind-solar farm back to the electrical grid; and this is done at half the price at which it is purchased.

The mathematical models that were pieced together to perform this work are presented. Detailed models of the solar and wind resource are utilized. The conversion of solar energy into electricity by the solar panels is handled with a solar panel efficiency. The conversion of wind energy into electricity is handled with a wind turbine power curve. Demand profiles for a given location are obtained from those published on the internet. The net present cost analysis is done including the time value of money. A MATLAB program was written to obtain numerical results from the mathematical models brought together to simulate the performance and costs of a wind-solar farm with gird backup.

Many results are presented in this thesis for three different cities in the United States. These cities are Rio Vista, California, Dallas, Texas, and Dayton, Ohio. For each of these locations, electricity demand profiles, wind and solar resource profiles, electricity produced by different sizes of wind-solar farms, excess electricity produced by these wind-solar farms over the required demand, and the net present cost of these wind-solar farms with grid backup using different cost constraints are presented. A base case of costs is developed and then single changes to these base case costs are investigated. The results show that combining wind turbines with photovoltaic panels can reduce the cost of providing a specified electricity demand. In Rio Vista, California wind-solar farms are cost competitive, whereas in Dayton, Ohio they are not. Whether a wind-solar farm is cost competitive in Dallas, Texas depends on the cost conditions. A key factor in determining the attractiveness of wind-solar farms under the conditions used in this study, is the cost of grid electricity.

Table of Contents

List of Figures

List of Tables

Nomenclature

A_i	Anisotropic index
A_{FR}	Area of solar panels in front row
A_{BR}	Area of solar panels in back row
A_r	Swept area of wind turbine rotor
a,b	Coefficients of empirical relationship
B	Day fraction in year
B_{BR}	Beam radiation component impinging on shaded solar panels
B_{FR}	Beam radiation component impinging on unshaded solar panels
C_{CS}	Solar panel equipment installation cost
C_{CW}	Wind turbine equipment installation cost
C_{MW}	Wind turbine Maintenance cost
C_{MS}	Solar panels maintenance costs
$C_{el,d}$	Cost of getting deficit power from grid
$C_{el,ex}$	Cost of selling excess power to grid
D_r	Rotor diameter
D_{BR}	Diffuse radiation component impinging on shaded solar panels
D_{FR}	Diffuse radiation component impinging on unshaded solar panels
E	Equation of time
$E_{H,D}$	Hourly energy demand
$E_{H,BR}$	Hourly energy produced by all shaded row panels
$E_{H,ex}$	Hourly excess energy
$E_{H,FR}$	Hourly energy produced by entire front row of solar panels
$E_{H,WSF}$	Hourly energy produced by wind and solar farm
$E_{H,S}$	Hourly total energy produced by solar farm
$E_{H,W}$	Hourly wind turbine power generation
$E_{H,W}$	Hourly Power produced by wind turbine
$E_{Y,FR}$	Yearly energy produced by entire front row of solar panels
$E_{Y,BR}$	Yearly energy produced by entire shaded row of solar panels
$E_{Y,S}$	Yearly total energy produced by solar farm
$E_{Y,W}$	Yearly Power produced by wind turbine
$E_{Y,WSF}$	Yearly energy produced by wind and solar farm
$E_{Y,D}$	Yearly energy demand
$E_{Y,ex}$	Yearly excess energy
$E_{Y,d}$	Yearly energy deficit
F_{NS}	Fraction of panel not shaded in shaded rows
f_{GR}	Fraction of ground not shaded
F_{gvf}	Ground view factor
G	Extraterrestrial radiation
G_{FR}	Ground reflected radiation component impinging on unshaded solar panels

G_{BR}	Ground reflected radiation component impinging on shaded solar panels
G_{sc}	Solar constant
H	Panel vertical height from the horizontal
h	Hour of day
I	Global horizontal incident
$I_{d,cs}$	circumsolar portion of diffuse radiation component
$I_{d,iso}$	Isotropic diffusion
I_b	Incident beam radiation
I_d	Diffuse horizontal incident
I_o	Hourly extraterrestrial solar radiation on horizontal surface
I_{BR}	Total radiation impinging on shaded solar panels
I_{FR}	Total radiation impinging on unshaded solar panels
K_T	Hourly clearness index
L	Panel length
L_{loc}	Local meridian
L_{st}	Standard meridian
N_W	Number of wind turbines in wind farm
n	Day number
NPC	Optimization total costs in net present costs
P_{wind}	Power in wind
$P_{5,W}$	Power generates by wind turbine in five-minute interval
P_{NPW}	Name plate power capacity of wind turbines
P_{NPS}	Name plate power capacity of solar panels
R_b	Geometric factor
$R_{b\ avg}$	Integrated model Geometric factor
t_s	Solar time
t_{std}	Standard time
V	Scaled wind speed
V_{ref}	Wind speed at reference height
z	Height of wind turbine hub
z_{ref}	Reference height at which wind speed is available
z_o	Surface roughness
H,L,d,c,	Length constants for derivation of fraction of panel shaded in shaded rows
f,g,k,p	Length constants for derivation of fraction of panel shaded in shaded rows
r,m,p,e	Length constants for derivation of fraction of panel shaded in shaded rows
ρ_g	Ground reflectivity
Φ	Latitude angle
Θ	Angle of incidence
Θ_{mp}	Angle of incidence at the middle of the operating solar hour
Θ_z	Zenith angle
β	Panel slope angle
γ_s	Solar Azimuth angle
δ	Declination angle

δ_d	Daily Declination angle
δ_h	Hourly Declination angle
γ	Surface Azimuth angle
ω	Hour angle
ω_1	Hour angle at the beginning of the operating solar time
ω_2	Hour angle at the end of the operating solar time
ω_{sr}	Hour angle at sunrise
ω_{ss}	Hour angle at sunset
δ_g	Ground reflectivity
α_s	Solar Altitude Angle
η_{pv}	Efficiency of solar panel
ρ_{air}	Density of air

Acknowledgement

I would like to express my special thanks and gratitude to my thesis advisor Dr. James Menart, the Director of Renewable and Clean Energy Master's Degree Program at Wright State University who has given me an opportunity to work on a wonderful topic on “Optimization Study of a Combined Wind-Solar farm for a Specified Demand”. I appreciate all his valuable advices and time that spent to guide me with this project. I appreciate his knack teaching skills during my period of the program. I am humble to Dr. Mitch Wolff and Dr. Rory Roberts for spending their valuable time as my defense committee members during this COVID 19 quarantine to attend this conference.

I would also like to express my extreme gratitude to my family for their love, prayers and sacrifices they has gone through to educate and preparing me for my future.

Finally, I would thank all my friends and people who helped me during my stay in the United States, thank you for your support and being a part of my life. I am really blessed for having these people in my life.

Chapter 1
Introduction

1.1. Objective of Work

Renewable energy technologies like wind, solar, hydropower, geothermal, wave and tidal, and biofuels produce sustainable and clean energy from sources such as the atmosphere, sun, rivers, earth, oceans, and plants. Renewable energy technologies can reduce environmental degradation and increase energy security, while at the same time boosting a region's economy [2]. Figure 1 shows one of the changes that can occur to our environment as a result of relying too heavily on fossil fuels [3]. On the other hand, a difficulty with wind, solar, and most renewable energy technologies is their intermittency. Intermittency drives electricity providers to install expensive storage or to have backup facilities available when the renewable energy system is not providing the electric power demanded by a community. Thus, there is a need to reduce the intermittency of renewable energy systems.

The problems caused by the variable nature of renewable energy resources can be partially overcome by combining renewable energy sources in such a way that one renewable energy technology complements the weakness of the other [7]. Researchers have been developing the Integrated Renewable Energy Systems (IRES) program [2] to face the challenges of stand-alone systems due to source availability interruption. The integration of renewable energy technologies changes with the renewable energy source, location, load demands, and various other factors. The choice of renewable energy technologies to be used in combination is usually dependent on the energy sources that are locally available [8]. For this work combinations of wind and solar

renewable energy systems are studied. These two renewable energy sources are available in almost any location on the surface of the earth to varying degrees. In addition, these two renewable energy technologies are becoming the least expensive means to generate electrical power. It is only natural that studies should be done to see if the costs of meeting a specified demand can be reduced by combining these two renewable technologies into one installation which will be called a wind-solar farm in this thesis.

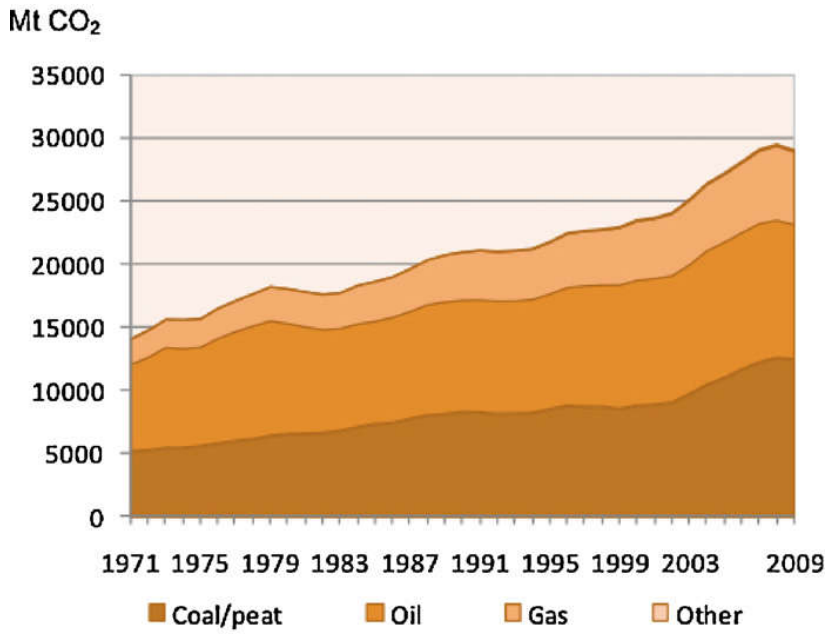

Figure 1.1: CO_2 produced by various fossil fuel power generation systems since 1971 [3].

1.2. Renewable Energy Systems

Before giving background on wind and solar systems, a brief discussion of a number of renewable energy sources is given. Renewable energy sources are those energies that nature continually provides and are essentially inexhaustible. Depending on how you want to categorize the primary sources of renewable energy on the earth, you can obtain different categories. In this work, six categories are utilized. These categories are:

1. Solar energy: This includes the use of radiant energy as it comes from the sun and does not include solar energy that has been converted to other forms before being used for producing an energy form useful to humankind. Because the net radiation the sun exchanges with the earth is based on the temperature differences between the sun and the earth, this is a form of thermal energy.

Because it is thermal energy at very high temperatures, conversion efficiencies can be very high.

2. Wind power: This only includes kinetic energy present in the movement of air in our atmosphere. Of course, this air movement is commonly called wind and originates as solar energy.
3. Hydropower: For this work hydropower includes the energy that can be obtained from the kinetic and potential energy stored in inland, surface water sources. In essence, this includes energy that can be obtained from lakes, ponds, rivers, and streams and excludes energy in ground water and oceans. Examples of this type of energy is the potential energy stored in fresh water as it is about to fall over a cliff and the kinetic energy in fast moving rivers.
4. Ocean energy: This includes potential, kinetic, and thermal energy that is obtained from our oceans. Potential ocean energy is harvested from the ocean's tides, kinetic and potential energy can be harvested from the ocean's waves, and thermal energy can be harvested from the ocean's temperature gradients.
5. Geothermal Power: This is the thermal energy that is stored in the earth, whether it be in the ground, in ground water, or in fresh, surface water. High temperature geothermal energy stored deep inside the earth is the energy residual left over from the creation of our planet and from radioactive decay of several elements present in the earth. Thermal energy stored in the earth within 10 meters of the surface or in surface water mostly comes from the sun.
6. Biomass energy: This includes the energy obtained from plant and animal matter. This is the oldest known renewable energy. Biomass energy was popularly used as people have been burning trees for cooking and warmth since humankind discovered fire. Though it is renewable, it takes a very long time for trees to regrow when compared to the rate at which they are used. Currently, biomass energy is being used safely by producing methane gas and alcohols to run automobiles.

Sometimes hydrogen energy and battery energy is placed in the renewable energy category. While it may be acceptable to call them renewable, they are not primary sources of energy. The energy that is stored in a battery, needs to come from some other sources. Likewise, the energy required to produce hydrogen from water or natural gas, comes from some other sources. Batteries and hydrogen should be looked at as energy storage systems, not primary renewable energy sources.

A schematic representation of the path that various energy conversion process naturally follow in the earth-atmosphere system is as shown in Figure 1.2. The usefulness of diagrams of this kind has been pointed out by King Hubbert in 1971 [4]. Different components of the earth-atmosphere system have been placed in horizontal rows. Vertical columns represent various energy types. The chambers in which energy may become stored are represented by boxes and the line

with arrows indicates the flow of energy with respective rates in terawatts. The part of the incoming short-wavelength solar radiation that has been reflected into outer space and the part that has been absorbed into various layers of earth's atmosphere are represented in the first column. Potential energy, latent chemical energy and nuclear energy are represented in the second column. Sensible heat energy is represented in third column. Kinetic energy in the wind and ocean is represented in the fourth column. Longwave radiation re-radiated into space from the earth is represented in the fifth column. Energies presented in the second column are not susceptible to characteristic weather patterns since these energies are constrained within matter. Sensible heat energy within the biosphere and various energies associated with kinetic energy like moving land masses, the movement of animals and the movement of ground water are ignored in Figure 1.2 due to the excessively complicated nature of these energies. This thesis project deals with the first column in Figure 1.2, short-wavelength solar radiation from sun, and the fourth column, kinetic energy of the wind.

1.3. Solar Energy

1.3.1. The Sun

Th sun has been providing the earth energy for billions of years. The diameter of the sun is 1.39 x 10^9 meters and, on average, it is 1.5x10^{11} meters away from the earth with an effective radiating temperature of 5777 K. The inner temperatures of the sun are much higher at approximately 8 x 10^6 to 40x10^6 K [11]. The sun undergoes a significantly energetic process called nuclear fusion in its core, where it creates high mass particles by fusing lower mass particles. Hydrogen atoms combine with each other and form helium atoms. There is a loss of mass in this reaction since the helium atom's mass is less than the hydrogen atoms that combine to form the helium. This mass is converted into energy. As the vacuum of space does not facilitate conduction and convection, any of the sun's energy that makes it to the earth gets here via radiation. Currently, the sun emits 3.9x10^{26} watts of energy through radiation in all directions. On average the earth's topmost layer of atmosphere receives about 1353 watts per square meter on a surface perpendicular to the propagation of the solar rays from sun. This is the earth's solar constant. Due to orbital motion of the earth around the sun every year, there is an oscillation around the solar constant value which is illustrated in Figure 1.3.

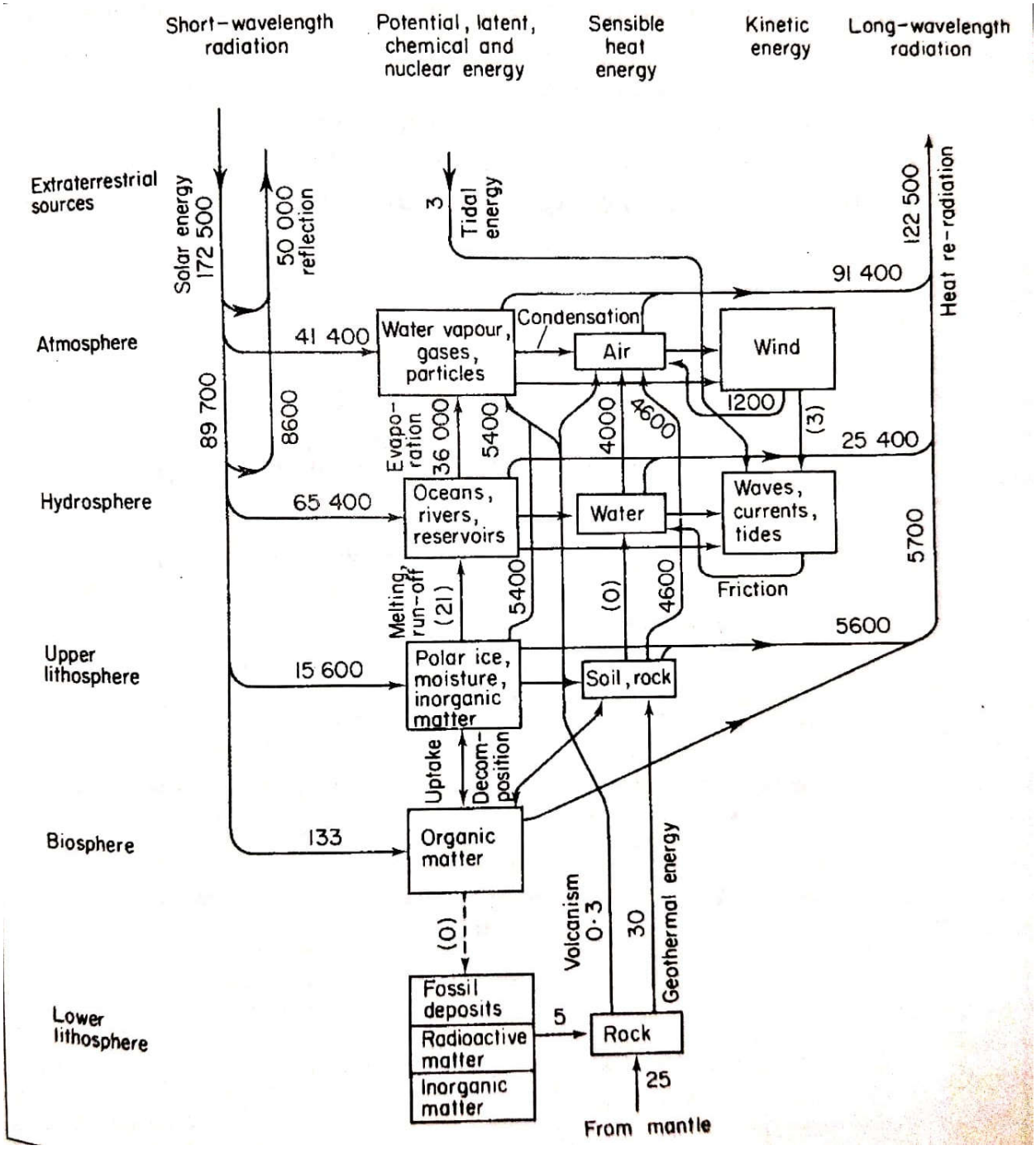

Figure 1.2: Schematic energy cycle without anthropogenic interference [4].

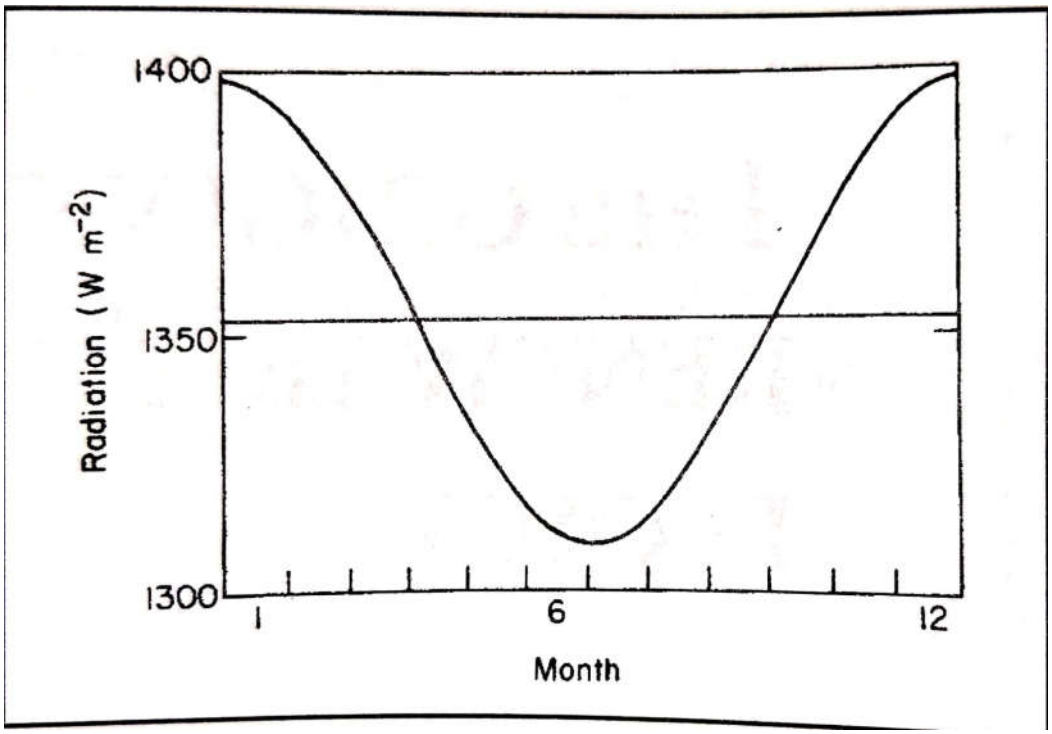

Figure 1.3: Yearly variation in the solar constant [11].

Having detailed spectral data about the solar extraterrestrial irradiation, i.e., the radiation that the earth receives at the edge of the atmosphere, is important. Below is a figure of the WRC standard spectral irradiance curve that has been produced by collecting information from high altitude weather and space equipment [12]. From this curve it can be seen that the spectral radiance is relatively smooth. While not illustrated in this figure, the suns irradiance just above the earth's atmosphere is close to the spectral profile a blackbody.

1.3.2. Solar Thermal and Solar Electric Systems

To take advantage of solar energy there has been various technologies developed for capturing the radiant energy from the sun. The renewable energy technology that makes use of the energy output from the sun in a thermal form is called solar thermal energy. This energy can be used for both comfort purposes, like home temperature control and producing hot water, and for production of electricity in appropriate locations. A system making use of solar thermal energy for electricity production is shown in Figure 1.5 and one used for hot water heating is shown in Figure 1.6.

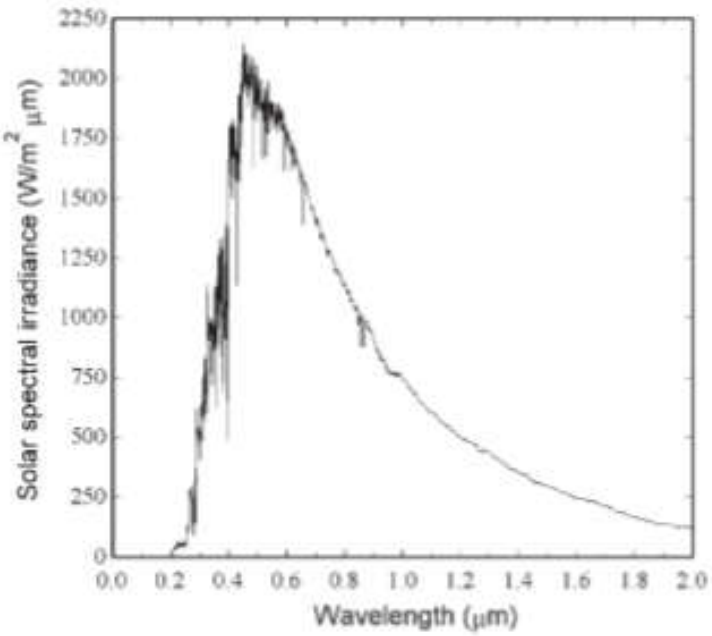

Figure 1.4: WRC standard spectral irradiance curve at mean earth-sun distance [11].

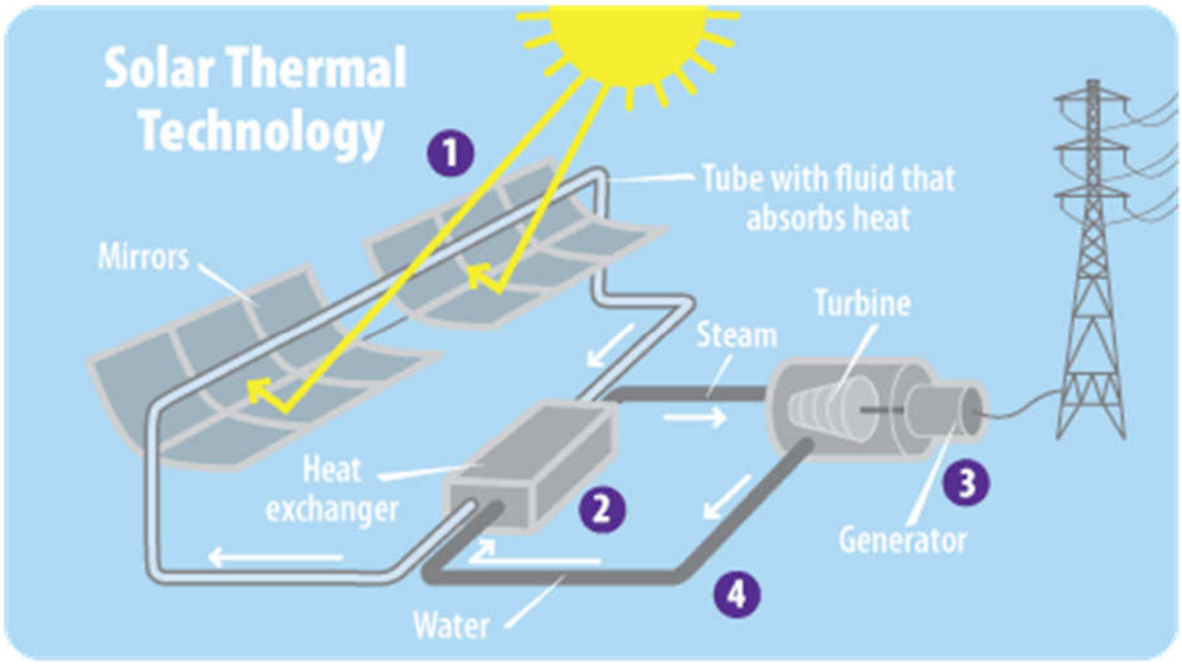

Figure 1.5: Solar thermal technology used for electric power production [13].

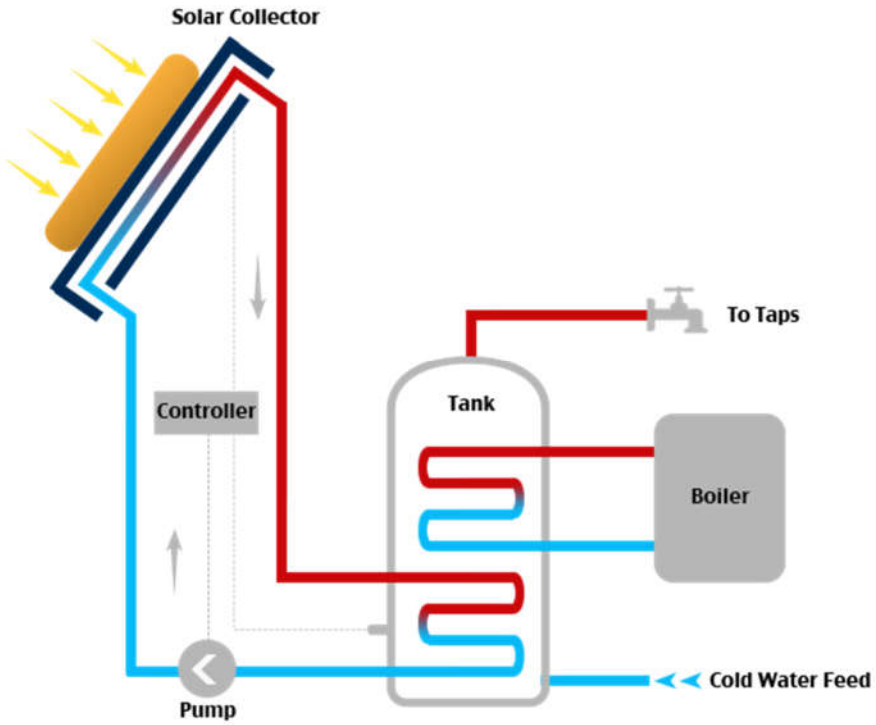

Figure 1.6: Solar thermal technology used for hot water production [14].

A second broad classification of solar energy systems is solar electric systems. These systems take the radiation from the sun and directly produce electricity (see Figure 1.7). This is done using the photovoltaic process. In fact, such solar electric systems will be called photovoltaic energy systems and these are the types of systems utilized in the wind-solar farms being investigated in this thesis. Photovoltaic systems are the most common way solar energy is utilized. The reason this is the most common way of harnessing solar energy is that it is the least expensive way to convert the radiant energy from the sun into electricity.

1.4. Wind Power

Wind power or wind energy comes from the kinetic energy present in the flow of air in the earth's atmosphere. People have been using the energy present in wind for thousands of years, although not extensively until the last 500 years. In the past 100 years, due to the invention of electric generators, this energy has been used to generate electricity. In the 400 years before wind turbines humankind mainly used wind mills. People tend to use the terms "windmill" and "wind turbine" interchangeably; but in reality, they are different. Windmills are devices that are used to

capture wind energy and use it for mechanical processes like grinding grain, pumping water, cutting logs etc. In contrast, wind turbines are advanced machines that capture the energy present in wind to generate electricity [16].

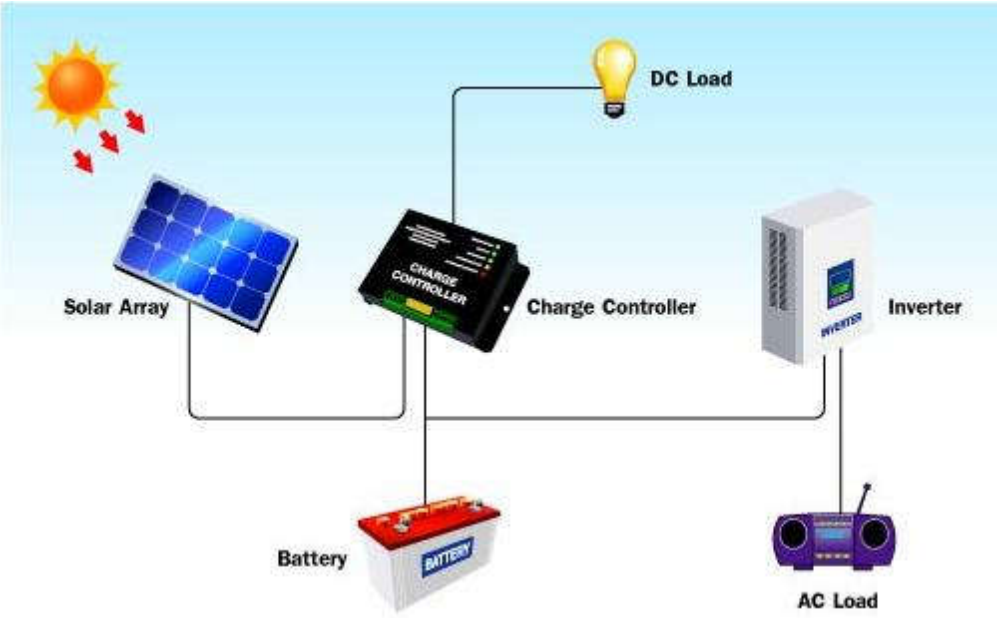

Figure 1.7: Solar photovoltaic system [15].

1.4.1. Utility Scale Wind

Wind turbines used for generating electricity at the utility scale tend to be quite large. Utility scale wind turbines produce more than 100 kilowatts of electricity per turbine and usually in the megawatt range. Wind turbines as large as 12 MW are currently being considered. These large-scale wind turbines cannot be used in all locations, they are often used in open fields or offshore which have the least obstruction to wind flow and are used in collections of wind turbines. Collections of wind turbines are called wind farms.

Wind is an important source of affordable, renewable energy, contributing 6.5% of the United States' electricity supply in 2018. With 7,588 megawatts (MW) of new wind capacity added to the nation's capabilities in 2018 and $11 billion invested, wind represents the third largest energy source added for generating electricity in the United States in 2018, behind solar and natural gas [17].

1.4.2. Land-Based Wind

The majority of the wind turbine projects in the United States are land based. There are more than 56,000 land-based wind turbines operating across 41 states, Guam and Puerto Rico [17]. Figure 1.8 shows the installed wind capacity in each state. The total wind turbine nameplate capacity of installed wind turbines in the United States is slightly over 97 gigawatts of electricity [20]. Land-based wind turbine projects have vastly proliferated due to the ease of construction and demand in the nearby communities. It has been estimated by the National Renewable Energy Laboratory that the United States has more than 10,000 gigawatts of wind energy potential at 80-meters above the ground [18]. There has been a 5% increase in the average nameplate capacity rating of recently installed wind turbines in the United States from the 2.43-megawatt average capacity in 2018 [17].

1.4.3. Offshore Wind

Compared to land-based wind, offshore wind has a higher capacity to produce electricity (since there are no obstructions to wind flow in oceans and the wind has higher and steadier velocities and thus higher kinetic energy potential). Due to recent advancements in the material sciences, there is a widespread growth of offshore wind energy projects across the globe. The overall size of the United States offshore wind pipeline grew from 25,464 megawatts to 25,824 megawatts in 2018 [19].

1.5. Outline of Thesis

In this thesis, a wind-solar farm which is a combination of on-shore wind turbines that tap into the land-based wind and solar photovoltaic panels which tap into the radiant energy from the sun are optimized for the least cost of providing electricity to 20,000 typical homes for 25 years. The wind resources, solar resources, and community load profiles of Riovista, California, Dallas, Texas and Dayton, Ohio are considered for this purpose. To perform these computations a computer program has been developed in MATLAB which has a capability to plot the necessary comparisons for each case studied. In this analysis, the solar panels are facing due south and have a 22% conversion efficiency. The wind turbines employed are 3 MW in size with a hub height of 84 m. All the costs associated with the project are converted into present day dollars with an interest rate of 10 percent.

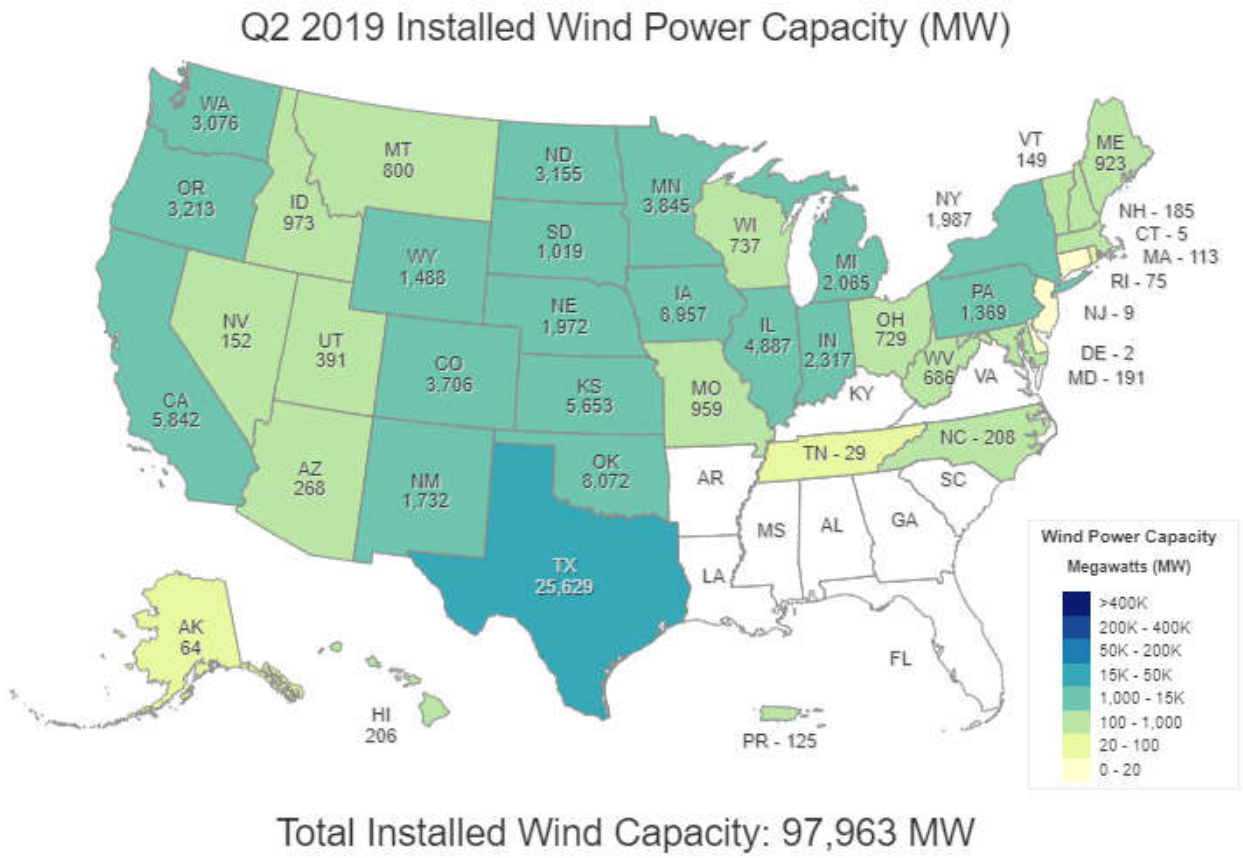

Figure 1.8: Wind power capacity in the United States [20].

Chapter 2 of this report looks at the work that has been published in the literature to optimize integrated renewable energy systems with several objectives like least cost or least loss of power capability using several optimization algorithms. Chapter 3 provides a detailed explanation of the mathematical models employed in this work. The first section of this chapter describes the fundamentals of calculating the solar energy resource, its capture and its conversion to electricity. This is followed by the fundamentals of calculating the wind energy resource, its capture, and its conversion to electricity. Shading of solar panels in rows behind the first row is included in this analysis. A method of calculating this shading was developed as part of this work. In Chapter 4, the results section is divided into five sections. The first section provides general information on the large number of results that are presented in Chapter 4. Sections 4.2, 4.3, and 4.4 present results for each of the three cities in the United States were survey results are produced. Section 4.2 presents results for Rio Vista, California, Section 4.3 presents results for Dallas, Texas, and Section 4.4 presents results for Dayton, Ohio. Lastly, Section 5.5 presents tabulated results

that make comparisons between the three cities much easier to perform. The last chapter of this thesis draws conclusions based on the wind-solar farm studies performed.

Chapter 2
Literature Survey

The literature that has been focused on optimizing integrated wind and solar systems is discussed in this chapter. There are a several optimization techniques that have been published; this chapter presents nine optimization methodologies that have been found in the literature. In the work presented in this thesis, a brute force method of optimization is used. In this thesis, several different sizes of wind and solar capacity are surveyed with the optimum found by plotting and looking for the minimum overall cost. This brute force technique has the advantage in that it shows how the optimum is approached with different combinations of wind and solar. Like some of the studies presented below, this thesis shows costs for pure solar and pure wind systems. Most of the optimization studies presented below are on the small size, whereas the study done in this thesis focuses on large wind-solar farms located in the United States. This is significant because wind does not become cost competitive to grid generated electricity until utility sized wind turbines are implemented. Some of the studies discussed below focus on wind-solar installations where grid electrical power is not available. This work is focused on determining if large amounts of electricity at a rate below the local grid price can be provided by wind-solar farms using the local grid as backup.

2.1. Simulated Annealing Algorithm

In research done by Alireza Askarzadeh [22], a special type of simulated annealing algorithm named discrete chaotic harmony search-based simulated annealing (DCHSSA) is considered. The DCHSSA method has been developed by combining chaotic search (CS),

harmony search (HS), a meta-heuristic approach to simulate improvisation process of musicians, and simulated annealing (SA), a popular generic probabilistic solo-algorithm used for global optimization problems with efficient discrete optimization methodology, for solving optimum sizing of integrated renewable energy systems. A desirable aspect of the DCHSSA method is that it considers every constraint variable without repetition. This methodology has been used to design photovoltaic and wind hybrid systems with inverter connected battery storage and backup power generator by varying sizes of the system components to have minimum total annual cost. The program developed has been used to design a system for a house in remote south-central Montana with varying demand profiles having a peak demand of 2.8 kW. Capital recovery factors using an interest rate of 6 percent for 20 years of system life are used to convert the initial capital cost to an annual cost. Three system configurations were studied including hybrid, photovoltaics alone and wind alone.

This method has been used to investigate two cases: Case 1 is where the power production is at the rated capacities of the individual photovoltaic panels and wind turbines and Case 2 is where the power produced by the photovoltaic panels is reduced by 50% and that for the wind turbines is reduced by 20% from rated capacities. In Case 1, the minimum cost is for a hybrid system with 2 photovoltaic panels, 2 wind turbines and 58 batteries is $9687. In Case 2, the minimum cost is also for a hybrid system with 18 solar panels, 2 wind turbines and 66 batteries with total minimum cost of $10944.

2.2. Biogeography Based Optimization

In research done by Rajesh Kumar, R. A. Gupta and Ajay Kumar Bansal [5] on the biogeography based optimization (BBO) method, an algorithm that is used to categorize evolutionary emigration and immigration rates of species in a habitat has been modified to predict the optimal sizing of wind and photovoltaic hybrid energy systems by minimizing total cost of the system. In their work, an integrated renewable energy system consisting of wind turbines, photovoltaic panels, storage batteries, and a diesel electric generator are combined to ensure a continuous supply of power that is reliable. Power generated by the wind turbines is calculated by using the wind speed and power coefficient for the wind turbine; and power generated by the photovoltaic panels is determined by using an efficiency along with rated currents and voltages of photovoltaic panels. Excess power produced is stored is in batteries. The total cost of the system

includes the costs of the photovoltaic panels, the wind turbine, the battery and the diesel generator in present day dollars. The time value of money is included by using a capital recovery factor along with a compensation coefficient which is used determine the cost value of energy.

The BBO optimization program has been used to design an IRES for an isolated area of Jaipur, Rajasthan, India. The daily energy consumption at this site is 2263 kWh/day with a peak demand of 261 kW and 30% variation of the load profile. The lifetime of this system is taken as 25 years, with an interest rate of 10%, a capital cost of $1,120/kW (Rs. 65,000/kW) for the wind turbine, $3,447/kW (Rs. 200,000/kW) for the photovoltaic panels, $345/kW (Rs. 20,000/kW) for the diesel generator running at maximum rated capacity, $172 (Rs.10,000) for each 6V, 360Ah Tarjan L16P battery, and $862/kW (Rs.50,000/kW) for an inverter. Peak loads that cannot be satisfied by the renewable systems are satisfied by diesel generators. The analysis keeps the minimum fraction of energy supplied by the renewable components of the system at 60%. For this case, BBO provides optimal system component sizes of 52 kW of photovoltaic panels, one wind turbine generator at 300 kW rated power, one 163 kW diesel generator, 813 batteries and a 93 kW capacity inverter. The net present cost for this system is $1.17 million (Rs. 67,877,356) and 1,059,639 kW-h of energy is produced per year at a LCOE of $0.18/kWh (Rs. 10.81/kWh).

2.3. Genetic Algorithm Based Optimization

In the research done by A. Arabali, M. Ghofrani, M. Etezadi-Amoli, M. S. Fadali and Y. Baghzouz [37] a genetic algorithm (GA) is modified by using fuzzy C-means clustering of similar data points for seasonal variations to optimize wind and solar energy systems with battery storage to meet heating, ventilation and air conditioning (HVAC) loads while minimizing the total cost of the system. This approach uses an interrogative search inspired by Charles Darwin's theory of natural evolution where the fittest of species are selected for reproduction to produce the next generation. Probability distribution functions are used to group data from the past 10 years into 10 clusters of days using fuzzy C-means. A Weibull distribution is used to model wind speed statistics, the clearness index is modelled by a beta distribution to obtain solar irradiation information and a Gaussian distribution is used for the lower and upper limits of the HVAC loads.

The GA optimization program developed is applied for a residential feeder to analyze the IRES according to the risk factors which involve the percentage of demand not met by the system and for given cost constraints given in references [43] and [44]. Two optimum cases for hybrid

wind-solar systems with battery storage are analyzed having optimum characteristics of 0 MW of photovoltaics, 1.9 MW of wind, and 2.92 MWh of battery storage capacity. This system provides 0.85 MW-h of excess energy production at a cost of $3.80 million for wind and $0.815 million for storage. In this analysis the photovoltaics and wind generation are normalized with maximum allowable load shifting of 30%. The optimization characteristics for a region with poor wind and high solar irradiation gives 0.0 MW of wind, 2.85 MW of photovoltaics and 6.4 MWh of storage with 4.58 MW-h of excess energy production. The cost for the photovoltaic system was $11.7 million and that for the storage was $1.73 million. the authors mention that 100% of the load power could be supplied by installing more solar panels.

2.4. HOMER, PSO and CPSO

In research done by Vikas Khare, Savita Nema and Prashant Baredar [38], the optimization of a hybrid wind-solar system with battery backup and a diesel generator to obtain minimum total net cost was done for a police control room in Sagar, India. This control room has a load demand of 17 kWh/day and peak demand of 1.5 kW. This location is dominated by solar resources. This analysis uses the hybrid optimization model available in the National Renewable Energy Software called HOMER. The results from HOMER are compared to particle swarm optimization (PSO) with innovative variations and the chaotic particle swarm optimization algorithm (CPSO). The photovoltaic system is modeled by a simple maximum voltage and current model while the wind system is modeled by using power coefficients. A Weibull distribution factor of 7.961 and autocorrelation factor of 0.86 is used for wind speeds. The diesel generator is modelled by an overall efficiency which includes engine efficiency and efficiency of the electric generator. The minimum annual capital cost is obtained using a capital recovery factor, a sinking fund factor, a penalty factor for capacity shortage and a penalty factor for emissions. The cost of installation of a 3 kW photovoltaic system is $3163 and cost of replacement of deteriorated units due to continuous use by new units is $2846. For the wind system a SW Whisper 500 wind turbine with a 3 kW rated capacity, 2.5 meter rotor diameter and a hub height of 25 m which costs $13,000 per unit and $11,000/unit for replacement is used. The batteries cost $0.156/kWh at 3 kW rated capacity with 80% round trip efficiency and 405-minute allowable state of charge (SOC). The inverter costs $200/kW and the diesel generator costs $2100 per 3.5 kW at a replacement cost of $1300. The annual interest rate used in the analysis is 6% and the lifetime of the system is 25 years.

The program was run for two cases, photovoltaics and a diesel generator and a hybrid system with photovoltaics, wind, and diesel generator. The costs of energy were cheaper for the hybrid system at $3163 as predicted by HOMER, $2777 as predicted by PSO, and $2700 as predicted by CPSO. The costs for the photovoltaics alone costs were $8435 as predicted by Homer, $8368 as predicted by PSO and $8200 as predicted by CPSO. Using the predictions from HOMER, the cost of fuel for the diesel generator are reduced 70-80% with the hybrid system and the reduction in total harmful gas emissions were reduced by 90%.

Getachew Bekele and Bjorn Palm [39] did research using the HOMER software to design a hybrid energy system in Ethiopia where at least 51% of the load demand of a village consisting of 1000 people is met by renewable energy systems. The daily energy consumption of the community is 147 kWh. The hybrid system is a combination of solar photovoltaics, wind turbines, a diesel generator, batteries and an inverter. Diesel and battery backup are used because only 15% of Ethiopia has grid coverage. The cost of installation of either photovoltaic panels or wind turbines is taken to be $4000/kW; while, the cost for diesel-based power is taken to be $1000/kW. When a system with 5 kW of photovoltaic panels, a 20-kW wind turbine, a 44-kW diesel generator, 40 (Serrette 6CS25P) batteries of 1156 Ah each, 20 kW inverter, and a 20 kW rectifier is used, a total initial capital cost of $121,320 is obtained. This system is able to supply 51% of the load demand of the village. Similarly, when a system with 20 kW of photovoltaic panels, a 20 kW wind turbine, a 44 kW diesel generator, 60 (Serrette 6CS25P) batteries of 1156 Ah each, a 40 kW inverter, a 40 kW rectifier is used the total initial capital cost is $205,980 This system is capable of supplying 81% of the electricity demand of the village. The lifetime of these systems was taken as 25 years.

Research was done by Sanjoy Kumar Nandi, Himangshu Ranjan Ghosh [40] on environmental aspects of a hybrid wind-solar system for the remote island of Kutubdia, Bangladesh where electricity is produced solely by diesel generators at an average daily demand of 160 kWh/day and a peak demand of 23 kW. The HOMER software was used to design a hybrid system with photovoltaic panels, a wind turbine, battery banks, an inverter and a diesel generator with total initial cost of $5000 and maintenance cost of $1000 for a 25-year time period. The interest rate for this analysis was 6%. There was approximately a 44% reduction in total pollution to 136,366 kg/year from 241,038 kg/year using the hybrid power system compared to diesel power generation only.

Ahmed M. A. Haidar, Priscilla N. John and Mohd Shawal [41] used HOMER to obtain a least net present cost of a hybrid wind-solar system in four Malaysia districts. Depending on the load requirements and energy available in the location different results were found. A total of 800,145 different configurations have been analyzed for least cost and least pollutants released into the atmosphere so that good economic and environmental decisions could be made on the way Malaysia provides its electricity production.

2.5. Genetic Algorithm with LPSP

In research done by Hongxing Yand, Wei Zhou, Lin Lu and Zhaohong Fang [7] the optimization of a photovoltaic and wind system with battery banks for minimum loss of power supply probability (LPSP) was undertaken. These investigators used a genetic algorithm (GA), which imitates evolutionary principles of natural genetics to find optimums. The solar irradiation in this model includes beam and diffuse components of solar radiation. The diffuse components use the Perez model [24] accounting for circumsolar, horizon brightening, and isotropic diffuse radiation using sky clearness coefficients and sky brightness parameters. The wind power system is modeled by scaling the wind speeds with the seventh power law. Wind turbines are modeled using aerodynamic power efficiencies coupled with mechanical transmission and electric conversion efficiencies. Lead acid battery banks are employed, and the battery model iconsiders charging rate, charging efficiency, capacity, state of charge (SOC), varying temperatures and self-discharge rates. The annualized cost of this hybrid system is calculated considering annualized capital costs calculated using a capital recovery factor, annualized replacement cost with sinking fund factor, and maintenance costs. The initial costs were $6500/kW for the photovoltaics, $3500/kW for the wind turbine without tower, $250/m of tower, $1500/kAh for the batteries, and $800 for other components.

A hybrid system used to supply power to a telecommunication relay station on the remote island of Dalajia in China was studied. The electrical load of this island is a continuous 1500 W. The integrated renewable energy system designed was a hybrid wind-solar system with one wind turbine with a hub height of 31 m, 128 photovoltaic panels at slope of 24.5^{o}, and 6 batteries with 0.97% LPSP. The annualized cost of this system is $10,600. Another integrated wind-solar system studied had one wind turbine with a hub height of 32.5 m, 115 photovoltaic panels at slope of 24^{o}, and 5 batteries with a 1.96% LPSP. This system has a slightly better annualized cost of $9708. A

nonintegrated system that only used 182 photovoltaic panels at slope of 25° with 8 batteries with a 1.96% LPSP had an annualized cost of $11,145 and a nonintegrated system that included 4 wind turbines with a hub height of 30 m coupled with 17 batteries with a 1.98% LPSP had an annualized cost of $16,889. It is clear that an integrated system with slightly more LPSP has lower annual costs. These systems were designed to supply 3-5 days of power to the relay station with battery alone.

2.6. Multiple Objective Optimization with Genetic Algorithm

Dhaker Abbes, Andre Martinez, and Gerard Champenois [42] studied wind-solar hybrid energy systems with battery banks using the multiple objective optimization with genetic algorithm. These investigators included life cycle costs (LCC), embodied energy (EE), and loss of power supply probability (LPSP) in an analysis to obtain multiple pareto front solutions. The energy is modelled by considering the wind turbine efficiency as 30% and the efficiency of the photovoltaic panels as 13%. Lead acid batteries are used by introducing an oversizing coefficient and using a maximum allowable depth of discharge of 70%. The life cycle cost of the system includes the cost of the equipment, the cost of installation, the cost of maintenance and the replacement costs. The time value of money uses a discount rate of 5%, inflation rate of 2%, and a system lifetime of 25 years. The embodied energy in the system is minimized by using an aluminum frame, polycrystalline silicon photovoltaic modules and a 90% recycle rate of scrap batteries. Less than a 10% energy contribution for manufacturing all other components in the system was assumed.

The integrated energy system was designed to supply electricity to a residential house with a 2193 kWh/year load that is located in Colorado. Studies of 120 different combinations of systems which consider LCC against EE and LPSP and are performed. A configuration with 9 sharp ND-240QCJ 240W solar panels of 14.8 m^2 total area, a 900 W Lacota S wind turbine with a swept area of 3.43 m^2 and 4 Numax Gel SLG180-12, 12 V batteries rated at 178.6 Ah. An embodied energy of 101,459 MJ and LCC of $32,471 were calculated. This system meets at least 95% of the electrical energy requirements of the home and the rest is supplied by the grid.

2.7. Hybrid Solar Wind System Optimization Tool

Hongxing Yang, Lin Lu, and Wei Zhou [44] developed what is referred to as the hybrid solar wind system optimization (HSWSO) tool. The HSWSO simulation tool optimizes for the least possible loss of power supply probability (LPSP) and for levelized cost of energy (LCE). Power from photovoltaic modules is tracked using regression constants for silicon photovoltaic modules operating at ambient temperature. The solar incident radiation on the panels is determined with the Perez model [24]. Power from the wind system is modeled by using power curves from the wind turbine manufacturer. Wind speeds at a given hub height are scaled from published data at one hub height using the 1/7 power law formula. Lead acid Battery banks are modeled by considering the state of charge (SOC) of the batteries and tracking energy into and out of the batteries. Batteries are sized to have the LPSP. The LCE was determined using capital costs for the photovoltaic panels, wind turbine, and batteries of $3330/kW, $2000/kW, and $80/kWh respectively. Maintenance costs of $10/kW, $20/kW and $25/kW-h for photovoltaic panels, the wind turbine, and batteries respectively. The photovoltaic panels used in this simulation have an area of 0.457 m^2 with 2.5 amps of short circuit current and 22 volts of open circuit voltage at 50 watts of maximum power. The simulation initially starts 20 photovoltaic panels facing south at an inclination angle of 29.5^o and an 0.5 kW wind turbine that increments by 0.1 kW. A 5% loss of power from all secondary aspects of system, like wires and connections, is included in the calculations.

This simulation is applied to design the optimum size of a power system for a communication relay stationed in Shanwei, China which has 1000 W of continuous daily demand. The system has zero LPSP when a 10 kW wind turbine and 270 modules of photovoltaic panels are coupled with a one-day battery storage bank. It has also been found that with 3 days of battery storage, zero LPSP can be obtained with less photovoltaic panels and less wind turbine capacity. A configuration with 75 modules of photovoltaic panels, a 5 kW of wind turbine, and a half-day of battery storage gives the lowest LCE at $0.22/kWh (1.6 HKD/kWh) at 5% LPSP. For the system to be reliable in a stand-alone configuration, it is necessary to have battery storage of at least 1.5 days of energy use.

2.8. Monte Carlo Simulation

Dheeraj Kumar Khatod, Vinay Pant and Jaydev Sharma [45] developed an approach to compare well-being performance using a Monte Carlo simulation technique. They also implemented an analytical procedure. These techniques were applied to small autonomous power systems (SAPS) comprised of photovoltaic panels and wind turbines coupled with a diesel generator. In the analytical model, a beta distribution is used to rank solar irradiations to obtain a probability distribution function for the solar irradiance, a Weibull distribution function is used to model wind speed distributions, and a probability distribution function is used to model the load distribution. Only a fraction of the load demand was to be met by the wind system as it has the highest fluctuations in its reliability factor. The energy not served (ENS), loss of healthy expectation (LOHE) and loss of load expectation (LOLE) are three calculated quantities used to evaluate the stability of the designed system with a given load demand. The power from photovoltaic panels is calculated by using temperature coefficients of current and voltage of the photovoltaic I-V characteristic, along with a fill factor. The power from the wind turbine is obtained with functions that provide the electrical power from the wind turbine as a function of the wind speed between the cut-in and cut-out speed.

These models are applied to a site in Gujarat, India that has a peak load of 60 kW. The analytical approach was compared to the Monte Carlo simulation by adding increments of wind and solar to the starting system with very small percentage changes, 0.07-0.4%, in the LOEE, LOHE, and LOLE. The analytical method had a run time of 10.53 minutes, while the Monte Carlo simulation had a run time of 8147 minutes.

2.9. Probabilistic Modeling

Probabilistic modeling has been performed by G. Tina, S. Gagliano and S. Raiti [46] on an integrated wind-solar system. In this case excess power was sent to the electrical grid and deficit power was taken from the electrical grid. The probabilistic approach used by these investigators produced an energy index of reliability (EIR) which is directly related to the energy expected but not supplied (EENS). A Weibull distribution was used for the wind speeds and a transformation theorem [23] for power from the wind turbine. The Hollands and Huget probability distribution [26] of hourly clearness indexes was used for solar irradiation so that power from a photovoltaics panel could be obtained.

The system was designed for a remote island in Italy which has a peak demand of 20.33 kW and yearly demand of 98,800 kWh. The average wind speed at this location is 4.55 m/s and an equivalent sunlight period is 5.5 hours. Simulations are done for wind alone, photovoltaics alone and hybrid systems. The solar panels were given an inclination angle of 0^o and an inclination angle equal to the latitude of the location. Calculated yearly EIRs of 0.418, 0.293, and 0.519-0.501 for photovoltaics alone, wind alone, hybrid configurations respectively were obtained when the inclination of the panels is equal to latitude of the location and yearly EIRs of 0.454, 0.293, 0.544-0.496 respectively were obtained when the inclination of the panels was zero. The authors clearly state in their paper that it is not possible to have a reliable energy system without energy storage.

Chapter 3
Mathematical Models

This chapter presents a number of mathematical models required to determine the net present costs of meeting specified electrical demands with a combination of wind, solar, and grid generated electricity. To do this a mathematical model predicting the electrical output of a given number of solar panels, of a specified efficiency, set in a specified location, at a given slope and given azimuthal orientation is required. This model is presented in the first section of this chapter. Also required is a mathematical model that predicts the electrical output of a given number of wind turbines that have a specified performance as a function of wind speed, that are set in a specified location. This model is presented in the second section of this chapter. After determining the electrical output of a specified wind-solar farm it is compared to the specified electrical demand. This comparison is done on an hour by hour basis so that the amount of positive excess electricity generated and negative excess, that is the deficit, electricity generated can be determined. For any hour in which the wind-solar farm cannot supply the required electrical demand, electricity is drawn from the local electrical grid. This comparison between the electricity produced by the wind-solar farm and the electrical demand is discussed in the third section of this chapter. Lastly a mathematical model is needed that properly describes the economics of fulfilling a given electrical demand with a combination of wind, solar, and grid generated electricity. This economic mathematical model is given in the fourth section of this chapter. Because results from such complex models must be generated by computers using a computer program, a fifth section is added to this chapter discussing a few of the numerical issues. All mathematical models presented

in this chapter have been implemented in a MATLAB computer program that was written from scratch as part of this thesis work.

The goal of this thesis work is not simply to determine the net present cost of a specified hybrid system for meeting a specified electrical demand, but to find the configuration that results in the minimum net present cost to achieve this goal. To perform this cost minimization study, the mathematical models presented in this chapter are used to predict the net present cost of many sizes of wind-solar farms. Plots of the net present cost versus wind nameplate capacity and solar nameplate capacity are produced so that the configuration that produces a minimum net present cost can be found. While this can be viewed as a brute force method of performing an optimization study, it provides information that more sophisticated optimization studies may gloss over. Seeing the trends in the net present cost as a function of wind nameplate capacity and solar nameplate capacity is beneficial for understanding the benefits of different combinations of wind and solar electricity generation. Even combinations that only use wind and grid generated electricity to meet a specified demand, or only use solar and grid generated electricity to meet a specified demand are displayed. Because of the brute force optimization technique used in this work, results are available for all these combinations and comparisons between these different types of wind-solar farms can be made.

3.1. Solar Model

The mathematical model to predict the amount electricity produced by the solar portion of the wind-solar farm is presented first because it is the most complex model. A large number of angles are required to perform these calculations and different aspects of the way the surface of the earth and its atmosphere affect the sun's rays need to be modeled. All the required angles are given in the following subsection and the equations giving the solar energy incident on a solar panel of a given slope and azimuthal orientation, including the effects of the earth's surface and atmosphere are given in the second subsection. The third subsection provides the relatively simple equations required to determine how much of this incident solar energy is converted to electricity.

3.1.1. Fundamental Angles

A number of the angles required for the solar calculations are shown in Figure 3.1. To calculate some of these angles, the time of day is required. However, the time of day needs to be

given in what is called solar time. The difference between solar time and standard time is what instant is called noon. In solar time, noon is when the sun is directly above the latitude of the location of the solar panel. Standard time is the same for all latitudes within a time zone. All the latitudes in a given time zone have the same noon time. Only one location in each time zone can possibly have standard time match solar time; and this location will vary throughout the year.

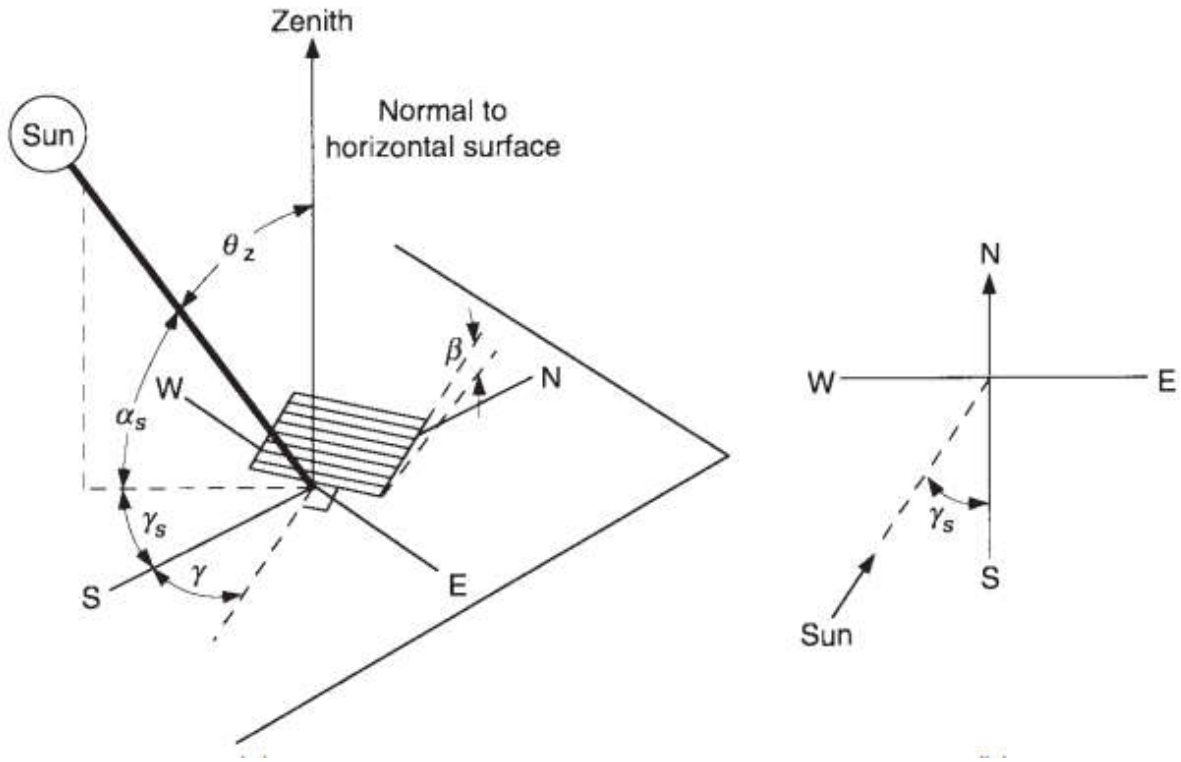

Figure 3.1: Zenith angle, surface slope angle, surface azimuthal angle, solar azimuthal angle and polar view of solar azimuthal angle [11].

3.1.1.1. Solar Time

In solar calculations, all times must be in solar time. Normally solar time only varies from standard time at a given location by less than an hour. Solar time, t_S, is determined from the local standard time, t_{Std}, as

$$t_S - t_{Std} = \frac{4(L_{st} - L_{loc}) + E}{60} \tag{3.1}$$

where L_{st} is the standard meridian for the time zone of the longitude where the solar panel is located, L_{loc}, and E is the equation of time given as

$$E = 229.2(0.000075 + 0.001868\, cosB - 0.032077\, sinB - 0.014615\, cos\, 2B - 0.04089\, sin2B. \tag{3.2}$$

The B in this equation is the year fraction converted to a degree fraction and can be determined by

$$B = (n-1)\frac{360}{365}, \tag{3.3}$$

where n is the day number from January 1. In Equation (3.1), the quantities on the righthand side are in minutes and the 60 in the denominator converts the minutes to fractions of an hour. Equation (3.2) provides the equation of time, E, in minutes. Thus Equation (3.1) provides the difference between solar time and standard time in hours. Solar time can easily be determined by adding this difference to the standard time at the panel location. With this solar time, the location of the sun in an east to west direction can be determined as an angle. This angle is called the hour angle and will be discussed next.

3.1.1.2. Hour Angle

The hour angle is a measure of the sun's location east or west of the location of the solar panel in degrees of longitude. This angle is measured from the center of the earth between a plane that encompasses the longitude of the panel location and a plane that encompasses the longitude that the sun is located over. The hour angle changes with the time of the day having a negative value before noon and positive value after noon. Positive hour angles occur in the morning and negative hour angles occur in the afternoon. The hour angle changes by 15° every hour and is zero at solar noon. Thus, the hour angle, ω, can easily be determined once solar time is known using the equation

$$\omega = 15\ (t_S - 12). \tag{3.4}$$

The hour angle at sunset, ω_{ss}, can be determined from

$$cos\ \omega_{ss} = -tan(\emptyset)\ tan(\delta_d). \tag{3.5}$$

In this equation $\emptyset$ is the latitude of the location of the solar panel and δ_d is the daily declination angle. These two angles are discussed below. Since the sun rises and sets in a symmetric manner around solar noon, the sunrise time can be determined as

$$\omega_{sr} = -\omega_{ss}. \tag{3.6}$$

Knowing sunrise and sunset is important because it is only between these times that the sun's energy is available. Times before sunrise and after sunset are considered nighttime. The bending of the sun's rays as they travel through the atmosphere are not included in Equation (3.5). Ray bending makes sunset slightly later in the day and sunrise slightly earlier in the day, thus increasing the time in which the sun's rays can be collected.

3.1.1.3. Declination Angle

The declination angle is the angle between a line extending from the center of the sun to the center of the earth and the earth's equatorial plane. It is a function of the time of year with its value ranging from -23.45° to +23.45°. Most texts present the declination angle as being a function of the day only,

$$\delta_d = 23.45\, sin\left(360\frac{(284+n)}{365}\right). \tag{3.7}$$

In parts of this work, the declination angle is calculated on an hourly basis using

$$\delta_h = 23.45\, sin\left[360\left(\frac{284}{365}+\frac{h}{8760}\right)\right] \tag{3.8}$$

where h is the total number of hours that have passed from midnight on January 1. Calculating the declination angle on an hourly basis does not affect the final results in any noticeable way, but it does make the computer programing easier.

3.1.1.4. Zenith Angle

The zenith angle is the angle between the sun rays and a normal vector to a horizontal plane on the surface of the earth at the location of the solar panel. Its value ranges from 0° to 90° and has a value of 0° when the sun is directly overhead and 90° when the sun is on the horizon. The zenith angle is equal to 90° at sunrise and sunset. The zenith angle, θ_z, is related to the latitude, $\emptyset$, declination angle, δ_h, and hour angle, ω, as

$$\cos\theta_z = cos\,\emptyset\, cos\,\delta_h\, cos\,\omega + sin\emptyset\, sin\delta_h. \tag{3.9}$$

3.1.1.5. Altitude Angle

The solar altitude angle, α_s, is nothing more than the compliment of the zenith angle,

$$\alpha_s = 90 - \theta_z. \tag{3.10}$$

This angle represents how high the sun is in the sky. An altitude angle of 90° indicates the sun is directly overhead and an altitude angle of 0° means the sun is on the horizon getting ready to rise or set.

3.1.1.6. Azimuthal Angle

The azimuthal angle is an angle in a horizontal plane between a line pointing due south and line that is the projection of the sun's rays on this horizontal plane. Its value ranges from -180° to

+180° having negative values when the projection of the sun's rays on horizontal plane is east of due south and is positive values when the projection of the sun's rays on a horizontal plane are west of due south. For latitudes between 23.45° and 66.45° north and -23.45° and -66.45° south, solar azimuth angle values range between -90° to +90° on days with less than 12 hours of sun light and take on a value that is greater than 90° in the late evenings and less than -90° during the early mornings when the day length is greater than 12 hours. The azimuthal angle of the sun can be related to other angles using

$$\gamma_s = sign(\omega)\ \left|cos^{-1}\left(\frac{cos\theta_z sin\emptyset - sin\delta_h}{sin\theta_z cos\emptyset}\right)\right|. \quad (3.11)$$

An absolute value sign is placed around the inverse cosine portion of this equation so the sign of the azimuthal angle of the sun is determined by the sign on the hour angle.

3.1.1.7. Latitude

The latitude, ∅, is the angle between a line joining the location of the solar panel to the center of the earth and the equatorial plane. Latitudes are marked on maps as an angle from the equator. This angle is measured from the center of the earth. The latitude values range from -90° to +90° with positive values for locations north of the equator and negative values for locations south of the equator. In this work, three different latitudes are used, 38.21° N for Rio Vista, California, 32.77° N for Dallas, Texas and 39.83° N for Dayton, Ohio. Latitudes of any city in the world can be found on the internet. The latitudes listed for the three cities above should be taken as representative latitudes for those cities, as latitudes vary for different locations within a large city.

3.1.1.8. Surface Azimuthal Angle

The surface azimuthal angle, γ, is the angle between the projection of a normal vector from the solar panel surface to a horizontal plane and due south. Its value ranges from -180° to +180° having negative values when the surface is orientated east of due south and positive values when the surface is orientated west of due south. In this work, all solar panels are orientated due south and have an azimuthal angle of 0°.

3.1.1.9. Surface Tilt Angle

The slope of the solar panel surface is represented by the angle between the plane of the surface and a horizontal surface, β. Its value is between 0° and 90°. Any angle greater than 90° would have the sun collecting surface facing down towards the ground, which does not make sense. The solar panel surface is horizontal when its slope angle is 0° and is vertical when its slope angle is 90°. In this work, all solar panels are tilted at an angle equal to the latitude of the location

$$\beta = \emptyset. \tag{3.12}$$

This is a rule-of-thumb used in the solar industry to collect the most solar energy from a fixed panel over the course of one year. If two axis tracking were used, the panel would always face directly towards the sun. Since tracking devices add undesired initial costs to the system, fixed panels are used throughout this work. Using fixed solar panels, as opposed to solar panels with two axis tracking, reduces the yearly solar energy collected by about 25 to 40%.

3.1.1.10. Angle of Incidence

The angle of incidence, θ, is the angle between a line joining the location of interest to the center of the sun and the normal to the solar panel surface. This angle is a function of longitude, declination angle, hour angle, slope angle of the surface, and surface azimuth angle. The value of the incidence angle changes as a function of time of day and day of the year. The cosine of the incidence angle is given by

$$\cos\theta = \sin\delta_h \sin\emptyset \cos\beta - \sin\delta_h \cos\emptyset \sin\beta \cos\gamma + \cos\delta_h \cos\emptyset \cos\beta \cos\omega + \cos\delta_h \sin\emptyset \sin\beta \cos\gamma \cos\omega + \cos\delta_h \sin\beta \sin\gamma \sin\omega. \tag{3.13}$$

This is a rather lengthy expression, but it is an important one. This equation provides the fraction of the beam radiation normal to the sun's rays that impinges on the surface as the sun moves across the sky and the panel orientation remains fixed. When the incident angle of the sun's rays is large, little solar energy hits the panel. When the incident angle of the sun's rays is small, more solar energy is captured by the solar panel.

3.1.2. Solar Radiation Incident on Tilted Solar Panel

While the sun's radiant energy travels through the vacuum between the sun and earth's atmosphere as beam radiation, in the earth's atmosphere beam radiation is disturbed. In the earth's atmosphere, a portion of the sun's beam radiation is scattered into what is called diffuse radiation.

At the surface of the earth, a portion of the sun's radiant energy is reflected from the ground and this called ground reflected radiation. These are the three primary components of solar radiation that need to be tracked in order to determine the amount of solar energy incident on a solar panel located on the surface of the earth. Beam, diffuse, and ground reflected solar radiation components are included in the Hay and Davis solar radiation model [29] which is used in this work.

In some models the diffuse radiation component is subdivided into three parts: isotropic diffuse, circumsolar diffuse, and horizon brightening diffuse. The isotropic diffuse part is the portion of the incoming solar radiation that has interacted with the earth's atmosphere and is scattered with the same strength in all directions. The circumsolar portion is the forward scattered solar radiation and has almost the same direction of travel as the beam radiation. The horizon brightening portion is nonisotropic scattered radiation that comes from the horizon. For certain atmospheric conditions more or less scattered radiation is received from the horizon than what a purely isotropic model would predict. In the Hay and Davis model used in this work, diffuse radiation is subdivided into circumsolar diffuse radiation and isotropic diffuse radiation. Hay and Davis assume that horizon brightening is adequately modeled with isotropic radiation coming from the horizon. Thus the radiation model used in this work has detailed models for the beam, circumsolar, isotropic diffuse, and ground reflected radiation reaching a tilted solar panel and neglects the effects of horizon brightening.

For this work, shading of the solar panels by the panels in front of them is included. For this reason, the solar radiation collected by the front row of panels is discussed separately from the solar radiation collected by the succeeding rows. Any row of solar panels behind the front row may be partially shaded depending on a number of conditions. For this work the front is never shaded, but the succeeding rows are checked for any shading by doing detailed trigometric calculations. The front row panels will be referred to as front row panels and the succeeding rows of panels will be referred to as back row panels.

Before discussing the nonshaded models and shading models for incident solar energy on the front row and back rows of arrays of solar panels, a number of required quantities are presented. These quantities are required in the Hay and Davis model which predicts the amount of solar energy incident on a tilted solar panel, of any azimuthal orientation, at any location.

3.1.2.1. Extraterrestrial Radiation

The extraterrestrial solar radiation normal to the sun's rays present just above the atmosphere of the earth is required to determine the amount of scattering in the earth's atmosphere. From a simplistic viewpoint this is just the solar constant, G_{sc}, which is 1353 W/m^2. Figure 1.3 showed that the extraterrestrial solar radiation varies with the day of the year and this variation can be modeled using the formula

$$G = G_{sc}\left(1 + 0.033\, cos\frac{360n}{365}\right). \tag{3.14}$$

In addition to handling this issue, the extraterrestrial solar flux will be converted from a power flux normal to the sun's rays to an hourly energy flux on a horizontal surface. In this work, and in most solar modeling, solar energy is modeled on an hourly basis. This is done because the required experimental data on solar energy reaching the earth's surface are given for hourly time increments. Integrating Equation (3.14) multiplied by Equation (3.9) over a one-hour time period gives

$$I_o = \frac{12}{\pi}G_{sc}\left(1 + 0.033\, cos\frac{360n}{365}\right)\left[cos\,\emptyset\, cos\,\delta_h(sin\,\omega_2 - sin\omega_1) + \frac{\pi(\omega_2-\omega_1)}{180}sin\,\emptyset\, sin\,\delta_h\right] \tag{3.15}$$

where I_o is the solar radiation incident on a horizontal surface per unit area, located just outside of the earth's atmosphere, for a time period of one hour. The quantities ω_1 and ω_2 are the hour angles at the beginning and end of the hour respectively.

3.1.2.2. Components of Solar Radiation on a Horizontal Surface

To get the portion of the total solar radiation that interacts with the atmosphere, a clearness index is used. The clearness index is calculated as

$$\mathrm{k_T} = \frac{\mathrm{I}}{\mathrm{I_o}}. \tag{3.16}$$

Once the clearness index is found, it is used in the empirical relationships

$$\frac{\mathrm{I_d}}{\mathrm{I}} = \begin{cases} 1.0 - 0.09\mathrm{k_T} & \text{for} \quad \mathrm{k_T} \le 0.22 \\ 0.9511 - 0.1604\mathrm{k_T} + 4.388\mathrm{k_T^2} - 16.638\mathrm{k_T^3} + 12.336\mathrm{k_T^4} & \text{for} \quad 0.22 < \mathrm{k_T} \le 0.80 \\ 0.165 & \text{for} \quad \mathrm{k_T} > 0.8 \end{cases} \tag{3.17}$$

to determine the ratio of the diffuse flux, $\mathrm{I_d}$, to the total flux, I, on a horizontal surface. Notice that the denominator on the lefthand side of this equation is the measured solar energy flux on a

horizontal surface. This is a known quantity that comes from published data sets, and the clearness index is calculated with Equation (3.16). Therefore, the diffuse flux on a horizontal surface can be determined from these relationships. Once the total energy flux and the diffuse flux on a horizontal surface are known, the beam energy flux on that same horizontal surface can be found from

$$I_b = I - I_d. \tag{3.18}$$

At this time the total measured energy flux on a horizontal surface has been separated into beam and diffuse components. The ground reflected component on a horizontal surface, I_g, is the only one of the three primary radiation components left to determine on this horizontal surface. This can be done using the equation

$$I_g = I\rho_g \tag{3.19}$$

where ρ_g is the ground reflectivity to solar radiation. In this work the ground reflectivity is given the value of 0.6.

To get the portion of the diffuse component that is circumsolar, the anisotropic index is used. The anisotropic index is determined from the beam energy flux and the extraterrestrial solar energy flux as

$$A_i = \frac{I_b}{I_o}. \tag{3.20}$$

The circumsolar portion, $I_{d,cs}$, of the diffuse radiation component is determined from the anisotropic index as

$$I_{d,cs} = I_d A_i \tag{3.21}$$

and the isotropic, $I_{d,iso}$, portion of the diffuse component is

$$I_{d,iso} = I_d(1 - A_i). \tag{3.22}$$

Equations (3.21) and (3.22) show how the anisotropic index is used in the Hay and Davis radiation model to split the diffuse component into a circumsolar portion and an isotropic scattering portion.

Note that both the clearness index and the anisotropic index are calculated on an hourly basis just like the solar energy fluxes. Both of these indices make use of a ground radiation energy flux and an extraterrestrial radiation flux to indicate the amount of interaction the atmosphere has with the solar radiation traveling through it. For the clearness index the ground radiation flux is the total solar radiation on a horizontal surface, while for the anisotropic index it is the beam radiation on a horizontal surface.

3.1.2.3. Horizontal to Tilted Surface

The separate parts of the solar radiation that need to be summed to get the total solar radiation incident on the solar panel are the beam, circumsolar, isotropic diffuse, and ground reflected. Equations (3.18), (3.19), (3.21), and (3.22) provide these quantities for a horizontal surface. The beam component given in Equation (3.18) and the circumsolar portion of the diffuse component given in Equation (3.21) needs to be adjusted to that impinging on the tilted solar panel surface. This can be done using the geometric factor R_b, which represents the ratio of beam radiation on the tilted surface to the beam radiation on a horizontal surface. On an instantaneous basis, this geometric factor is defined as the cosine of the incident angle to the cosine of the zenith angle,

$$R_b = \frac{cos\theta}{cos\theta_z}. \tag{3.23}$$

Because this geometric factor approaches infinity close to sunset and sunrise an integrated average version is used,

$$R_{b,ave} = \frac{a}{b} \tag{3.24}$$

where

$$a = (sin\delta_h \sin \emptyset \cos\beta - \sin\delta_h cos\, \emptyset \sin\beta\cos\gamma)\frac{1}{180}(\omega_2 - \omega_1)\pi + (cos\delta_h cos\emptyset\cos\beta + \cos\delta_h sin\emptyset\sin\beta\cos\gamma)(\sin\omega_2 - sin\omega_1) - (cos\delta_h sin\beta sin\gamma)(cos\omega_2 - cos\omega_1) \tag{3.25}$$

and

$$b = (cos\emptyset cos\delta_h)(sin\omega_2 - sin\omega_1) + (sin\emptyset sin\delta_h)\frac{1}{180}(\omega_2 - \omega_1)\pi. \tag{3.26}$$

Using this average reduces problems that could occur at sunset and sunrise, but does not completely eliminate them.

Converting isotropic diffuse radiation on a horizontal surface to a tilted surface does not require a geometric factor like the beam and circumsolar radiation. Because isotropic diffuse radiation has the same strength in every direction, the flux is generally taken to be the same on a tilted surface as that on a horizontal surface. This is true as long as the surface has a full view of the atmosphere. Thus, changes in the isotropic diffuse radiation on a horizontal surface and that on a tilted surface are handled with a view factor. This view factor is presented latter.

3.1.2.4. Electrical Energy Produced by Front Row Solar Panels

In this model, solar panels are considered to be arranged in several rows that constitute a rectangular array pattern. There is a shadow cast by the first row of solar panels on the second row and by the second row on the third row and so on. The first row is special in that no shading occurs to it. Every row after the first will have shading affects and these rows will be labeled as back rows. The amount of shading occurring on the back rows is a function of the row spacing, the height of the top edge of the solar panels above the bottom edge and the position of the sun in the sky.

Since there is no shading on the front row of solar panels, the solar energy flux, I_{FR}, incident on the front row of solar panels is

$$I_{FR} = B_{FR} + D_{FR} + G_{FR} \tag{3.27}$$

where the beam including circumsolar, isotropic diffuse and ground reflected terms are symbolized by B_{FR}, D_{FR} and G_{FR} respectively. The subscript FR on these quantities indicates front row. Each of these three terms can be written in terms of quantities already defined in this thesis as

$$B_{FR} = (I_b + I_d A_i) R_{b,avg}, \tag{3.28}$$

$$D_{FR} = I_d (1 - A_i) \left(\frac{1+cos\beta}{2}\right), \tag{3.29}$$

and

$$G_{FR} = I\rho_g \left(\frac{1-cos\beta}{2}\right). \tag{3.30}$$

View factors for the isotropic diffuse radiation, $\frac{1+cos\beta}{2}$, and for the ground reflected radiation, $\frac{1-cos\beta}{2}$, have been included at this time.

The electrical energy produced by the entire front row of panels in one hour, $E_{H,FR}$, can be determined by multiplying the incident solar flux given by Equation (3.27) by the surface area of the front row panels, A_{FR}, then by the conversion efficiency of the photovoltaic panels, η_{pv}, then by the conversion efficiency of the inverters and other required electronics, c_f, as

$$E_{H,FR} = I_{FR} A_{FR} \eta_{pv}. \tag{3.31}$$

The yearly electrical energy produced by the front row of solar panels, $E_{Y,FR}$, is then obtained by summing the hourly values over the 8760 hours that compose one year as

$$E_{Y,FR} = \sum_1^{8760} E_{H,FR}. \tag{3.32}$$

3.1.2.5. Electrical Energy Produced by Back Row Solar Panels

The determination of the electrical energy produced by the back row solar panels is much more difficult to determine than the front row. All the complication comes from accessing what fraction of the solar panel area in a back row is shaded by the row in front of it. Of the three main components of solar radiation separately modeled in this work, the beam and ground reflected are affected by shading. The circumsolar portion of the diffuse radiation is also affected by shading and this is handled by combining the circumsolar diffuse radiation with beam component.

This is an involved geometric analysis that was developed specifically for this thesis. The geometry associated with this problem is shown in Figure 3.2. In Figure 3.2, the wedge in the front represents the row of panels doing the shading, and the wedge in the back represents the row of panels being shaded. For purposes of developing the shading model, the solar panel rows are taken to be infinitely long. Of course, this is never true, but if the rows of panels are long, it is a very good model. As the rows become shorter, this model will over predict the amount of shading. To better see some of the important distances involved on the shaded panel, Figure 3.3 has been prepared. Figure 3.3 only shows the shaded panel. These distances are important for determining where a ray of the sun just comes over the row of solar panels doing the shading, impinging on the row of panels being shaded. With the location of this impingement point, the fraction of the back row solar panels that is not shaded, F_{NS}, can be determined as

$$F_{NS} = 1 - \frac{l}{H}. \tag{3.33}$$

where H is the height of the upper edge of the solar panel above the lower edge of the solar panel; and l is the height above the lower edge where the sun beam coming over the shading solar panel hits the surface of the shaded solar panel. See Figure 3.3 for these dimensions.

Angles that are required in this analysis are β, the tilt of the solar panel, γ, the azimuthal orientation of the solar panel, α_s, the solar altitude angle, and γ_s, the solar azimuthal angle. The two solar panel angels are inputs to this analysis, and the two sun angles can be determined with Equations (3.10) and (3.11). Other inputs are the length of the solar panels, L, and the spacing between the solar panels, g. For all the results presented in this thesis the solar panel length is taken as 1 m and the spacing between the solar panels is taken as 5 m. Using these distances and trigonometry the following equations are produced

$$H = Lsin\beta, \tag{3.34}$$

$$d = \frac{H}{tan\alpha_s}, \tag{3.35}$$

$$c = d\ cos\gamma_s, \tag{3.36}$$

$$f = c - g, \tag{3.37}$$

$$p + k = \frac{f}{cos\gamma_s}, \tag{3.38}$$

$$o = \frac{pf}{p+k}, \tag{3.39}$$

$$l = o\ tan\beta, \tag{3.40}$$

and

$$\frac{l}{k} = tan\alpha_s. \tag{3.41}$$

With Equations (3.34) through (3.41), Equation (3.33) can be written as

$$F_{NS} = 1 - \frac{f tan\beta}{Lsin\beta(1+\frac{cos\gamma_s}{tan\alpha_s}tan\beta)} \tag{3.42}$$

and f can be written as

$$f = \frac{Lsin\beta}{tan\alpha_s}cos\gamma_s - g. \tag{3.43}$$

Equations (3.42) and (3.43) are written in terms of known quantities and can be solved.

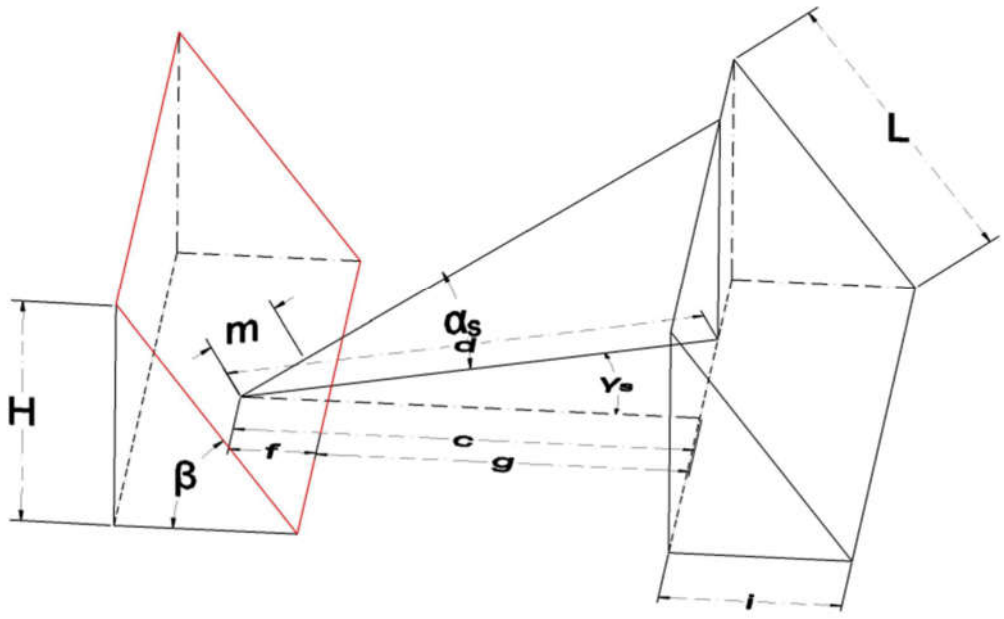

Figure 3.2: Important distances and angles for shading calculations.

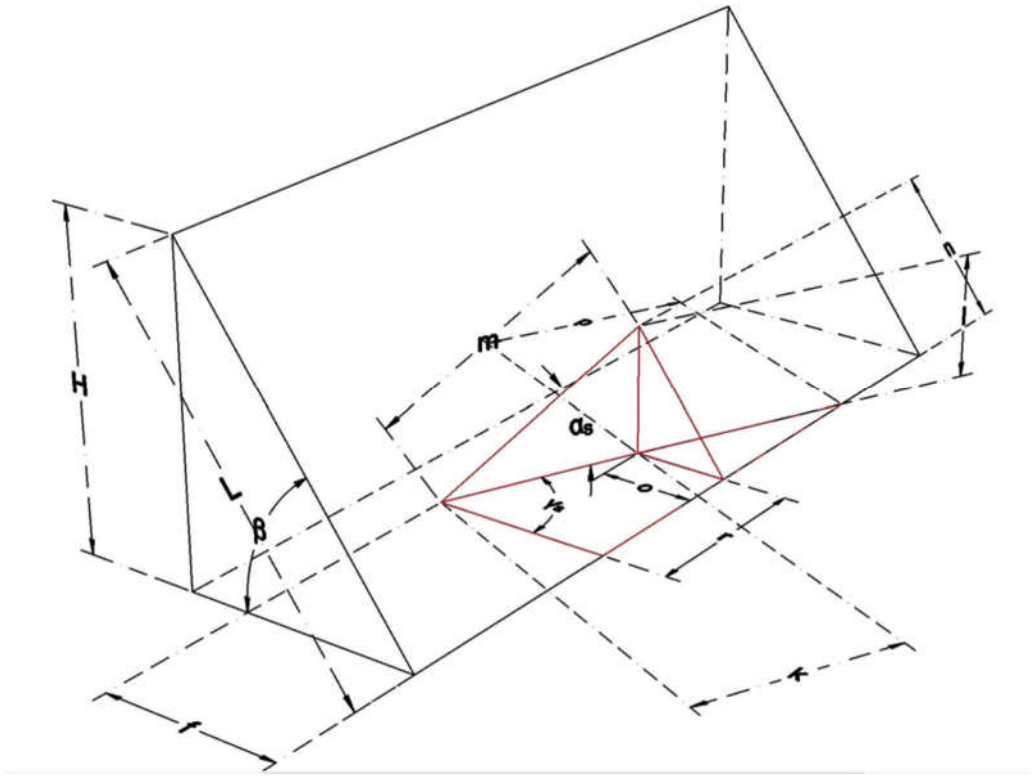

Figure 3.3: Enhanced view of shaded row solar panel with important angles and distances.

For the ground reflected component of the solar radiation, the length of the ground between the two rows of solar panels that is not shaded must be determined. This length is needed to calculate the ground view factor for the shaded panels. Here, f_{GR} is the length of ground not shaded,

$$f_{GR} = max[0, g - c], \tag{3.44}$$

and F_{gvf} is the corresponding ground view factor

$$F_{gvf} = \frac{L + f_{GR} - \sqrt{L^2 + f_{GR}^2 - 2\,L\,f_{GR}\ \cos(180 - \beta)}}{2\,L}. \tag{3.45}$$

With the fraction of the back row panels not shaded and the ground reflectivity view factor adjusted for shading, equations for the electrical energy produced by the back row panels can be written. These equations are similar to those for the front row solar panels given in Equations (3.27) through (3.32), but include reductions caused by shading. The average solar energy flux, I_{BR}, incident on the back rows of solar panels is

$$I_{BR} = B_{BR} + D_{BR} + G_{BR} \tag{3.46}$$

where the beam including circumsolar, isotropic diffuse and ground reflected pieces of the total incident solar energy flux are symbolized by B_{BR}, D_{BR} and G_{BR} respectively. The subscript BR on

these quantities indicates back row. This equation is the same as Equation (3.27) for the front row, except for the subscripts. These subscripts indicate that the components in this equation have different relationships than the front row and all three components are given as

$$B_{BR} = F_{NS}(I_b + I_d A_i)R_{b,avg}, \tag{3.47}$$

$$D_{BR} = I_d(1 - A_i)\left(\frac{1+cos\beta}{2}\right), \tag{3.48}$$

and

$$G_{BR} = I\rho_g F_{gvf}\,. \tag{3.49}$$

Since all the back rows behave similarly, the electricity generated by all the rows behind the front row are determined as one quantity. Just like for the front row of panels, the solar energy fluxes need to be multiplied by the surface area of the back row panels, A_{BR}. This surface area is the entire surface area of the back row panels, not just the unshaded surface area. The fraction of the area that is shaded has already been accounted for in the solar energy fluxes. Thus, the electrical energy produced by the all the back row panels over a one hour period is

$$E_{H,BR} = I_{BR}A_{BR}\eta_{pv}. \tag{3.50}$$

The yearly electrical energy produced by the back rows is

$$E_{Y,BR} = \sum_1^{8760} E_{H,BR}. \tag{3.51}$$

The electrical energy generated by the solar portion of the wind-solar farm, both the front row and all the back rows, can be found by summing the front and back row values. For one hour, the electricity generated by the solar portion of the wind-solar farm is

$$E_{H,S} = E_{H,FR} + E_{H,BR}. \tag{3.52}$$

For a year period, the electricity generated by the solar portion of the wind-solar farm is

$$E_{Y,S} = E_{Y,FR} + E_{Y,BR}. \tag{3.53}$$

3.2. Wind Model

The wind energy calculations are less involved than the solar energy calculations because a number of complex angles and different components do not have to be included. The wind energy parameter required is the wind speed and it is assumed that the wind turbine is yawed to face directly into the wind, so wind directions are not required. The wind speed at a given location is obtained from measured wind speeds over the course of a year at a specified location at a specified elevation.

The energy in the wind over the area swept out by the rotor, A_r, of the wind turbine is obtained by the simple relation

$$P_{wind} = \frac{1}{2}\rho_{air}\, A_r\, V^3 \tag{3.54}$$

where

$$A_r = \frac{\pi}{4} D_r^2. \tag{3.55}$$

and D_r is the diameter of the rotor of the wind turbine. The density of the air used in this work is always taken as the standard value of 1.225 kg/m^3. What remains to be done is to determine the fraction of this energy extracted by the wind turbine. This is done by using a manufacturer power curve for the chosen wind turbine. A power curve provides the electrical power a given wind turbine will produce at a given wind speed. The power curve used in this work is given below. The proper wind speed to enter into the power curve is the freestream wind speed at the height of the wind turbine hub.

3.2.1. Scaling Wind Speed Data for Different Heights

Wind speed data at every five-minute interval for the year of 2012 at the three locations studied in this thesis are obtained from the wind speed database published by the National Renewable Energy Laboratory [33]. Often, these wind speed data are tabulated at standard heights which may differ from the hub height of the wind turbine under consideration. This is the reason that wind scaling relations were developed. In this work a log wind scaling relation is used which is given as

$$V = V_{ref} \frac{ln\left(\frac{z}{z_o}\right)}{ln\left(\frac{z_{ref}}{z_o}\right)}. \tag{3.56}$$

In this equation, V is the speed of the wind at the hub height of the chosen wind turbine, z, and V_{ref} is the speed of the wind given in the measured data set which was measured at a height of z_{ref}. The parameter z_o is an effective surface roughness height which changes depending on the type of landscape located around the turbine. In this work, a surface roughness factor of 0.01 m is used which is representative of rough pastures. Other surface roughness factors can be obtained from published tables.

The measured wind speed used in this work has a high temporal resolution and is reported every 5 minutes over the course of a year. This means there are 105,120 wind speed values to

represent the wind at a given location for an entire year. Measured wind speeds are generally given on finer time intervals than measured solar data, because changes in the wind speed occur more abruptly than changes in the solar radiation incident on the surface of the earth. Thus, the wind calculations in this work are done over 105,120 time intervals, while solar calculations are done over 8760 time intervals. The only difficulty this causes is the computer has to perform more calculations to complete a year's worth of wind energy calculations. This is not difficult for modern day computers, and should not cause concern. Another point to be made is that the measured wind speed data used in this work was taken in 2012. The calculations performed in this work are meant to be valid for any year. While there may be some changes in temporal wind profiles from year to year, it is assumed that 2012's wind speed profiles are representative of any year's wind speed profiles.

3.2.2. Electricity Generation from Wind Turbine

The wind turbine used in this work is the Enercon E-82 E4 3.0 which has a cut-in wind speed of 3 m/s, a cut-out wind speed of 34 m/s, a hub height of 84 m, and rotor diameter of 82 m. The power curve for this wind turbine is shown in Figure 3.4. This power curve shows the maximum rated capacity of this turbine to nominally be 3 MW. This is the peak electrical power that this wind turbine can produce. To find the energy that this wind turbine can produce at a given location, electrical power outputs for each of the 105,120 wind speeds at the hub height are found. These electrical power outputs are labeled with the symbol $P_{5,W}$. This quantity is found for each 5 minute wind speed by linearly interpolating the discrete tabulated data used to produce the wind turbine power curve given in Figure 3.4.

When the electrical power output from all the wind turbines in the wind-solar farm is numerically integrated over a one hour time period an hourly electrical energy output, $E_{H,W}$, can be found. This is done as

$$E_{H,W} = N_w \frac{5}{60} \sum_1^{12} P_{5,W} \tag{3.57}$$

where N_w is the number of wind turbines in the farm. This equation simply adds the five minute wind turbine powers, $P_{5,W}$, multiplies them by a five minute time increment in hours, 5/60, for one hour. There are 12, five minute time increments in an hour. This quantity is useful for comparing hourly electricity generation from the wind portion of the wind-solar farm to the hourly electricity

generation from the solar portion. The electrical energy produced over the course of a year by the wind turbines in the wind-solar farm is found from

$$E_{Y,W} = N_w \frac{5}{60} \sum_1^{105,120} P_{5,W}. \tag{3.58}$$

This equation will produce a yearly energy output in kW-h or MW-h depending on the power units used for $P_{5,W}$. The $\frac{5}{60}$ factor dictates that the time units in the energy result is in hours.

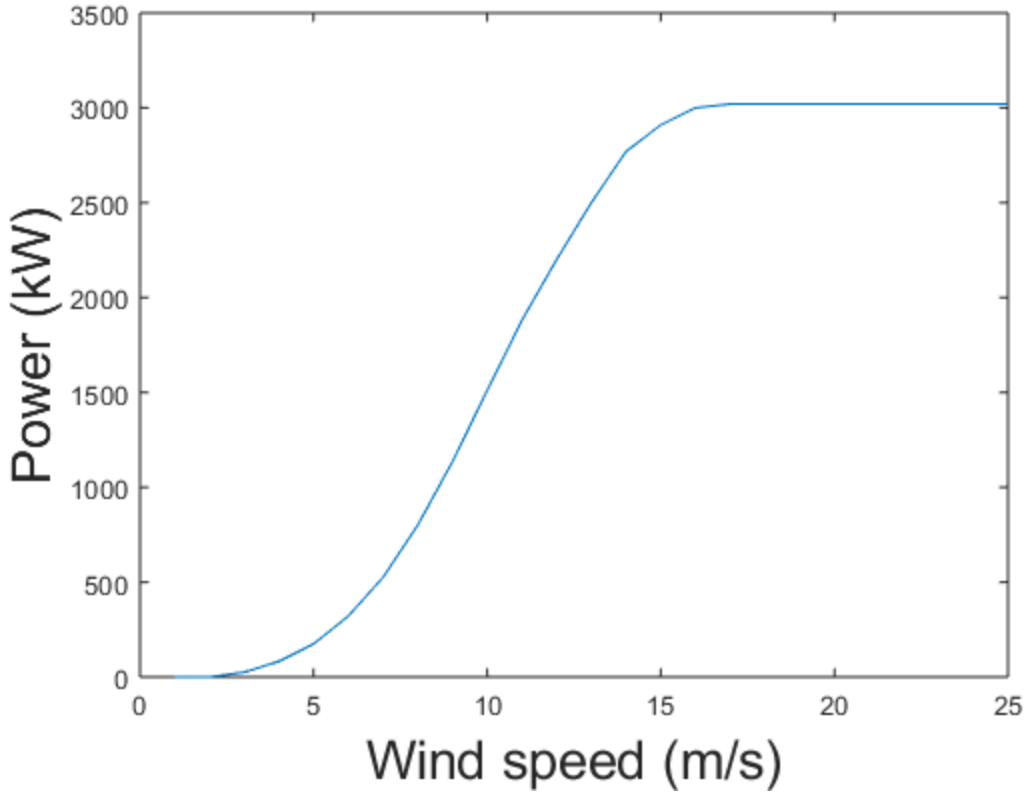

Figure 3.4: Wind power curve for the Enercon E-82 E4 3.0 wind turbine.

3.3. Electricity Demand

Electricity demand curves are obtained from the OpenEI energy datasets that are located on the web [32]. These demand curves were determined using the NREL developed software ENERGY PLUS. These demands are given as average powers that occur on an hourly basis. A key criteria for this study is that all of the electrical demand has to be met. If the wind-solar farm cannot meet the demand, electricity has to be purchased from the local electrical grid.

From the electricity produced by all the solar panels and the electricity produced by all the wind turbines in the wind-solar farm, the hourly electricity production from the wind-solar farm is

$$E_{H,WSF} = E_{H,W} + E_{H,S}. \tag{3.59}$$

This same sum can be done on a yearly basis as well giving

$$E_{Y,WSF} = E_{Y,W} + E_{Y,S}. \tag{3.60}$$

The electricity demand on an hourly basis, $E_{H,D}$, can be directly compared to the hourly wind, $E_{H,W}$, and solar, $E_{H,S}$, electrical energy productions. Yearly demand can be found by simply summing the hourly demands as

$$E_{Y,D} = N_w \sum_1^{8760} E_{H,D}. \tag{3.61}$$

No time increment is needed because the hourly demands are energies and not average hourly powers.

Now the excess energy produced by the wind-solar farm on an hourly basis, $E_{H,ex}$, can be determined as

$$E_{H,ex} = E_{H,WSF} - E_{H,D}. \tag{3.62}$$

To calculate the excess electrical energy produced on a yearly basis, care has to be taken to understand that electricity purchases are made on an hourly basis and thus the yearly positive excess energy should be calculated as

$$E_{Y,ex} = \sum_1^{8760} max\left(0, E_{H,ex}\right), \tag{3.63}$$

and the negative excess energy (deficit energy) should be calculated as

$$E_{Y,d} = -\sum_1^{8760} min\left(E_{H,ex}, 0\right). \tag{3.64}$$

The yearly deficit electrical energy, $E_{Y,d}$, is the electricity that has to be purchased from the local electrical grid every year. The minus sign in Equation (3.65) makes the yearly deficit electrical energy a positive number. The yearly positive excess electrical energy, $E_{Y,ex}$, is the yearly electrical energy that may be sold back to the grid.

3.4. Net Present Cost Model

The means of comparing different wind-solar farms studied in this work is through the net present cost of providing electricity to 25,000 typical homes in the city of interest for 25 years. The wind-solar farm with the lowest net present cost is considered to be the best wind-solar farm for that location. A constraint on this analysis is that all the demand must be met on an hourly

basis. If the demand cannot be met by the wind-solar farm, electricity must be purchased from the local grid at local grid prices. For most of the cases, excess electricity produced by the wind-solar farm is considered waste, and is not sold back to the gird. In one case for each location, electricity is sold to the grid at half the price at which it is purchased. No onsite energy storage is utilized in this study. Not using onsite storage eliminates capital costs, but is paid for as annual costs to obtain electricity to supply unmet demand.

The cost included in this analysis are rather simple. They include capital costs, operation and maintenance costs, and cost of purchasing electricity from the grid. The capital costs include the costs to purchase and install the wind turbines and solar panels at the site. Maintenance costs are given on a yearly basis and include the costs to keep the wind turbines and solar panels running throughout the 25 years of operation. A critical cost in this analysis is the amount of electricity that must be purchased to meet the portion of the electricity demand that cannot be met by the wind-solar farm. The key trade-off in this study is between the capital costs and the cost of purchased electricity. The capital costs are incurred at the start of the 25 year period and do not need any adjustment to be included in the net present cost. The maintenance costs and electricity purchases are annuitized costs and have to be multiplied by a time value of money factor to obtained their net present value.

The net present cost, *NPC*, including capital, maintenance, and electricity purchases or sales is determined with

$$NPC = C_{CW}P_{NPW} + C_{CS}P_{NPS} + C_{MW}E_{Y,W}\frac{(1+i)^{n_y}-1}{i(1+i)^{n_y}} + C_{MS}E_{Y,S}\frac{(1+i)^{n_y}-1}{i(1+i)^{n_y}} + C_{el,d}E_{Y,d}\frac{(1+i)^{n_y}-1}{i(1+i)^{n_y}} - C_{el,ex}E_{Y,ex}\frac{(1+i)^{n_y}-1}{i(1+i)^{n_y}} \quad (3.65)$$

Each of the terms in this equation represent a cost or a cash flow. All but the last term on the righthand side is a cost. The minus sign on this term indicates that it is a net cash influx. Each of the terms on the righthand side of this equation has the following meanings:

$C_{CW}P_{NPW}$ - the capital cost of placing wind turbines at the site where C_{CW} is the cost per unit of nameplate capacity and P_{NPW} is the wind nameplate capacity

$C_{CS}P_{NPS}$ - the capital cost of placing solar panels at the site where C_{CS} is the cost per unit of nameplate capacity and P_{NPS} is the solar nameplate capacity

$C_{MW}E_{Y,W}$ - the annual cost to operate and maintain the wind turbines where C_{MW} is the annual cost per unit of electricity produced and $E_{Y,W}$ is the yearly electricity produced by the wind turbines

$C_{MS}E_{Y,S}$ - the annual cost to operate and maintain the wind turbines where C_{MS} is the annual cost per unit of electricity produced by the solar panels and $E_{Y,S}$ is the yearly electricity production of the solar panels

$C_{el,d}E_{Y,d}$ - the annual cost of purchasing electricity from the grid to make up for deficit production by the wind-solar farm where $C_{el,d}$ is the cost per unit of electrical energy and $E_{Y,d}$ is the yearly amount of electrical energy bought from the grid

$C_{el,ex}E_{Y,ex}$ - the annual money received by selling excess electricity to the grid where $C_{el,ex}$ is the selling price per unit of electrical energy and $E_{Y,ex}$ is the yearly amount of electrical energy sold to the grid

The factor $\frac{(1+i)^{n_y}-1}{i(1+i)^{n_y}}$ shows up many times in Equation (3.65). This quantity is the inverse of the capital recovery factor and is used to convert an annuitized cost to a present cost. The i in this equation is the interest rate and the n_y is the lifetime of the system in years. Essentially the interest rate is the cost of money and is taken as 10% for all time value of money calculations. The lifetime of the system is taken as 25 years. Using this interest rate and lifetime gives

$$\frac{(1+i)^{n_y}-1}{i(1+i)^{n_y}} = 9.077. \tag{3.66}$$

For most of the cases studied in this work, electricity is not sold back to the grid. This means the last term in Equation (3.66) is taken to be zero. For the few cases where electricity is sold back to the grid, the selling price is taken to be half the purchase price. This type of constraint is an onerous one on the wind-solar farm. This was a choice made early in the study so that the economics of the wind-solar farm does not lean on the electrical grid for free storage capacity.

The goal of this work is to find the least cost combination of wind turbines, solar panels, and electricity purchased from the electrical grid. If the cost of producing a unit of electricity is high with wind and solar, the optimum system should be no wind turbines and no solar panels; all of the community's electricity needs should be purchased from the grid. Due to variations in the wind and solar resources, there will always be times when neither wind or solar energy is available. Thus, it is not possible to supply all the electrical demands of the community without purchasing some electricity from the grid. There will always be some hourly intervals where it is more beneficial, from a cost stand point, to purchase electricity from the grid. This cost analysis aims to show what is the least costly way to deliver electricity for a 25,000 home community. This is done accounting for the intermittency of wind and solar energy.

3.5. Numerical Issues

3.5.1. Discretization of Time

A time period of 8760 hours that begins at the start of the day on January 1 and terminates at the end of the day on December 31 is the temporal computational domain for the numerical calculations performed for this work. The primary time increment used in these computations is one hour, which means there are 8760 time increments. One hour is a natural time increment to use because the measured solar data is given in one hour time increments and the demand data is given in one hour time increments. The measured data that is not given in one hour time increments is the wind speeds. These are provided in 5 minute increments. So that wind results can be combined with solar results, the calculated five minute wind powers are converted to one hour wind energies using Equation (3.58). In addition, to doing most of the computations using one hour time increments, all results are plotted on an hourly basis, except the fundamental resource data which are plotted using 5 minute time intervals.

As mentioned in prior sections of this chapter, sun ray bending is not included in the solar model. This is the norm in these types of calculations. The beginning and end times when the sun's rays shine on a specified location on the surface of the earth is taken to be when the sun's rays are parallel with a horizontal surface at that location. This occurs at sunset and sunrise as determined by Equations (3.5) and (3.6) respectively. In these computations, all solar energy reaching the surface of the earth stops at sunset and begins at sunrise. So that matching with wind results in the night and plot results are continuous, solar energies are assigned a value of zero during the night which includes times from sunset to sunrise.

Another place in the numerical calculations where one hour time increments are not used is at sunset and sunrise. Sunset and sunrise usually occur between the beginning and the end of the hour time increments used in the MATLAB program. For this reason, the time increments for calculations at sunrise and sunset are shorten to match the portion of the sunset hour and the sunrise hour where the sun is shining. After calculating these partial hour energies, they are reassigned to the full hour for combination with wind energies and plotting.

3.5.2. Sunset and Sunrise Adjustments

In this work, most quantities are calculated at the middle of the one hour time increments; or at the middle of the shortened time increments at sunset and sunrise. When the shortened time

increments at sunset and sunrise become small, some solar quantities acquire unrealistically large values. The effect of this problem is minimized by using Equation (3.24) for the ratio of the solar radiation on a tilted surface to that on a horizontal surface, but it is not eliminated. To eliminate this problem completely, hour angles were calculated at the beginning of the hour increment where sunset occurs and at the end of the hour increment where sunrise occurs. This eliminated the few remaining unrealistic large numbers that Equation (3.24) does not eliminate.

Another difficulty at sunset and sunrise comes in through the anisotropic index. For some days anisotropic indexes are calculated that give rise to circumsolar and isotropic portions of the diffuse radiation component that do not make sense. This problem is mitigated by setting the anisotropic index to zero for the sunset and sunrise time increments. This simply puts all the diffuse solar energy into the isotropic diffuse portion and eliminates the circumsolar portion at sunrise and sunset.

The numerical adjustments made at sunset and sunrise have very little effect on the overall results generated in this work. Collected solar energy is small at these times.

3.5.3. Shading Adjustments

Depending on the slope of the panels and the day of the year the sun may be above the horizon, but behind the solar panels. If the sun is completely behind the solar panels the nonshaded fraction is zero, $F_{NS} = 0$. This occurs whenever the incidence angle becomes greater than or equal to 90º. Since the sun is behind the shaded panel in this situation, the distances f should become

$$c = abs(dcos\gamma_s) \tag{3.67}$$

and

$$f = max[0, c - (g - L\,cos\,\beta)] \tag{3.68}$$

and the nonshaded ground length is

$$f_{GR} = min[f, g]. \tag{3.69}$$

For times when the sun is at azimuthal angles less than -89º or greater than 89º and the incidence angle is still between 0º and 90º the back row solar panels are unshaded and $F_{NS} = 1$. These are times when the sun may be parallel or north of a line running along the rows of solar panels. The length of nonshaded ground in this case is should be taken as shown in the equations above.

Chapter 4
Results

A great deal of results from the mathematical models developed in Chapter 3 of this report are presented in this chapter. To keep the amount of repetition in the writing to a minimum, the first section of this chapter, Organization of Results, is provided. This should aid the reader in understanding the results presented.

The major reason for generating these results is to determine what combination of wind turbines, solar panels, and grid generated electricity provides the lowest cost in meeting a given electricity demand for a 25-year period. Of course, this lowest cost depends on a number of factors. The overall factor that determines a number of other factors that influence the benefits of using a wind-solar farm is location. Location determines the magnitude of the wind and solar resource, the magnitude of the electrical demands, and the cost of buying electricity from the grid. Of course, larger wind and solar resources are going to make wind-solar farms more attractive. For systems that do have energy storage, demand profiles that match resource profiles will make wind-solar farms more attractive. None of the wind-solar farms used in this study have on site energy storage, however, one case for each location will sell power back to the grid at a reduced price: effectively using the grid as energy storage. Not utilizing onsite storage, forces the analysis to optimize the number of wind turbines and number of solar panels in the combined facility against the local price of grid electricity. It also forces the analysis to use only that wind and solar capacity that generates demand electricity at a price lower than local grid generated power. In order for a wind-solar farm to be attractive from a purely economic perspective, it must produce electricity at a lower cost than

simply purchasing electricity from the gird. Thus, the price of buying electricity from the grid sets an upper limit on the unit electricity cost that a wind-solar farm must fall below to be economically desirable. One factor studied in this work, that is not taken to be a function of location, is the capital cost of wind and solar equipment. This cost will be increased and reduced by given percentages at each location, but the same base values are used for all locations.

4.1. Organization of Results

The major grouping of results in this chapter is by location. Location is the way the next three sections of this chapter are labeled. Three locations are studied:

1. Rio Vista, California,
2. Dallas, Texas, and
3. Dayton, Ohio.

As mentioned above, location affects a number of other quantities; these quantities will be treated as subsections and sub-subsections. The reason Rio Vista, California is chosen is that it has a good wind resource, a good solar resource and high grid electricity costs. The reason Dallas, Texas was included in this study is that it has a decent wind resource, a decent solar resource, and fair electricity costs. The wind and solar resources in Dallas, Texas are less than those in Rio Vista, California; and their cost of electricity is lower. The last location chosen for this study is Dayton, Ohio. This location was picked because it is the location where this work is being performed. More importantly, Dayton, Ohio has lowest wind and solar resources of the three locations studied, and very low electricity rates. This combination of factors is a severe test on the economic viability of a wind-solar farm. Dayton does not have the worst wind and solar resources in the country, but they are much less than Rio Vista, California and less than Dallas, Texas. The fact that Dayton's solar and wind resources are not as good as other parts of the country and grid generated electricity is inexpensive is supported by the fact that a small amount of wind and solar energy facilities have been built around Dayton, Ohio.

Within each location section of this report, four subsections are given. These four subsections are

1. Electricity Demand,
2. Wind and Solar Resources,
3. Wind-Solar Farm Electricity Production, and
4. Wind-Solar Farm Economics.

The Electricity Demand subsection presents a plot of the electricity used by 25,000 typical homes located in the city being studied. The demand varies from location to location, but does not vary for any of the results generated for that location. The demand for a typical home at each of the three locations studied was obtained from the OpenEI energy datasets [32]. As will be seen from these demand curves, air conditioning electricity requirements increase the amount of electricity demanded in the summer. For locations where electrical heating is used, electricity requirements increase in the winter. Dallas, Texas and Dayton, Ohio use electrical heating. Compared to heating and cooling, electricity used for appliances and lighting does not vary appreciably, but lighting usage is usually slightly higher in the winter time. The horizontal axis on each of these plots, and several others presented in this chapter, have the time of year marked out in hours. In general, spring runs between the hours of 1416 to 3624, summer from 3624 to 5832, and fall from 5832 to 8016. Winter is located on the beginning and end of the graph and goes from 0 to 1416 and 8016 to 8760.

To present the hourly wind and solar resource at a given location, it was decided to put the wind resource, the solar resource, and the sum of the two resources on the same graph. This graph has three curves with the blue one representing the wind resource, the yellow one representing the solar resource, and the black one representing the sum of the solar and wind resources. Wind resource data is given on 5 minute intervals, while solar resource data is given on 60 minute intervals. All resource data is plotted on 5 minute intervals; however, the solar resource data uses the same magnitude for the 12 five minute intervals that land in a given hour. Having these three curves on one graph is crowded, but it allows comparisons to be made between the wind and solar resources. It also allows the reader to determine the relative magnitude of these resources at different times of the year. For example, at some sites the wind resource may be larger in the winter, but the solar resource may be larger during the summer. The reader should also note that the wind and solar resource results are given in MW/m^2. This was done because the wind-solar farm dependent results are given in MW or MW-h. All wind resource data is obtained from NREL's wind energy database [33] and all solar resource data is obtained from the NREL's solar energy database [34].

The third subsection, Wind-Solar Farm Electricity Production, contains results for the yearly electricity production of different sized wind-solar farms and the excess energy produced by these wind-solar farms. On both of these plots, the size of the solar capacity is varied along the

horizontal axis and the size of the wind capacity is treated as a parameter and varies from curve to curve. Also, for both of these graphs, pure wind farm performance can be ascertained by looking at the location where the wind capacity lines intersect the vertical axis; and pure solar farm performance can be ascertained by looking at the wind capacity line marked 0 MW. For the energy production graphs, the yearly electricity produced by the wind turbines and the solar panels combined is shown on the vertical axis. For the excess energy production graphs, the electricity produced above the demand is shown on the vertical axis. If the wind-solar farm cannot meet the demand, the excess electricity is shown as a negative number. A negative number indicates a deficit of electricity for the year. A certain size of wind-solar farm can have a positive excess electricity, and still require that electricity be purchased from the grid. The timing of the excess electricity affects the results and yearly excess energy graphs do not show this timing. Detailed plots showing the timing of excess energy are given in the next subsection.

The last subsection, Wind-Solar Farm Economics, is where most of the graphs are located. As indicated in the subsection title, most of the results in this subsection depend on the cost associated with various aspects of electricity production. Obtaining these results is the reason the results in the prior subsection were generated. Five different cost scenarios are shown in these subsections for Rio Vista, California and Dallas, Texas, while six different cost scenarios are shown for Dayton, Ohio. Each of these cost scenarios is placed in its own sub-subsection. The first cost scenario presented is the base case; the remaining four or five cost scenarios have one cost altered from the base case.

The base case uses the inputs shown in Table 4.1. As seen in Table 4.1, these inputs are mostly related to costs. These costs include the cost to purchase a kW-h of electricity to make up for any demand that cannot be met by the wind-solar farm, the capital cost of the wind turbines, and solar panels, the time value of money and operations and maintenance costs for wind turbines and solar panels. For the base case, the cost of electricity is taken as the low industrial rate as provided by the Electricity Local website [35]. Industrial rates are much lower than residential rates and using these rates makes it tougher for wind and solar to compete with traditional grid generated electricity. All cases studied use the industrial rate for grid electricity, except one case that investigates the effects of using the higher commercial rate.

Table 4.1: Inputs used for base case net present cost scenario.

Quantity	Value
Electricity rate	Industrial Rate which equals \$0.0898/kW-h for Rio Vista, California, \$0.0557/kW-h for Dallas, Texas, and \$0.0196/kW-h for Dayton, Ohio.
Cost of wind turbines installed	\$1300 per kW of nameplate capacity
Cost of solar panels installed	\$1000 per kW of nameplate capacity
Operations and maintenance costs of wind turbines	\$0.00368 per kW-h of electricity produced
Operations and maintenance costs of solar panels installed	\$0.0012 per kW-h of electricity produced
Lifetime of capital equipment	25 years
Interest rate	10%

For the base case, none of the excess power generated by the combined wind-solar farm is sold back to the grid. This limits the attractiveness of wind-solar farms; however, it is felt to be a necessary restraint. If infinite, free storage capacity were made available to the wind-solar farm, there would be no optimization of the wind and solar capacity. One objective of this work is to show the complementarity of wind and solar. This constraint is relaxed in one case for each location to see the effect of selling excess wind-solar farm generated electricity back to the grid. To keep this relaxed constraint from completely eliminating the complimentary of wind and solar, the selling price is half of the purchase price.

For long term projects the time value of money is important. All wind-solar farm dependent results are based on a 25-year life. Most wind turbines and solar panels are capable of operating for this time span. The remaining critical number in a long lifetime economic analysis is the interest rate. A 10% interest rate is used for all economic analyses done in this thesis. These time value of money numbers make the capital costs of equipment a more significant factor in the economic analysis. In this work, three capital costs of equipment are studied. One case uses the baseline capital costs of equipment shown in Table 4.1, another case uses a capital cost of equipment increased by 50% from the baseline values, and yet another case uses capital costs of equipment

decreased by 50% from the baseline values. For Dayton, Ohio the base case capital costs are further reduced by 75% in hopes of obtaining a minimum cost using wind and solar energy.

Each of the five or six cost scenarios will show three plots, as long as the plots are not trivial. The first plot shown is the cost of delivering all the demanded electricity at a given location for 25 years in present day dollars for a range of wind turbine capacities and solar panel capacities. For all cases, the range of wind turbine capacities run from 0 to 108 MW and the range of solar capacities run from 0 to 125 MW. This provides ample scope to find a minimum cost. To find the present-day cost of running any combination of wind and solar farm, one simply has to find the intersection of the solar farm capacity, located on the horizontal axis, and the wind farm capacity curve. This intersection corresponds to one point on the vertical axis which is the present-day cost to deliver 25 years of electricity. For pure wind farm costs, simply look at intersections of the wind curves with the vertical axis. For pure solar farm costs, look for the intersection of the solar farm capacity value with the 0 MW wind capacity curve and trace it over to the vertical axis. To find the cost of providing all 25 years of electricity from the grid, find the intersection of the 0 MW wind capacity curve with the vertical axis. One can see that this graph provides a great deal of information on the costs of delivering 25 years of electricity to 25,000 homes.

The other two curves provided in each of these cost scenario sub-subsections are hourly details on the electricity produced and hourly details on the excess electricity produced by the wind-solar farm determined to provide the minimum cost of electricity in the graph described in the prior paragraph. The hourly electricity produced includes the electricity produced by all wind turbine capacity and all solar panel capacity. It does not include electricity purchased from the grid. The hourly excess electricity produced shows the amount of electricity produced by the wind and solar capacity above the demand. A negative excess energy means deficit electricity production by the wind-solar farm. Negative excess energy production is the amount of electricity that has to be purchased from the grid for that particular hour.

4.2. Rio Vista, California

4.2.1. Electricity Demand

The hourly electricity demand of 25,000 homes in Rio Vista, California is shown in Figure 4.1. Because electricity demand curves were not available for Rio Vista, those for Sacramento, California were used. Sacramento is just 40 miles from Rio Vista. The electricity load demand

ranges between 16 MW to 46 MW and has high demands during summer and early fall peaking at 96 MW. These occasional high electricity load demands during summer conditions are typical for air conditioning usage. The total electricity demand for the entire year is 218,470 MW-h.

The dark blue portion of the curves in Figure 4.1 provide the reader an idea of the most common demands. The same color was used for the entire curve, but the curve appears darker where the lines are more densely packed in the time direction. Because of the scales used in this plot it is not possible to see the daily variations of electricity usage. This information is contained in this plot, as all demand curves are done on an hourly basis. In general, daytime electricity demands are larger than nighttime electricity demands. Cooling electricity demands essentially run from hour 2904 to hour 6552 for Rio Vista. This is from the beginning of May to the end of September. Outside of the summer and early fall demands, December and January show higher demands than October and March. This is due to shorter days which require more lighting.

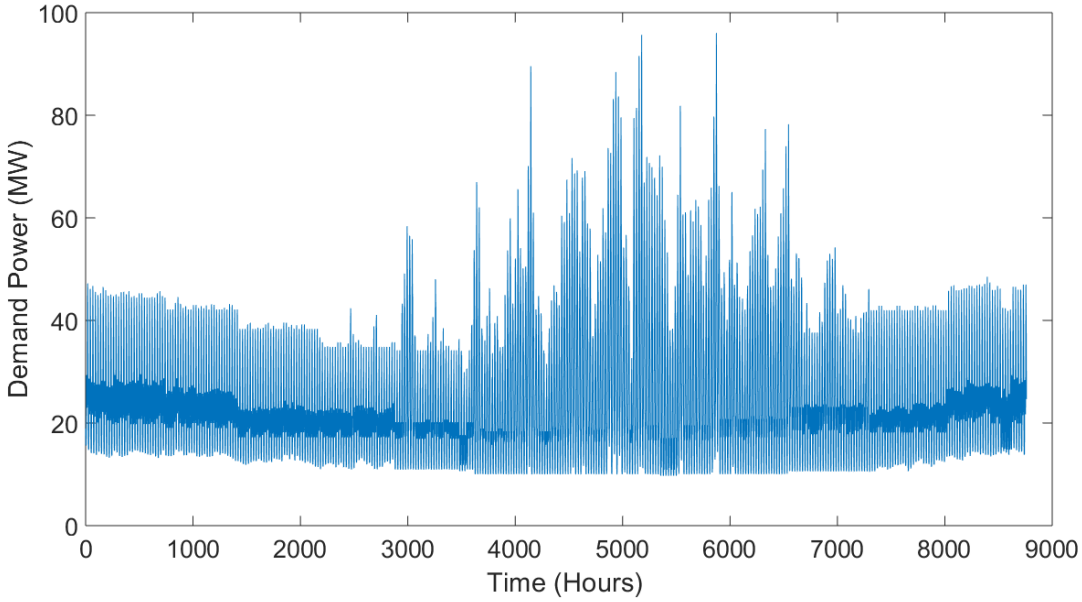

Figure 4.1: Electricity demand for 25000 typical homes located in Rio Vista, California.

4.2.2. Wind and Solar Resources

The wind and solar resources available in Rio Vista, California are shown in Figure 4.2. The solar energy resource in Figure 4.2 is for solar panels tilted from the horizontal at the latitude

of Rio Vista. This tilt angle is commonly recommended to collect the most solar energy over a one-year period using fixed panels [36]. It may be that other tilts better match the demand profile, but that is the subject of a future study. The wind power available at a height of 84 meters is also given. While the black line representing the combination of wind and solar power somewhat covers up the wind power curve and the solar power curve, putting these curves on one plot allows for comparison. All the large spikes of the combined wind-solar curve in Figure 4.2 are caused by the wind; the solar power never goes over 1.3 kW/m^2. Rio Vista has good resource availability with strong wind and exceptional solar illumination. Both the wind and solar resource show their largest values in the summer.

When the wind resource is integrated over one-year a value of 4.02 MW-h/m^2 is obtained. When the solar resource is integrated over one year a value of 2.28 MW-h/m^2 is obtained. These are good wind and solar resources. A nice aspect of the wind and solar energy resources available in Rio Vista is that they tend to peak in the summertime. This means these resources can address the peak cooling loads caused by air conditioning.

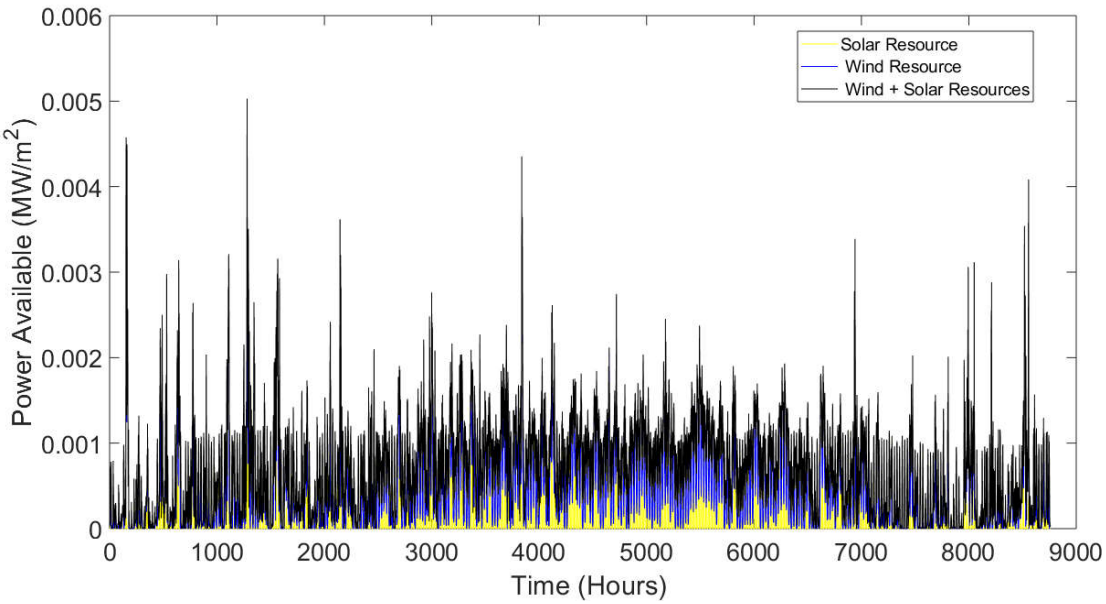

Figure 4.2: Wind and solar resource power densities for Rio Vista, California.

4.2.3. Wind-Solar Farm Electricity Production

Yearly energy produced by various sizes of wind-solar farms has been plotted in Figure 4.3 and yearly excess energy produced by the same sizes of wind-solar farms has been plotted in

Figure 4.4. Figure 4.3 shows the annual energy generation by the wind-solar farms ranging from 0 to 5.7×10^5 MW-h. Annual yearly excess energy for various configurations ranges from -2.18×10^5 MW-h to 3.58×10^5 MW-h. Figure 4.3 clearly shows a linear increase in total energy generated with increasing solar panel capacity. A linear relationship also exists in yearly energy produced versus the wind turbine capacity. Both of these trends are expected. A more surprising result is the close to linear relationship seen in the excess energy plot. As expected for lower wind and solar capacities, yearly net energy produced by the wind-solar farms is not enough for yearly electricity needs; even if there were battery storage on site to store the excess energy produced.

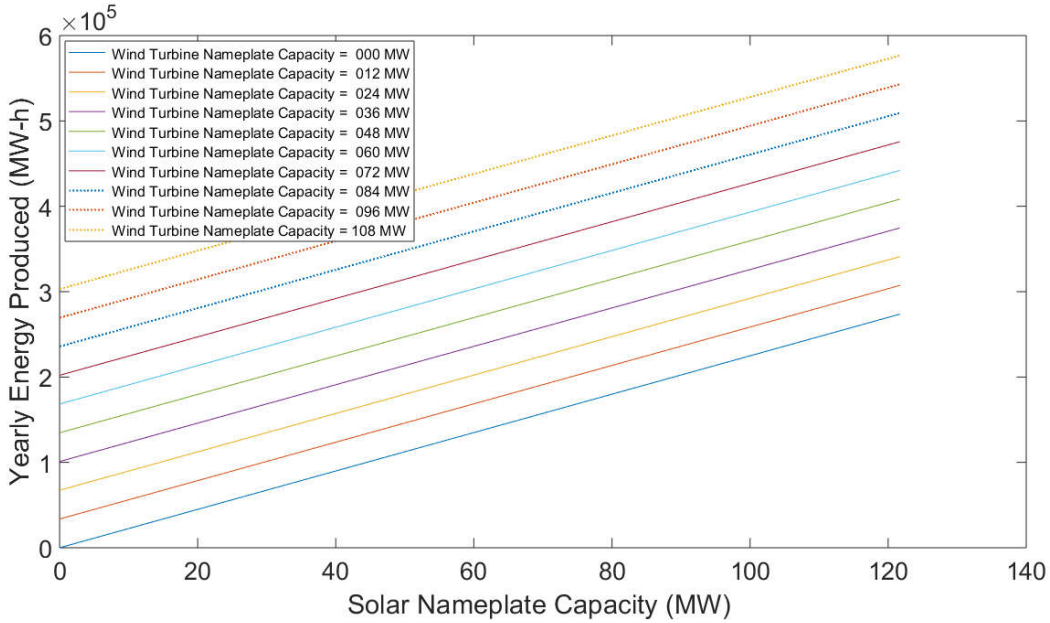

Figure 4.3: Yearly energy produced by different sizes of combined wind and solar installations located in Rio Vista, California.

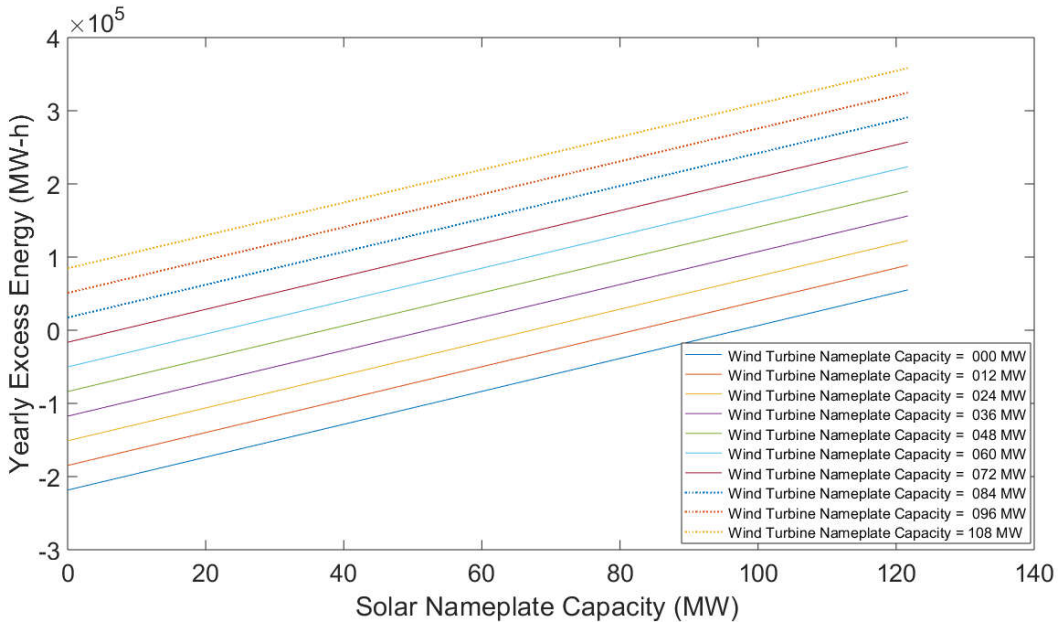

Figure 4.4: Yearly excess energy produced by different sizes of combined wind and solar installations located in Rio Vista, California.

4.2.4. Wind-Solar Farm Economics

4.2.4.1. Base Case

The net present cost of producing electricity for 25,000 homes located in Rio Vista, California for 25 years using various configurations of wind-solar farms using the economic values given in Table 4.1 are shown in Figure 4.5. The key point on this plot is where these costs reach a minimum value. This can be seen to occur with 24 MW of wind capacity and 25 MW of solar capacity. This configuration provides a minimum net present cost of electricity for 25,000 homes for 25 years of $149 million. The cost of supplying this electricity from the grid is $178 million. Thus, building a wind-solar farm in Rio Vista will save the community $29 million present day dollars. The other interesting result from this plot is the nearly equal wind and solar capacities required to obtain the minimum cost. This equal balance occurs even though savings of $17 million can be obtained with a pure wind farm of 36 MW and $17 million of savings can be obtained with a pure solar farm of 27 MW. This shows that a combined wind-solar farm is better than wind alone or solar alone. The combination helps to reduce the intermittency cost associated with wind alone or solar alone.

Detailed hourly power generated by the minimum cost wind-solar farm determined from the results presented in Figure 4.5 are given in Figure 4.6. For this same wind-solar farm, hourly excess power generated is given in Figure 4.7. Figure 4.6 clearly shows that the combined wind-solar farm is generating significantly more electrical power in the summer than the winter. This is desirable to meet the summer air conditioning loads. Summer power generation peaks at 47 MW due to high wind and solar resources. The excess power plot shows that the summer demands are being met better than winter demands. It appears that the minimum cost wind and solar capacities is obtained by sizing the wind-solar farm to meet summer demands. This means that electric power has to be purchased from the grid for many hours during the year. For Rio Vista, most of this purchasing is being done in the wintertime with the larger summer demands being met to a greater extent by the increased wind and solar resource in the summer.

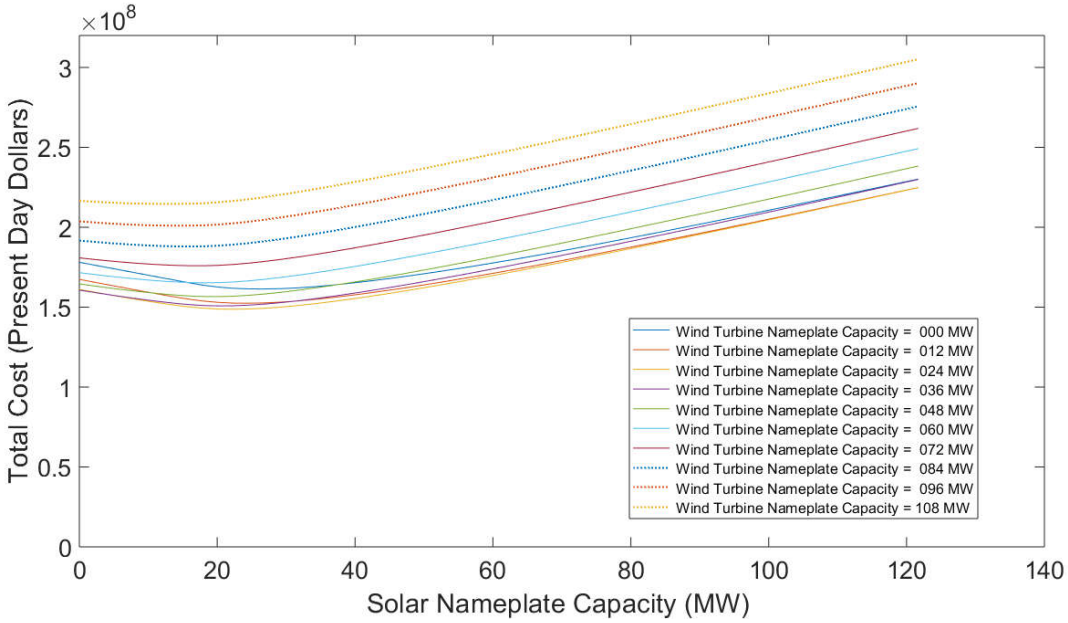

Figure 4.5: Yearly net present cost of energy for different sizes of combined wind and solar installations located in Rio Vista, California using $1300 per kW nameplate capacity for wind, $1000 per kW nameplate capacity for solar, and an industrial electricity price of $0.0898 per kW-h for purchasing electricity to cover energy deficits.

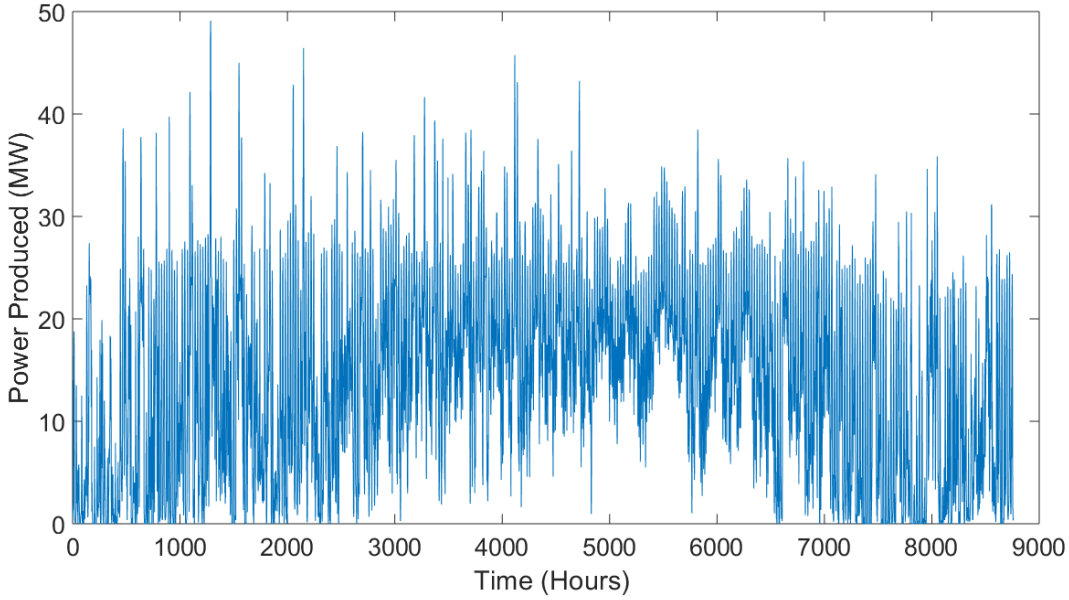

Figure 4.6: Power produced by a 24 MW nameplate capacity wind and 25 MW nameplate capacity solar installation located in Rio Vista, California. This combined wind and solar installation provides the minimum cost of energy and is the lowest plotted value in Figure 4.5.

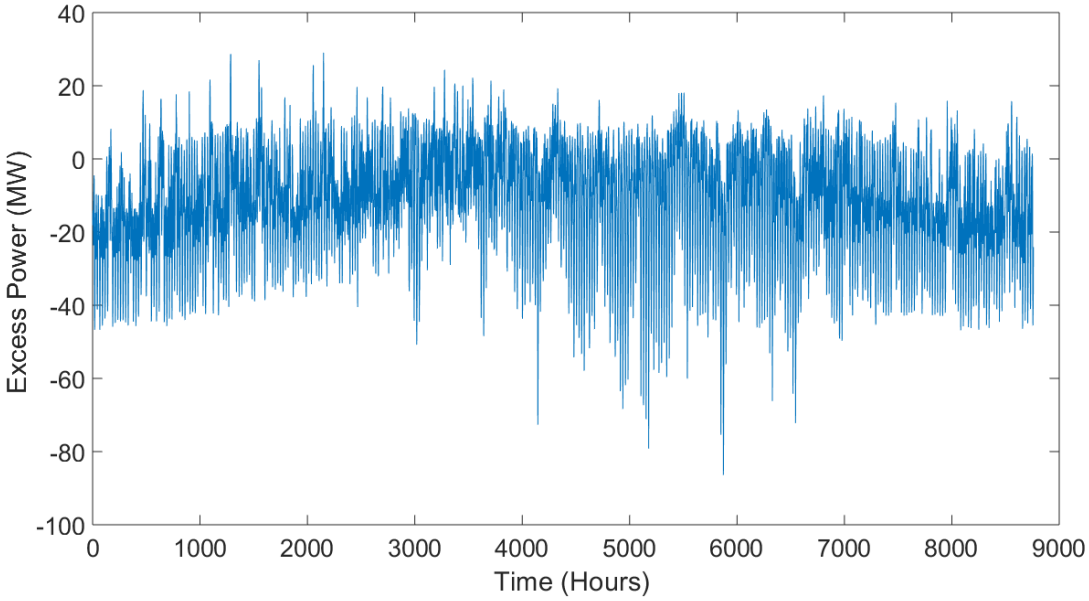

Figure 4.7: Excess power produced by a 24 MW nameplate capacity wind and 25 MW nameplate capacity solar installation located in Rio Vista, California. This combined wind and solar installation provides the minimum cost of energy and is the lowest plotted value in Figure 4.5.

4.2.4.2. Electricity Sold Back to Grid

The results in this section are different from the base case results because electrical energy is sold back to the grid. So that an optimization between wind and solar sizes is still obtained, electrical energy is sold back to the gird at half the price it is bought from the grid. For Rio Vista, excess wind-solar farm produced electricity is sold back to the grid at $0.0449 per kW-h. There are three graphs presented in this sub-subsection: Figure 4.8 shows the present day costs of supplying power to 25,000 homes for one year, Figure 4.9 shows the hourly power produced at the minimum cost point in Figure 4.8, and Figure 4.10 shows the excess power produced at the minimum cost point. Figure 4.9 corresponds to Figure 4.5 for the base case, Figure 4.10 corresponds to Figure 4.6, and Figure 4.11 corresponds to Figure 4.7. Figures 4.3 and Figures 4.4 for the base case which show the yearly energy produced and yearly excess energy for different sizes of wind-solar farms still applies, the only difference here is the excess energy is sold back to the gird.

Figure 4.8 shows that selling electricity back to the grid moves the minimum cost point to 60 MW of wind capacity and 52 MW of solar capacity. This results in a minimum cost of $134 million. This compares to 24 MW of wind capacity and 25 MW of solar capacity with a minimum cost of $149 million for the base case. Thus, selling excess electrical energy produced back to the grid in Rio Vista will save the community 44 million present day dollars. Selling power drops the cost of providing 25 years of electricity by $15 million when compared to base case. Selling power noticeably increases the wind capacity and the solar capacity. This trend indicates that the levelized cost of wind produced electricity is lower than the levelized cost of solar produced electricity for Rio Vista. These optimum sizes for minimum cost also indicate that the levelized cost of wind and solar are higher than $0.0449 for the conditions used in this analysis. It is also interesting to note that steepness of the curves to the left of the minimum cost point relative to the steepness of the curves to the right of the minimum cost point. This behavior has flipped from the base case. Selling excess electricity to the grid has made larger wind and solar capacities more economically attractive.

Figure 4.9 shows that the ability to sell power to the grid increases the excess electricity produced overall, of course all of this excess is sold. At 60 MW of wind capacity and 52 MW of solar capacity the yearly excess electricity produced is 1.25×10^5 MW-h. There is still a net yearly

deficit, but it is not as large as the deficit seen for the base case which has an excess of 5.89×10^4 MW-h.

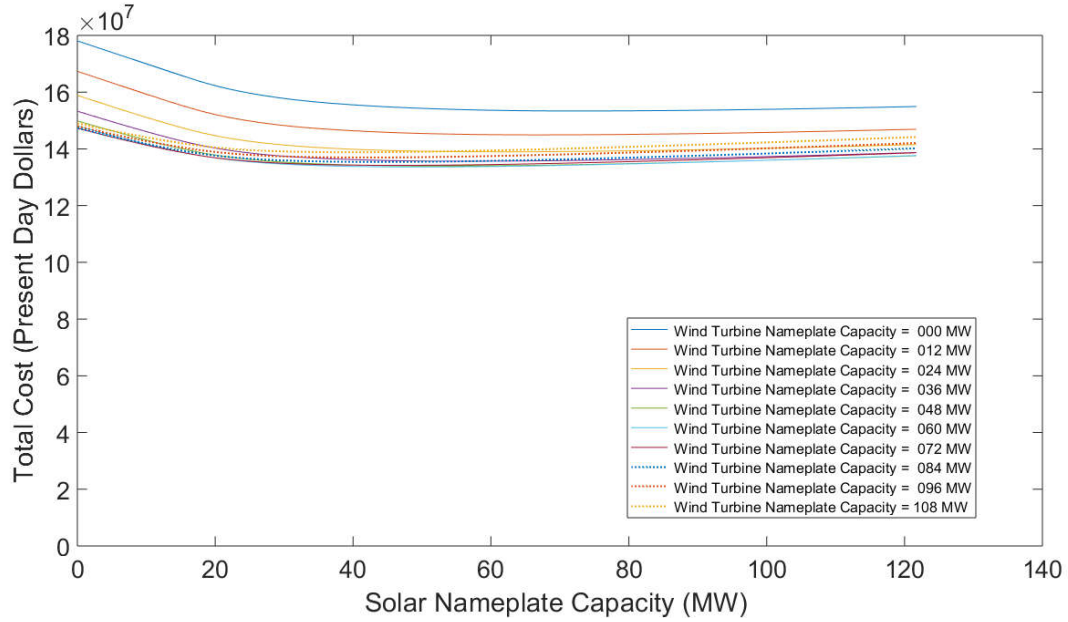

Figure 4.8: Yearly net present cost of energy for different sizes of combined wind and solar installations located in Rio Vista, California using $1300 per kW nameplate capacity for wind, $1000 per kW nameplate capacity for solar, an industrial electricity price of $0.0898 per kW-h for purchasing electricity to cover energy deficits, and a selling price of $0.0449 per kW-hr for excess electricity generated.

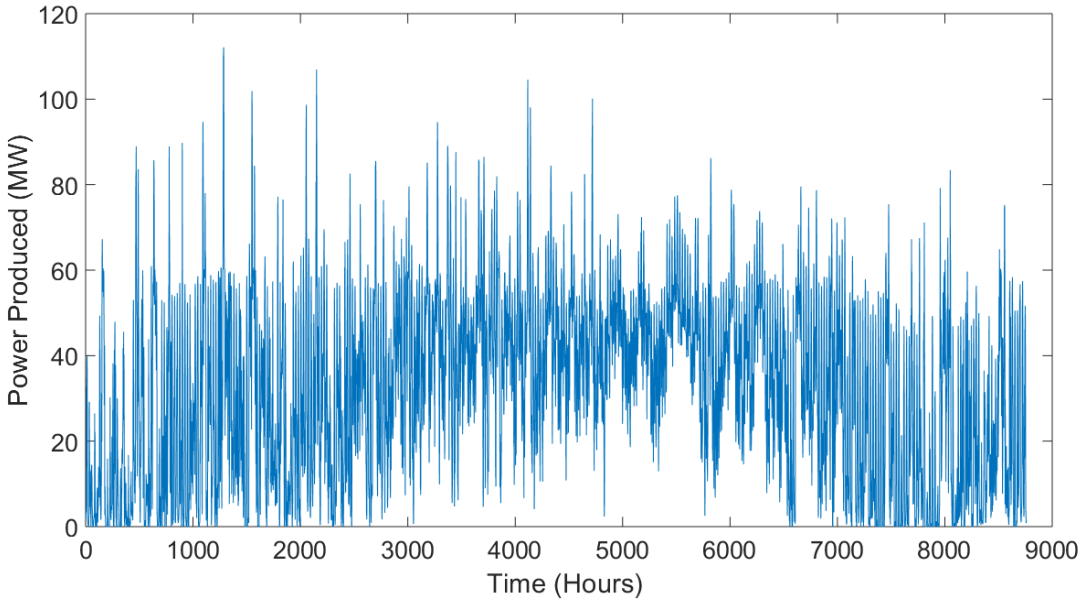

Figure 4.9: Power produced by a 60 MW nameplate capacity wind and 52 MW nameplate capacity solar installation located in Rio Vista, California. This combined wind and solar installation provides the minimum cost of energy and is the lowest plotted value in Figure 4.8

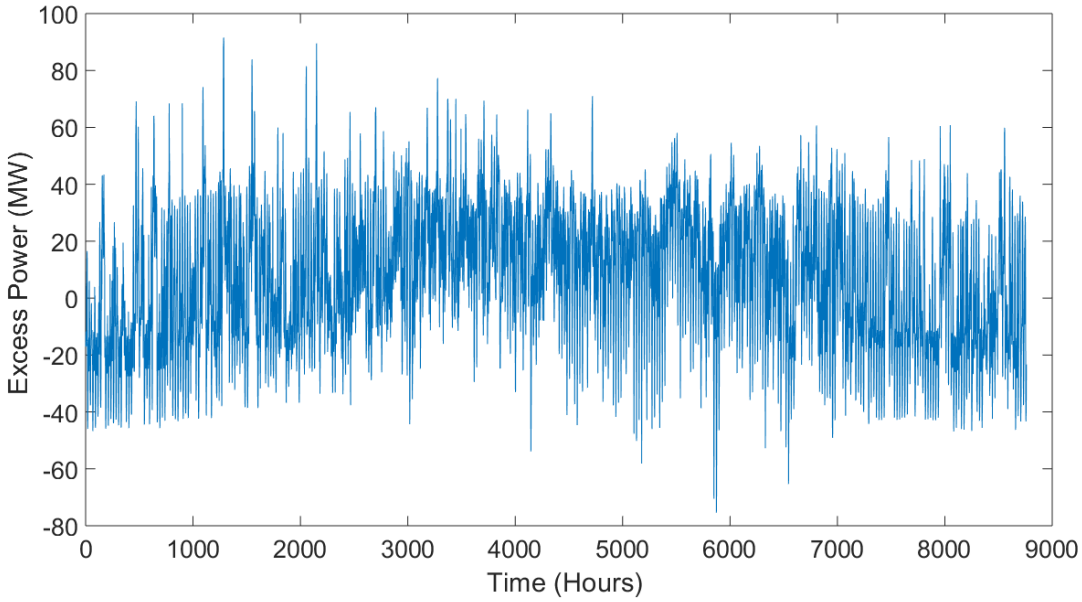

Figure 4.10: Excess power produced by a 60 MW nameplate capacity wind and 52 MW nameplate capacity solar installation located in Rio Vista, California. This combined wind and solar installation provides the minimum cost of energy and is the lowest plotted value in Figure 4.8.

4.2.4.3. Commercial Price of Electricity

In this sub-subsection, base case inputs shown in Table 4.1 replace the industrial cost to purchase electricity with the higher commercial cost. This makes a wind-solar farm more attractive economically. In the base, the cost used to buy electricity from the grid was $0.0898 per kw-h, in this case it is $0.1408 per kW-h. It is typical for commercial electricity rates to be more than industrial rates. Making this alteration to the inputs produces the results shown in Figure 4.11. Using commercial rates causes the lowest cost point to move to 36 MW nameplate capacity of wind and 29 MW name plate capacity of solar, providing a minimum cost of $194 million. This compares to 24 MW of wind capacity and 25 MW of solar capacity with a minimum cost of $149 million for the base case. All three of these numbers increase because the cost to cover demand increases. It must be recognized that the cost of using a grid only supply of electricity has increased to $279 million. This is one of the higher costs shown in Figure 4.11. Obviously as the cost of grid power increases, the benefits of using wind and solar increase. It is interesting that the wind capacity increased by 50% while the solar capacity increased by only 16% from the base case. The total cost of power increased by $46 million when compared to the base case. When commercial

electricity rates are in effect, the total savings garnered by using wind and solar compared to buying all electricity from the grid is $85 million.

The hourly power generated by the minimum cost configuration of a wind-solar farm is plotted in Figure 4.12 and hourly excess power generated by the minimum cost configuration of a wind-solar farm is plotted in Figure 4.13. Both Figure 4.12 and Figure 4.13 have similar shapes to Figure 4.6 and Figure 4.7, respectively. The difference between these two cases is magnitude, the commercial cost case having larger wind-solar farm electricity generation, and thus more excess power, than the base case. The higher amount of electrical power that is wasted in the commercial power case over the base case is justified by reducing the amount of grid power that needs to be purchased by 36.2% compared to the base case, as the commercial price is significantly higher than the industrial purchase price.

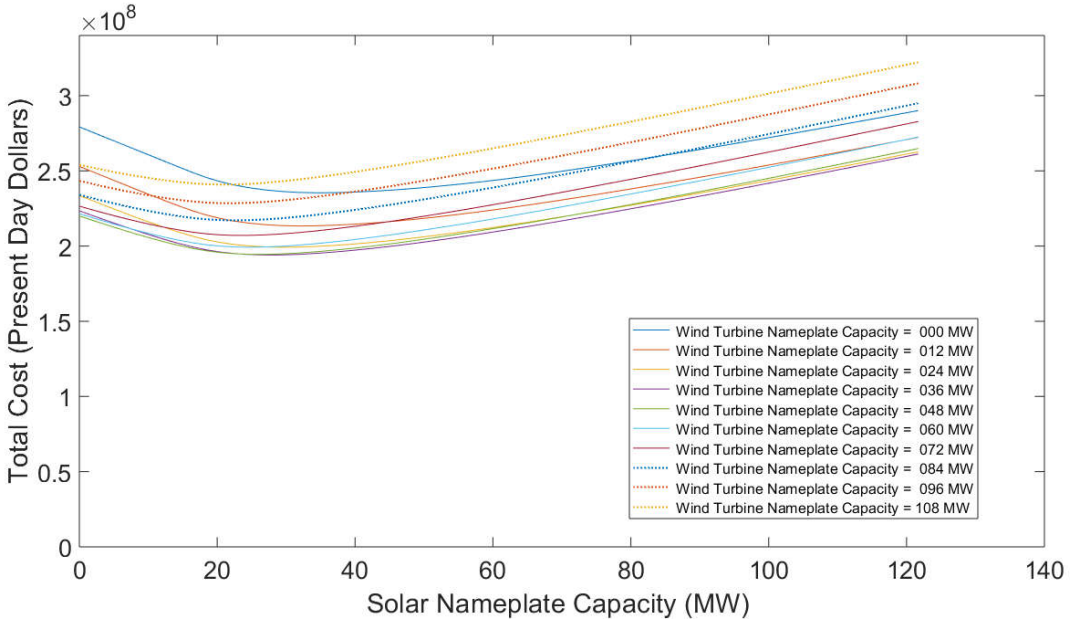

Figure 4.11: Yearly net present cost of energy for different sizes of combined wind and solar installations located in Rio Vista, California using $1300 per kW nameplate capacity for wind, $1000 per kW nameplate capacity for solar, and a commercial electricity price of $0.1408 per kW-h for purchasing electricity to cover energy deficits.

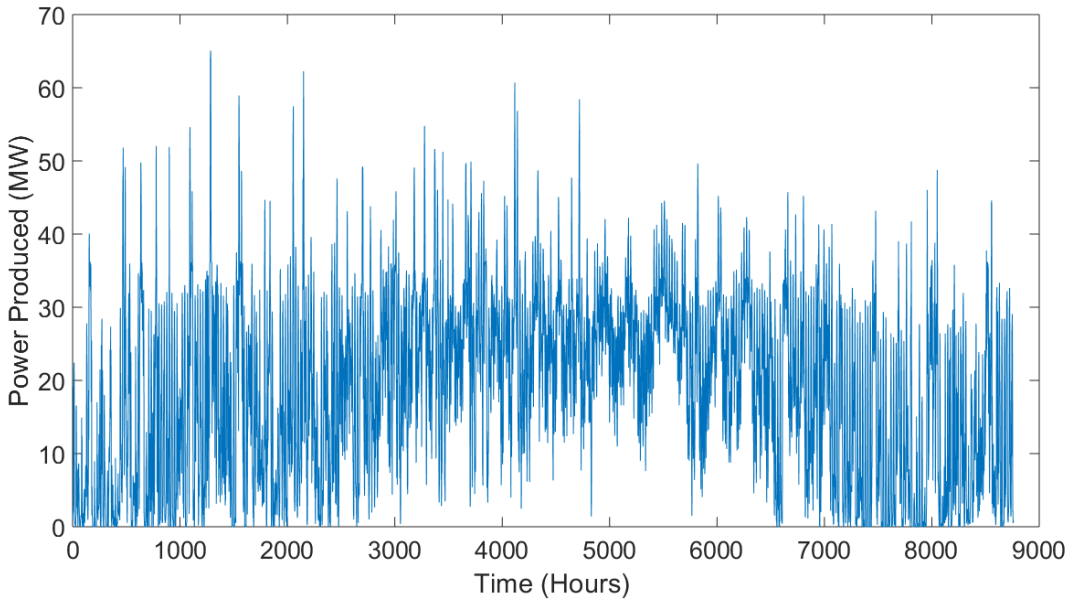

Figure 4.12: Power produced by a 36 MW nameplate capacity wind and 29 MW nameplate capacity solar installation located in Rio Vista, California. This combined wind and solar installation provides the minimum cost of energy and is the lowest plotted value in Figure 4.11

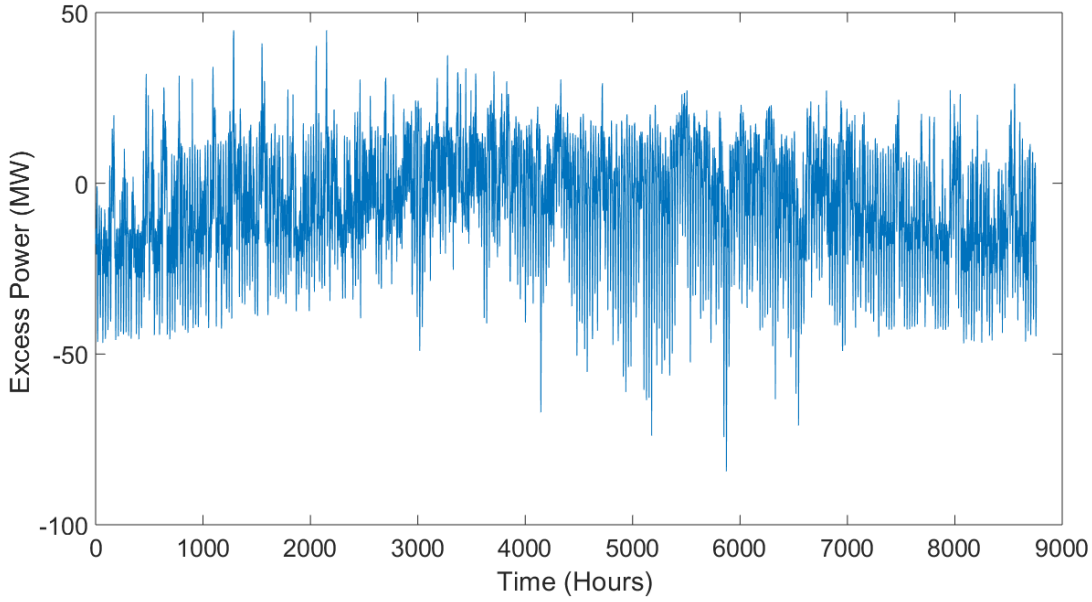

Figure 4.13: Excess power produced by a 36 MW nameplate capacity wind and 29 MW nameplate capacity solar installation located in Rio Vista, California. This combined wind and solar installation provides the minimum cost of energy and is the lowest plotted value in Figure 4.11.

4.2.4.4. Capital Costs Increased by 50 Percent

In this case, the costs for installing wind and solar equipment are increased by fifty percent. The cost to install wind is now $1950 per kW nameplate capacity and the cost to install solar is $1500 per kW nameplate capacity. Even at these increased capital costs some wind and solar is still the lowest cost option. The lowest cost point is for 12 MW nameplate capacity of wind and 20 MW nameplate capacity of solar. This results in a minimum cost of $171 million. This is below the $178 million to directly buy power from the grid. This minimum cost point is inflated from the base case cost of $149 million. Thus, building a wind-solar farm in Rio Vista with a 50 percent increase in installation prices will save the community $7 million present day dollars when compared to purchasing power from grid.

The hourly power generated by the minimum cost wind-solar farm is shown in Figure 4.15 and the hourly excess power generated is shown in Figure 4.16. Figure 4.16 shows that positive excess power generated is rare. Most excess power is generated in the spring and summer. The higher costs of capital used in this case drive the minimum cost point to a smaller capital installation, and thus more deficit power.

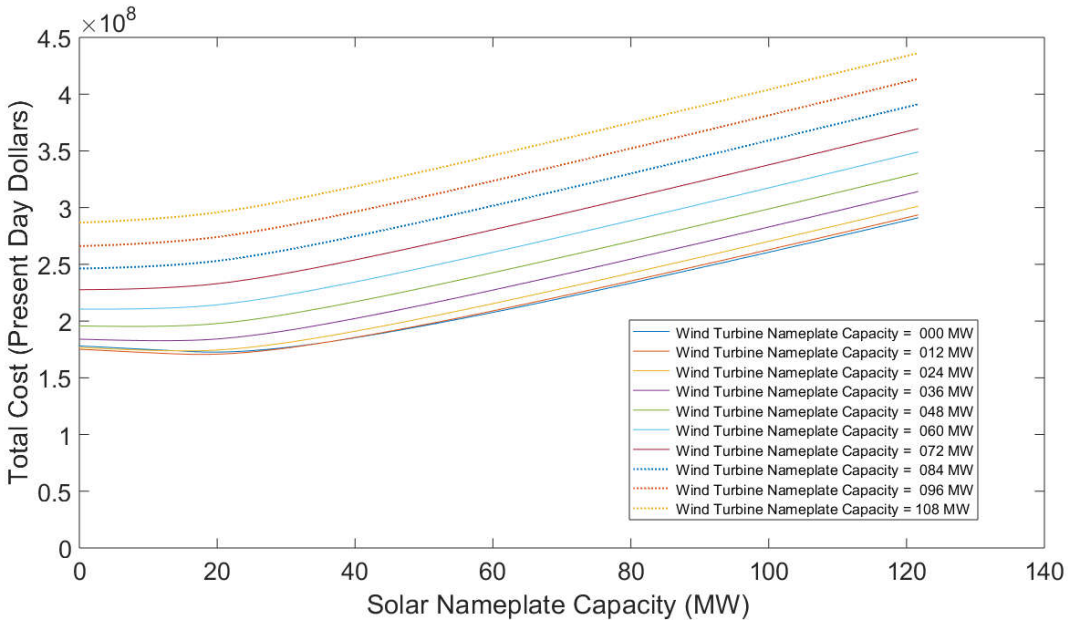

Figure 4.14: Yearly net present cost of energy for different sizes of combined wind and solar installations located in Rio Vista, California using $1950 per kW nameplate capacity for wind, $1500 per kW nameplate capacity for solar, and an industrial electricity price of $0.0898 per kW-h for purchasing electricity to cover energy deficits.

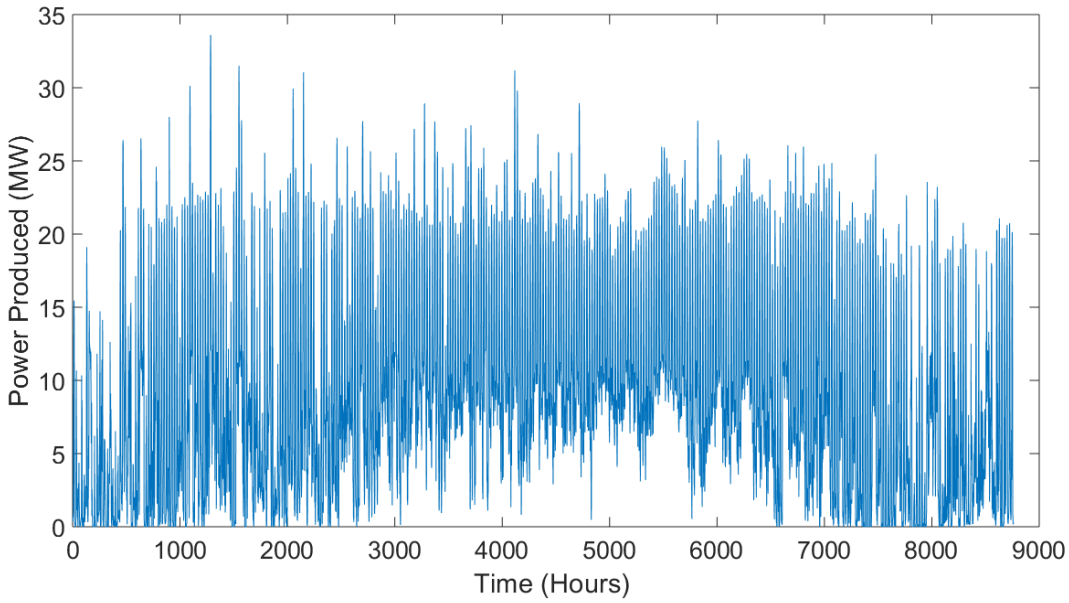

Figure 4.15: Power produced by a 12 MW nameplate capacity wind and 20 MW nameplate capacity solar installation located in Rio Vista, California. This combined wind and solar installation provides the minimum cost of energy and is the lowest plotted value in Figure 4.14.

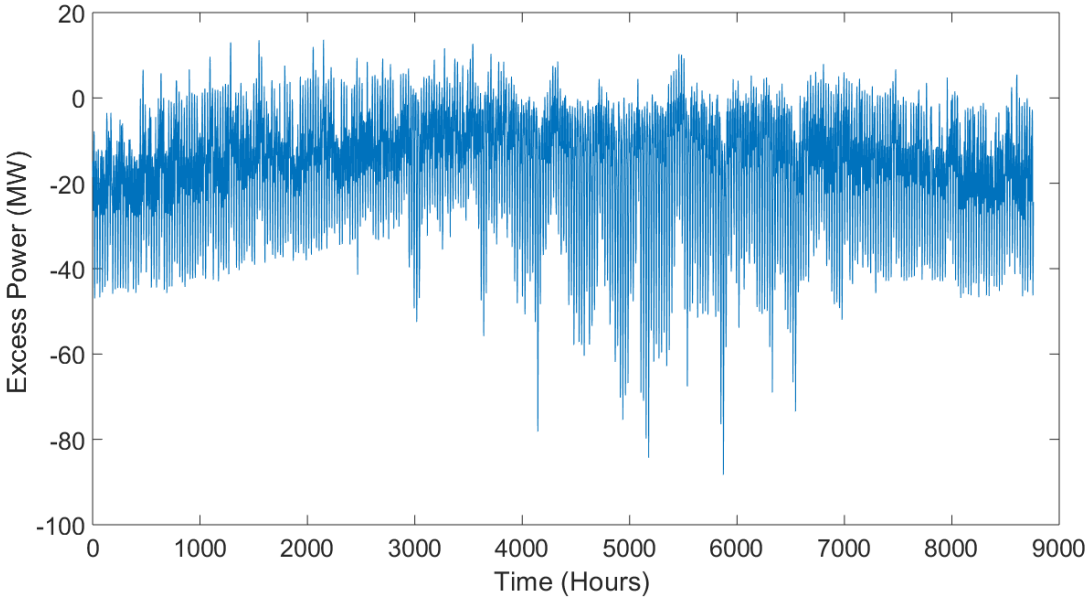

Figure 4.16: Excess power produced by a 12 MW nameplate capacity wind and 20 MW nameplate capacity solar installation located in Rio Vista, California. This combined wind and solar installation provides the minimum cost of energy and is the lowest plotted value in Figure 4.14.

4.2.4.5. Capital Costs Decreased by 50 Percent

In this case, capital costs for installing wind turbines and solar panels is decreased by fifty percent to $650 per kW nameplate capacity for wind and $500 per kW nameplate capacity for solar. Figure 4.17 shows that the minimum cost installation nameplate capacities are 48 MW for wind and 32 MW for solar. The minimum present-day cost for 25 years of electricity is $113 million. This is a reduction of $36 million from the base case minimum cost and a reduction of $65 million compared to buying all electricity from the grid.

Because of the lower cost of capital in this case, Figure 4.17 shows more electrical energy being produced by the minimum cost wind-solar farm as compared to the minimum cost base case wind-solar farm in Figure 4.6. More energy being produced for the same demand drives the production of more excess power as shown in Figure 4.19. At these low capital rates, it is advantageous to cover more of the demand, even if this means more electricity is wasted.

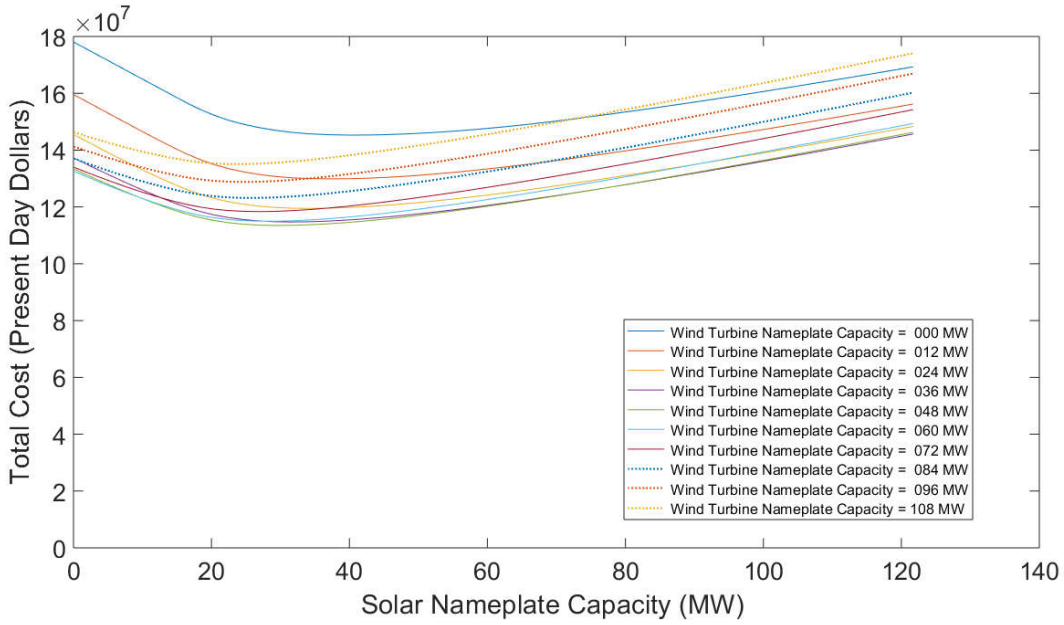

Figure 4.17: Yearly net present cost of energy for different sizes of combined wind and solar installations located in Rio Vista, California using $650 per kW nameplate capacity for wind, $500 per kW nameplate capacity for solar, and an industrial electricity price of $0.0898 per kW-h for purchasing electricity to cover energy deficits.

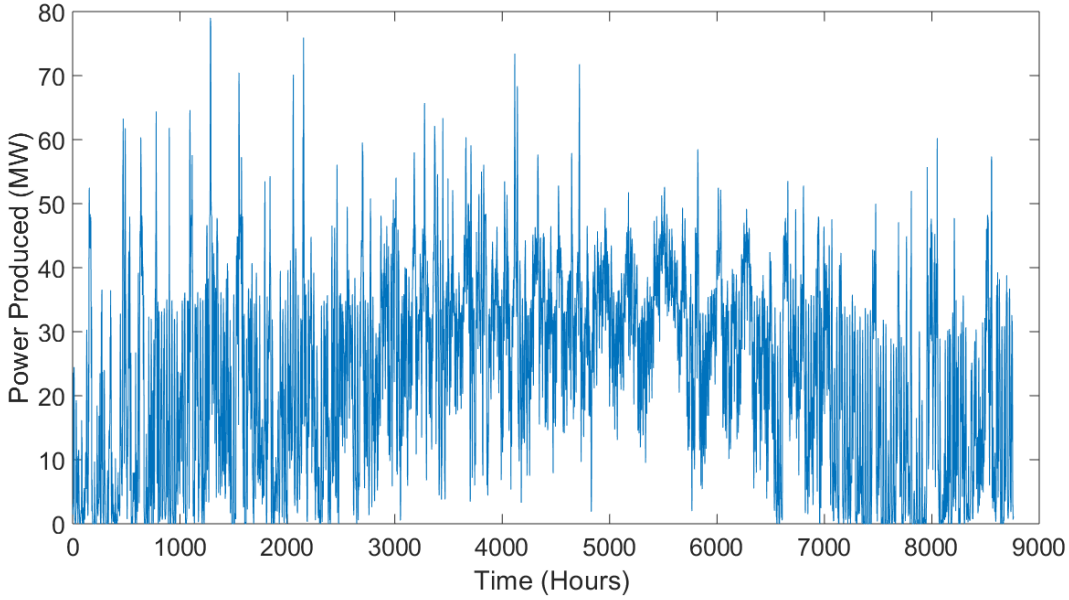

Figure 4.18: Power produced by a 48 MW nameplate capacity wind and 32 MW nameplate capacity solar installation located in Rio Vista, California. This combined wind and solar installation provides the minimum cost of energy and is the lowest plotted value in Figure 4.17.

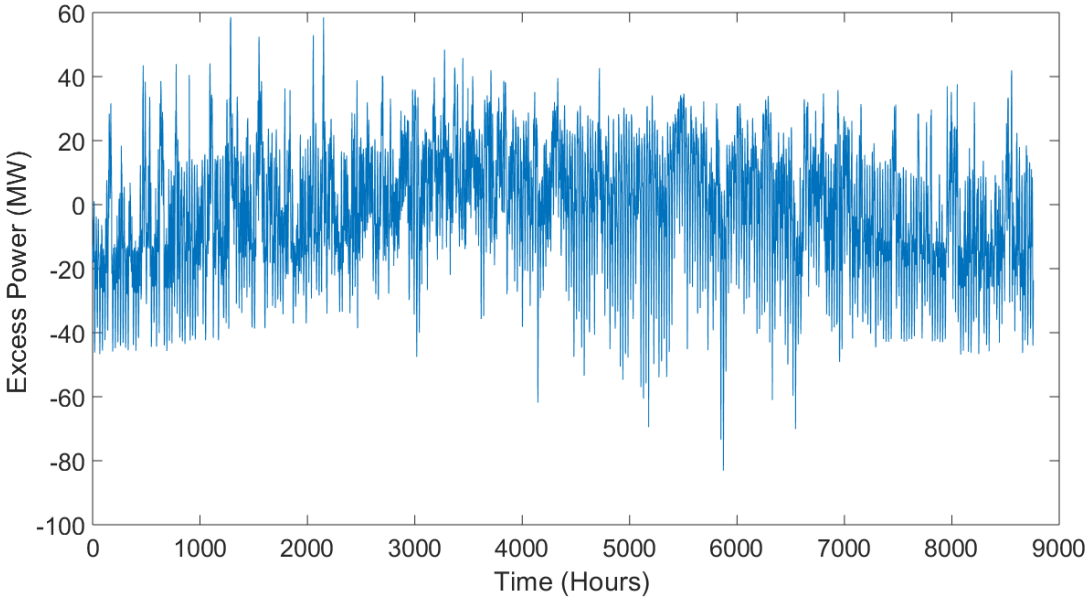

Figure 4.19: Excess power produced by a 48 MW nameplate capacity wind and 32 MW nameplate capacity solar installation located in Rio Vista, California. This combined wind and solar installation provides the minimum cost of energy and is the lowest plotted value in Figure 4.17.

4.3. Dallas, Texas

4.3.1. Electricity Demand

The electricity demand shown in Figure 4.20 for Dallas, Texas is very different from the electricity demand for Rio Vista, California shown in Figure 4.1. Immediately obvious is the much larger demands seen in the winter. This is due to electrical heating that is probably pure resistance heating. While these heating demands are large, they tend to occur on isolated days in December, January, February, and early March. The electricity load for Dallas ranges between 16 MW to 150 MW with peaks in the winter up to 196 MW. The total electricity demand for one year is 431,851 MW-h.

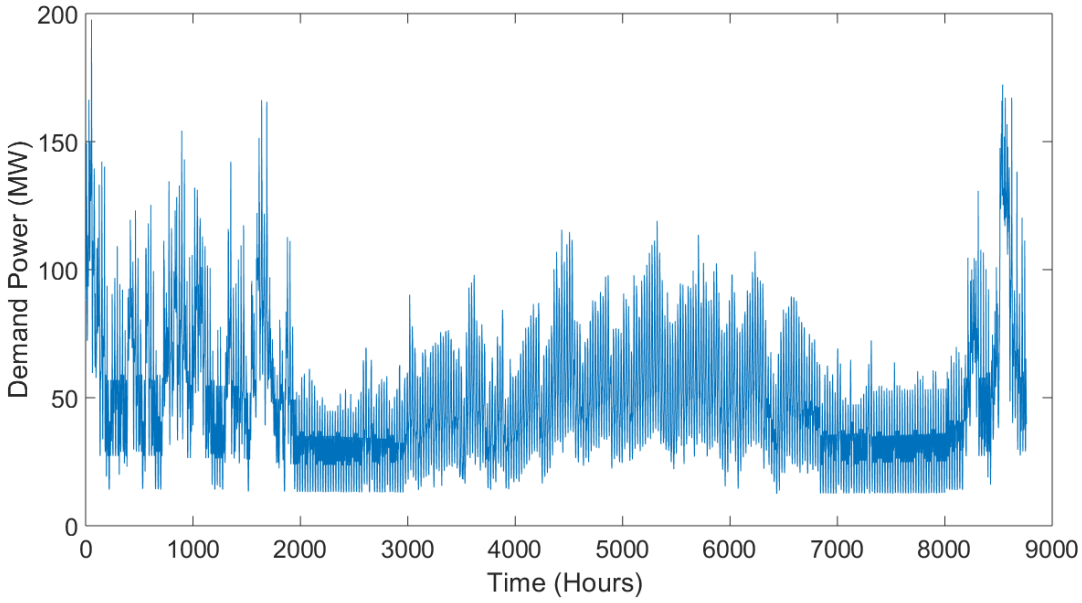

Figure 4.20: Electricity demand for 25000 typical homes located in Dallas, Texas.

4.3.2. Wind and Solar Resources

The wind and solar resources available in Dallas, Texas are shown in Figure 4.21. The solar energy resource is for a panel tilted at the latitude of Dallas. The wind power available in Dallas is at a height of 84 meters. When the wind resource is integrated over one-year, a value of 2.53 MW-h/m^2 is obtained; and when the solar resource is integrated over one year a value of 1.90 MW-h/m^2 is obtained. The combined resources provide 4.43 MW-h/m^2 for one year. Both the wind and solar yearly resources are smaller in Dallas, Texas than Rio Vista, California.

When making comparisons between the wind resource in Dallas, Texas (Figure 4.21) and the wind resource in Rio Vista, California (Figure 4.2) you need to watch the scale difference. Dallas has a maximum *y*-value of 0.008 MW/m^2 and Rio Vista has a maximum *y*-value of 0.006 MW/m^2. Keeping this in mind, it can be seen that the wind gusts in Dallas are larger than Rio Vista. However, the yearly wind resource in Dallas is less than that in Rio Vista. Overall it appears that Dallas has wind and solar distributions that are more similar during the winter and summer than Rio Vista.

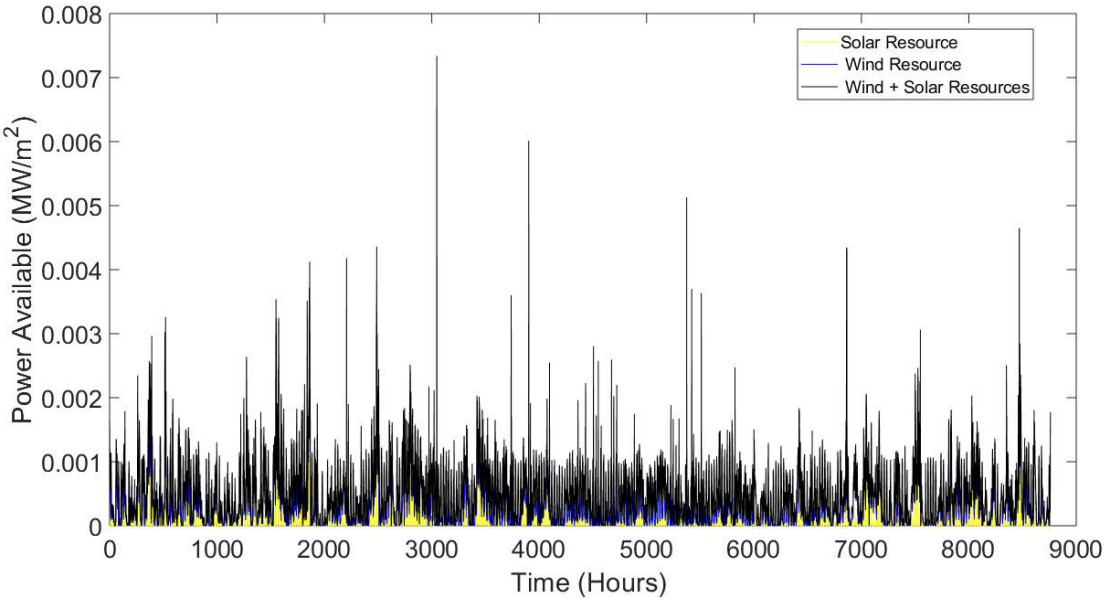

Figure 4.21: Wind and solar resource power densities for Dallas, Texas.

4.3.3. Wind-Solar Farm Electricity Production

Yearly energy produced by various configurations of wind-solar farms in Dallas, Texas has been plotted in Figure 4.22 and total excess energy produced by the configurations of wind-solar farms for an entire year has been plotted in Figure 4.23. Annual total energy generated for various configurations ranges from 0 to 4.4 x 10^5 MW-h. It is interesting to note that this maximum annual energy generation is 23% less than that in Rio Vista, California. The annual excess energy generated ranges from -4.3x10^5 MW-h to 0.06x10^5 MW-h. The same range of wind capacities and solar capacities were considered for both Dallas, Texas and Rio Vista, California, but Dallas, Texas cannot produce net positive electricity over the course of a year for most wind-solar farm sizes simulated. This is mostly due to the large electrical demands required in Dallas as compared to

Rio Vista. This can be seen by comparing Figure 4.20 to Figure 4.1 and realizing that Dallas' yearly electrical demand is 98% larger than Rio Vista's.

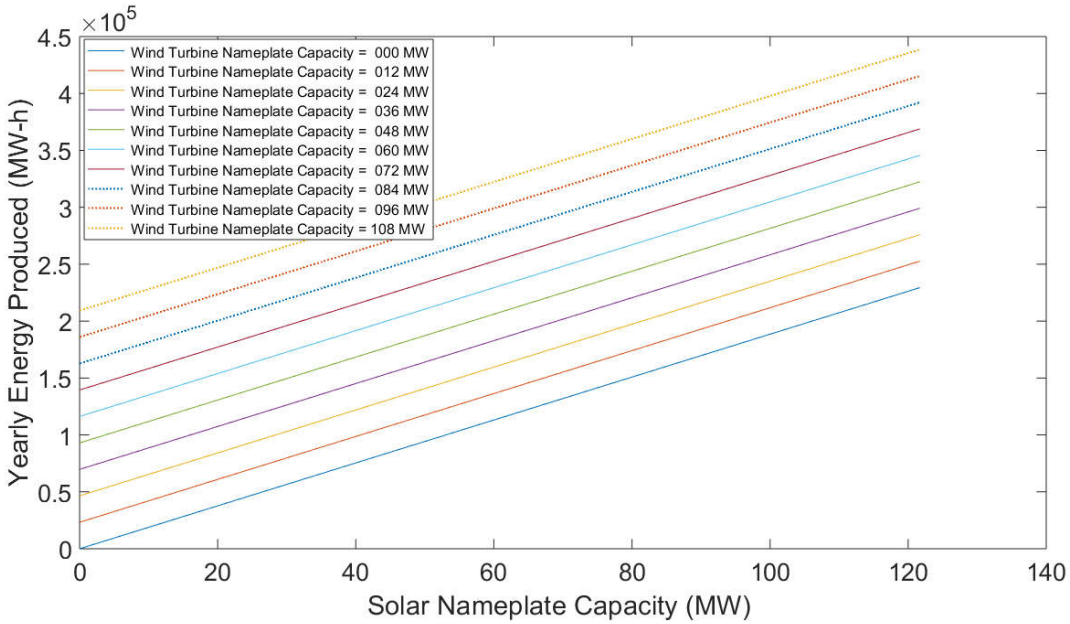

Figure 4.22: Yearly energy produced by different sizes of combined wind and solar installations located in Dallas, Texas.

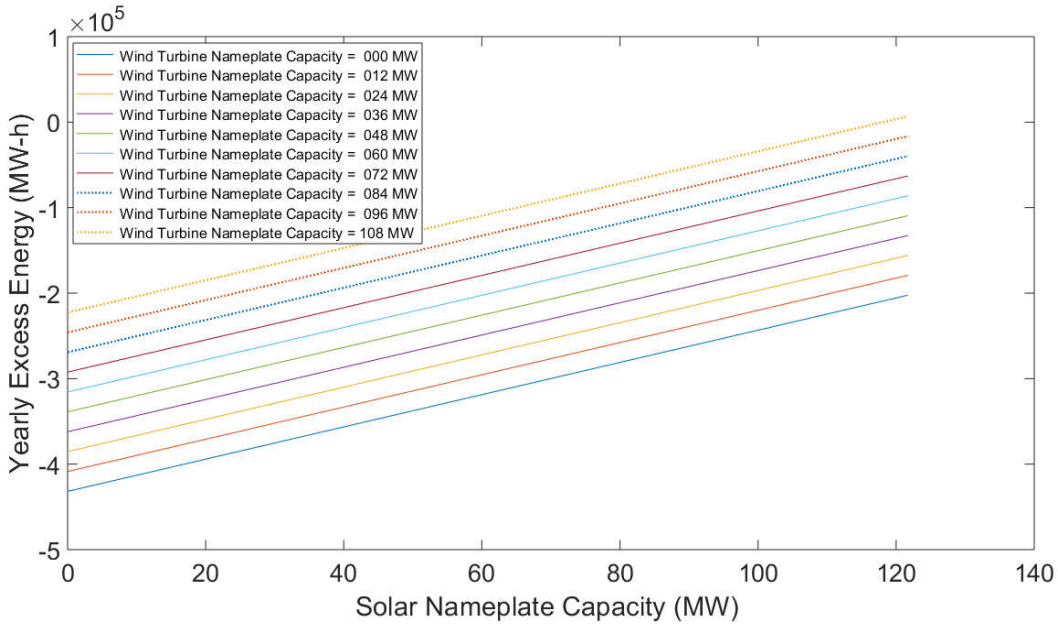

Figure 4.23: Yearly excess energy produced by different sizes of combined wind and solar installations located in Dallas, Texas.

4.3.4. Wind-Solar Farm Economics

4.3.4.1. Base Case

Costs for producing power for 25 years with different sized wind-solar farms in Dallas, Texas is shown Figure 4.24. This curve has no minimum for any sized wind-solar farm. The minimum occurs when there is no wind and no solar. This results in a present-day cost for 25 years of electrical energy of $218 million. Because the minimum cost point is at 0 MW of wind capacity and 0 MW of solar capacity, no figures are shown for the hourly energy produced or the hourly excess energy. The hourly energy produced is simply a horizontal line at zero production. The excess power produced is simply an inversion of the demand curve shown in Figure 4.20.

The primary reason why wind and solar are not cost effective under base case conditions in Dallas, Texas is the low cost of grid electricity. The cost of gird electricity in Dallas is $0.0557 kW-h. This is 38% below the $0.0898 cost of grid generated electricity in Rio Vista, California. The bend in the curves in Figure 4.24 close to the vertical axis indicate that a minimum is getting close. The Capital Costs Decreased by 50% sub-subsection below shows that decreasing the cost to purchase and install capital equipment makes wind-solar farms cost competitive in Dallas, Texas.

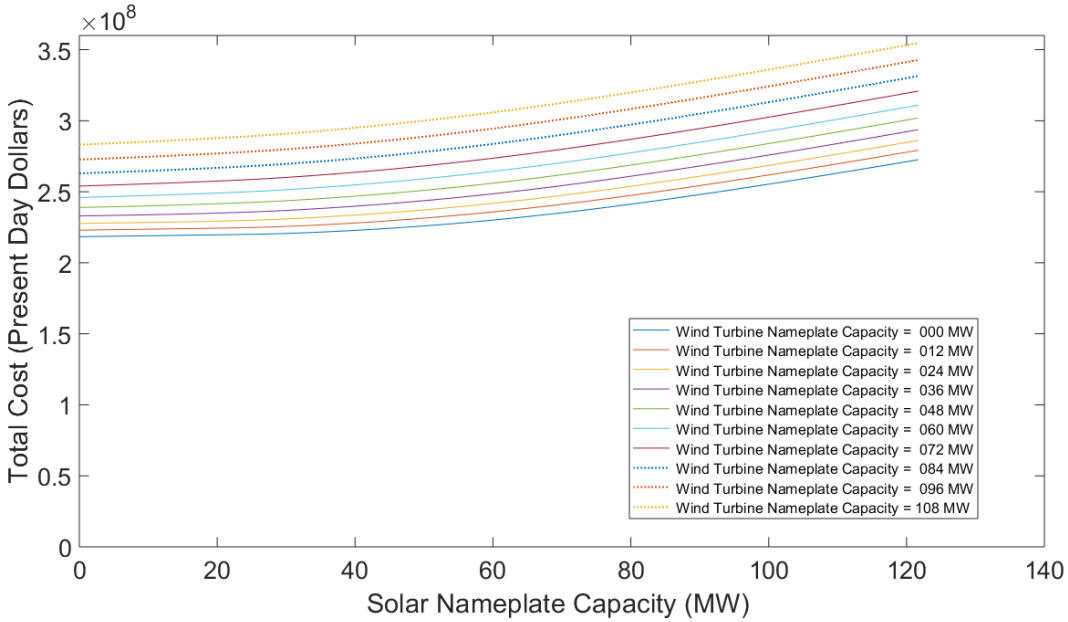

Figure 4.24: Yearly net present cost of energy for different sizes of combined wind and solar installations located in Dallas, Texas using $1300 per kW nameplate capacity for wind, $1000 per kW nameplate capacity for solar, and an industrial electricity price of $0.0557 per kW-h for purchasing electricity to cover energy deficits.

4.3.4.2. Electricity Sold Back to Grid

Figure 4.25 shows that using some wind and solar does not reduce the cost for 25 years of electricity when excess power is sold back to the grid at half the industrial rate, $0.02785 per kW-h. It is still cheaper to purchase all required electricity from the local grid. This curve has no minimum for any sized wind-solar farm. The minimum occurs when there is no wind and no solar. Because the minimum cost point is at 0 MW of wind capacity and 0 MW of solar capacity no figures are shown for the hourly power produced or the hourly excess power. The hourly energy produced is simply a horizontal line at zero production. The excess power produced is simply an inversion of the demand curve shown in Figure 4.20.

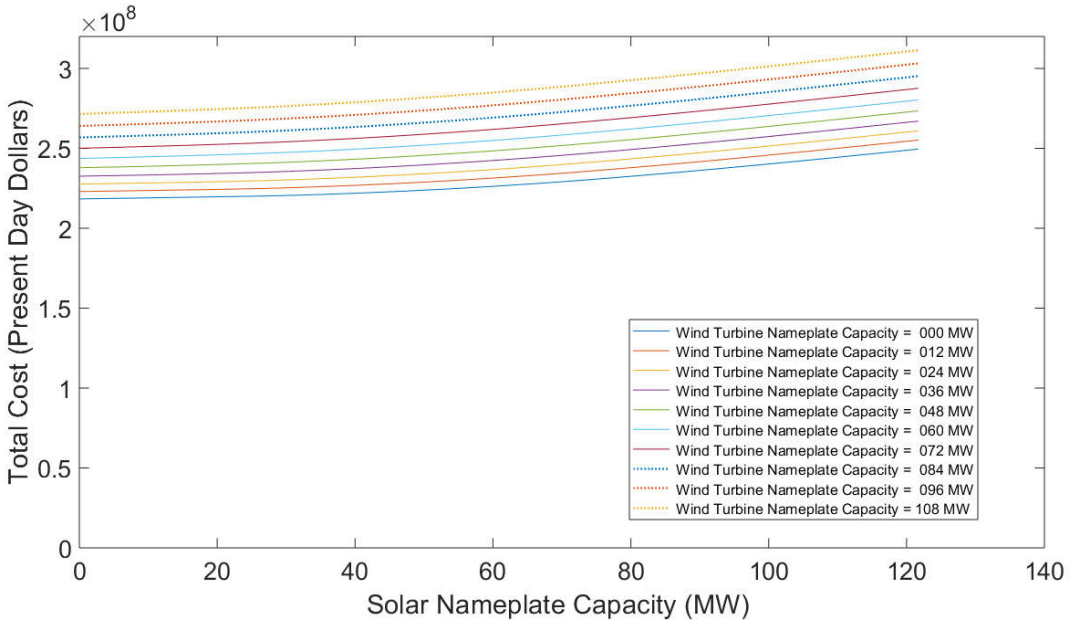

Figure 4.25: Yearly net present cost of energy for different sizes of combined wind and solar installations located in Dallas, Texas using $1300 per kW nameplate capacity for wind, $1000 per kW nameplate capacity for solar, an industrial electricity price of $0.0557 per kW-h for purchasing electricity to cover energy deficits, and a selling price of $0.02785 per kW-h for excess electricity generated.

4.3.4.3. Commercial Price of Electricity

Increasing the cost of grid electricity makes some solar capacity profitable, but wind capacity is not. Figure 4.26 shows that only solar capacity is cost competitive. A minimum now occurs at a wind nameplate capacity of 0 MW and solar nameplate capacity of 49 MW. The minimum cost of supplying 25 years of electricity with 49 MW of solar is $307 million. This is

much higher than the $194 million minimum found for the Rio Vista, California commercial electricity price. This is due to the larger demand in Dallas, as compared to Rio Vista.

This is a rather surprising result because the wind resource is better than the solar resource in Dallas, Texas. However, yearly integrated numbers do not show the match between the timing of the wind resource and the demand and the timing between the solar resource and the demand. It is believed that the solar resource must be better matched to the demand than the wind resource to have this result. This case is an example of where the intermittence of the solar resource is not helped by tapping the wind resource.

The detailed power production and detailed excess power production are given in Figure 4.27 and Figure 4.28, respectively. These graphs show larger power production and more excess power than Rio Vista, California. There are high amounts of power generated over the year, peaking at 56 MW. These plots show a relatively uniform power generation throughout the year, but excess power seems to peak in the spring and the fall when heating and cooling are low and deficit power peaks during the winter. The differences in the excess power curve in Dallas from the comparable curve in Rio Vista, California (Figure 4.13), is due to the different loads in the two locations and the different prices of grid electricity.

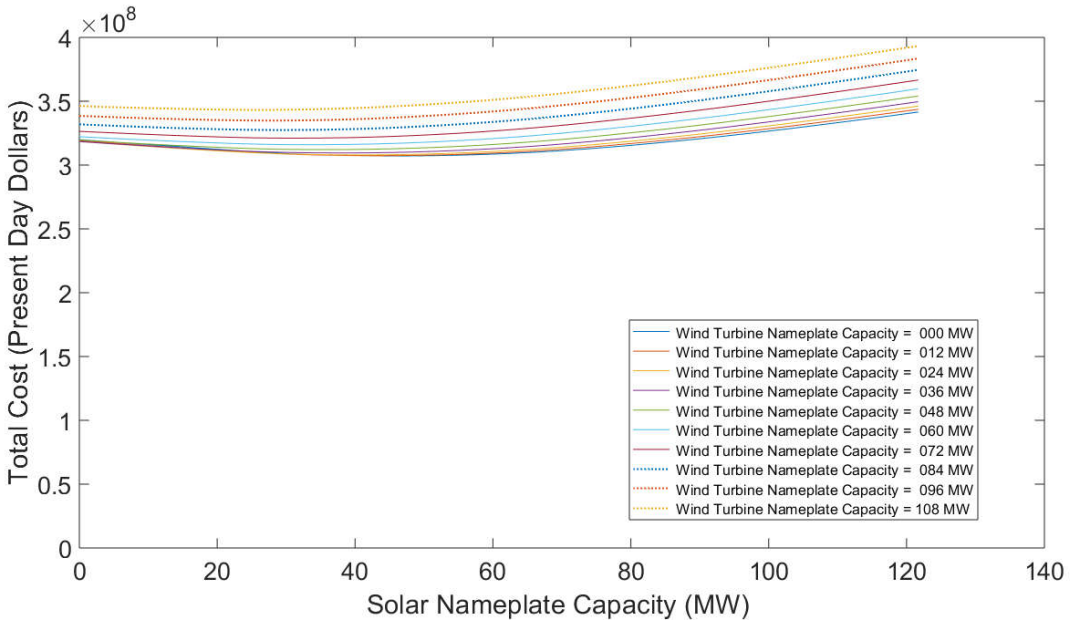

Figure 4.26: Yearly net present cost of energy for different sizes of combined wind and solar installations located in Dallas, Texas using $1300 per kW nameplate capacity for wind, $1000 per kW nameplate capacity for solar, and a commercial electricity price of $0.0816 per kW-h for purchasing electricity to cover energy deficits.

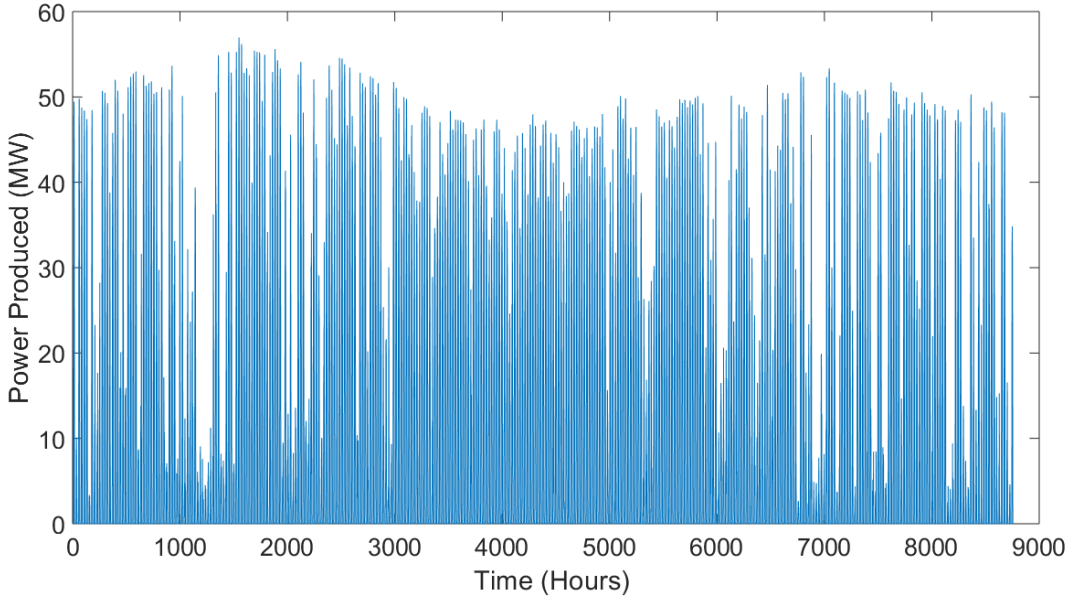

Figure 4.27: Power produced by a 0 MW nameplate capacity wind and 49 MW nameplate capacity solar installation located in Dallas, Texas. This combined wind and solar installation provides the minimum cost of energy and is the lowest plotted value in Figure 4.26.

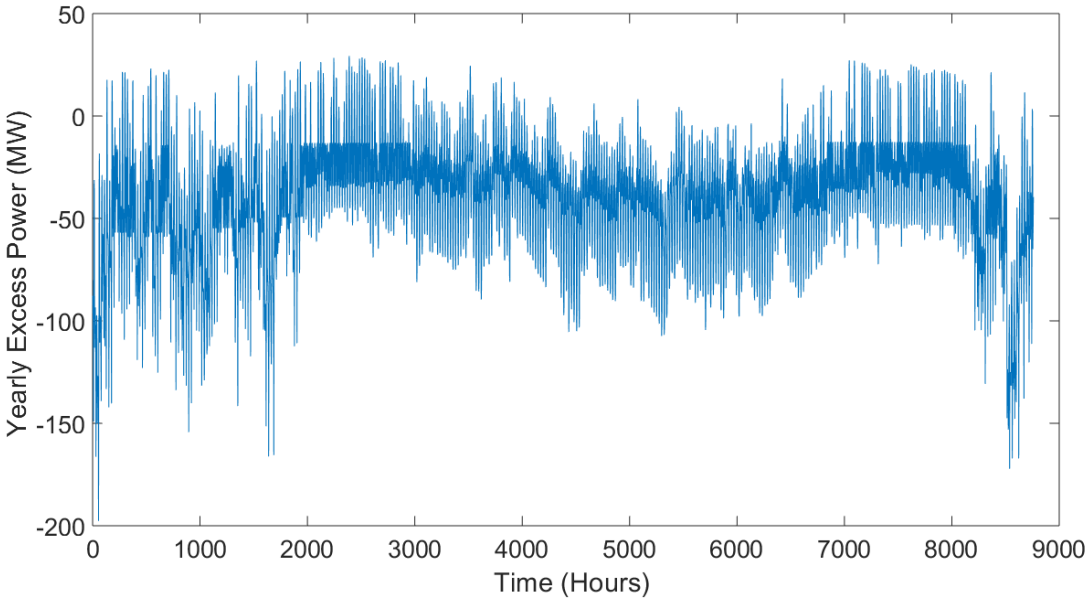

Figure 4.28: Excess power produced by a 0 MW nameplate capacity wind and 49 MW nameplate capacity solar installation located in Dallas, Texas. This combined wind and solar installation provides the minimum cost of energy and is the lowest plotted value in Figure 4.26.

4.3.4.4. Capital Costs Increased by 50 Percentage

Just like the base case shown in Figure 4.24, no minimum cost of energy is obtained when the cost of wind capacity is increased by 50% and the cost of solar capacity is increased by 50%. The yearly cost of energy for this case, for different capacities of wind and solar, is shown in Figure 4.29. The results on this plot show no signs of a minimum, even less so than the base case results. In fact, the slopes on these curves are steeper and the separation between the different capacity wind power curves are larger compared to the base case. These are results of the increased cost of wind and solar capacity. This means all electric demand is satisfied by grid purchased electricity and the present day cost of 25 years of electricity for this case remains the same as the base case at $218 million.

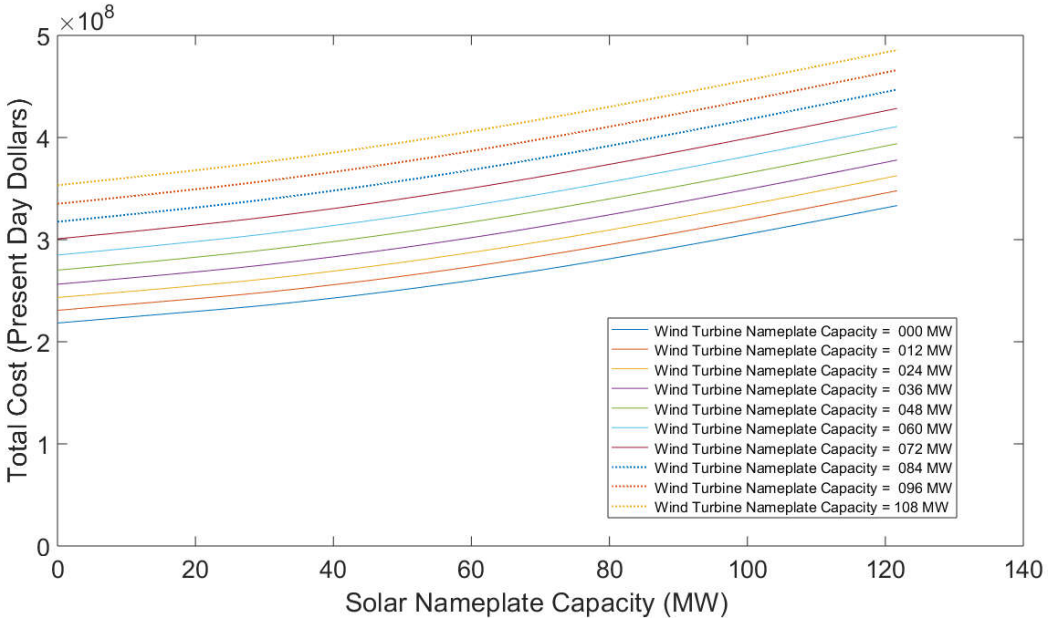

Figure 4.29: Yearly net present cost of energy for different sizes of combined wind and solar installations located in Dallas, Texas using $1950 per kW nameplate capacity for wind, $1500 per kW nameplate capacity for solar, an industrial electricity price of $0.0557 per kW-h for purchasing electricity to cover energy deficits.

4.3.4.5. Capital Costs Decreased by 50 Percent

As the base case yearly cost of energy plot shown in Figure 4.24 indicated, the cost of using a wind-solar farm was close to being less expensive than buying power from the grid, it is reasonable to expect a wind-solar farm to be cost competitive when the cost of wind turbines and solar panels is reduced. Thus, when capital cost are decreased by 50%, Dallas, Texas should show

wind and solar lowering the cost compared to buying all the required power from the electrical grid. This is exactly what Figure 4.30 shows. The minimum present day cost occurs when 48 MW of wind nameplate capacity is used, and 59 MW of solar nameplate capacity is used. These are larger wind and solar capacities than any of the Rio Vista, California cases and any of the other Dallas, Texas cases presented in this thesis. The present-day cost of 25 years of electricity using this size wind-solar farm is $195 million, saving $23 million compared to providing all electricity from the grid. While $23 million is a significant amount of money, this is not as much as the $65 million of savings obtained in Rio Vista, California for the comparable case. These reduced savings in Dallas, Texas are due to the much lower cost of grid purchased electricity.

Hourly power generated by the minimum cost configuration of a wind-solar farm in Dallas, Texas is given Figure 4.31 and the hourly excess-deficit power generated is given in Figure 4.32. There are high amounts of power generated for the least cost configuration peaking at 113 MW. It is interesting that positive excess power occurs in the spring and fall and negative excess powers occur in the winter and summer. This is a different behavior than seen in Rio Vista, California.

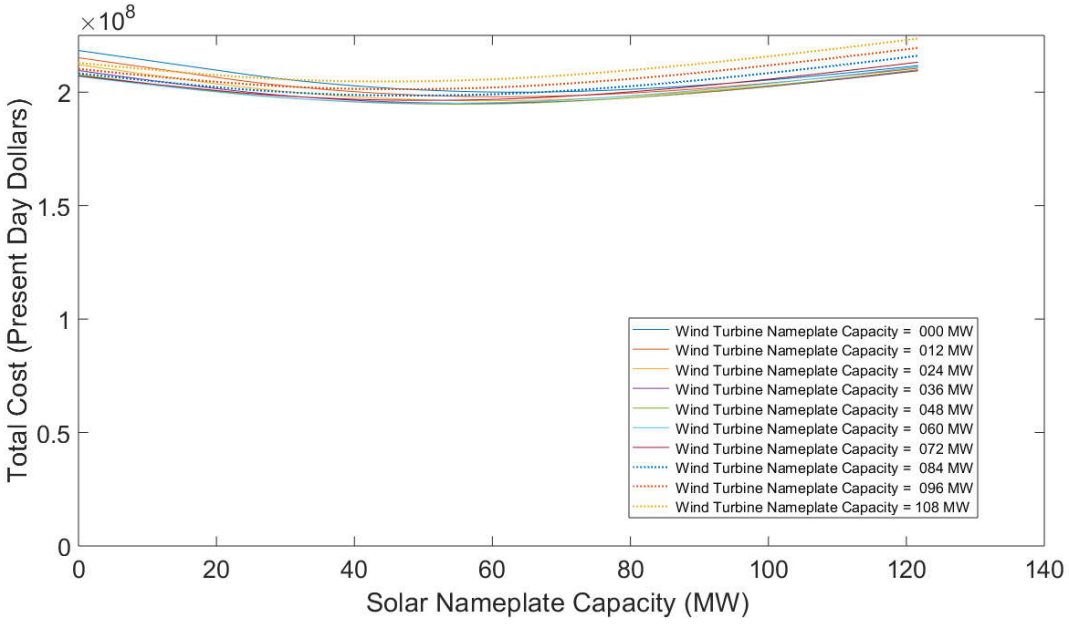

Figure 4.30: Yearly net present cost of energy for different sizes of combined wind and solar installations located in Dallas, Texas using $650 per kW nameplate capacity for wind, $500 per kW nameplate capacity for solar, and an industrial electricity price of $0.0557 per kW-h for purchasing electricity to cover energy deficits.

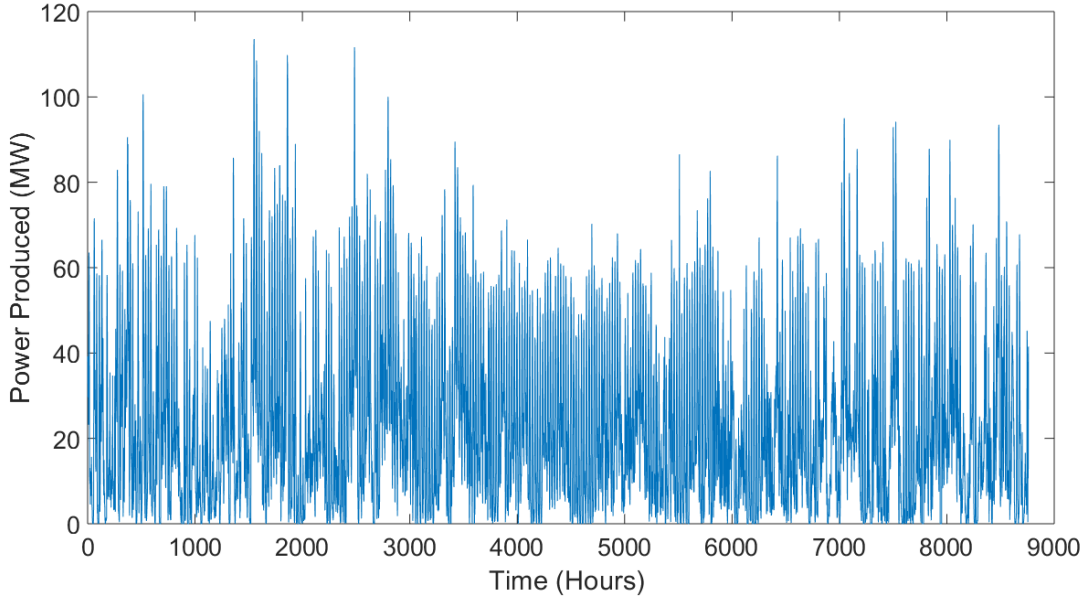

Figure 4.31: Power produced by a 48 MW nameplate capacity wind and 59 MW nameplate capacity solar installation located in Dallas, Texas. This combined wind and solar installation provides the minimum cost of energy and is the lowest plotted value in Figure 4.30.

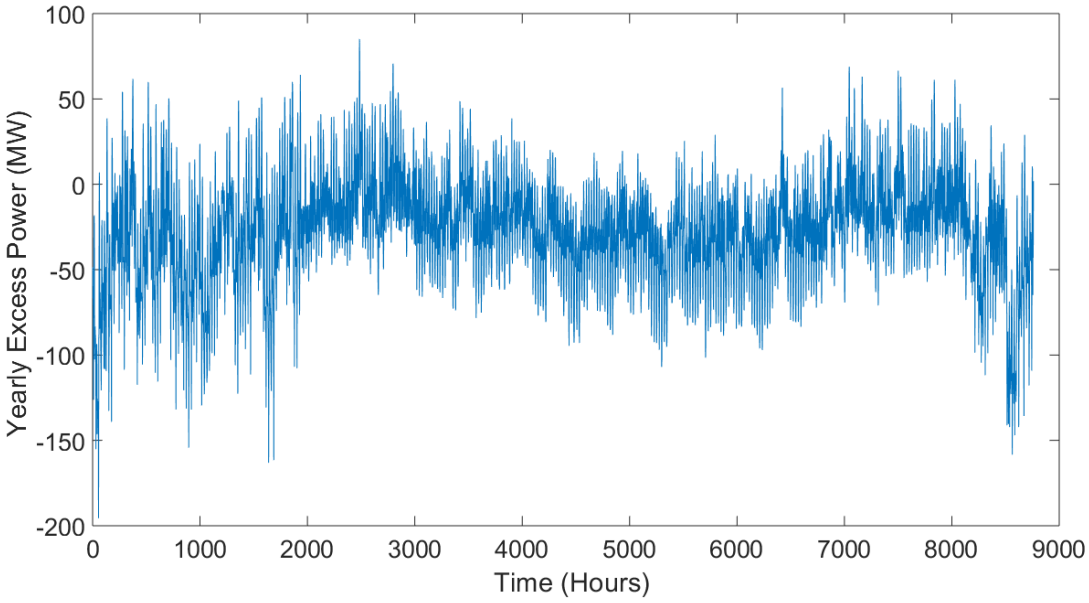

Figure 4.32: Excess power produced by a 48 MW nameplate capacity wind and 59 MW nameplate capacity solar installation located in Dallas, Texas. This combined wind and solar installation provides the minimum cost of energy and is the lowest plotted value in Figure 4.30.

4.4. Dayton, Ohio

4.4.1. Electricity Demand

The electricity demand for Dayton, Ohio is shown in Figure 4.33. This demand has different characteristics than Dallas, Texas and Rio Vista, California. The first difference is the cooling loads are not as big. The second difference is the heating loads are larger than those in Rio Vista, California, but do not reach the magnitudes of those seen in Dallas, Texas; however, the heating loads are more consistent in Dayton than Dallas. These demand plots should not be taken to mean that more heating is required in Dallas, Texas than Dayton, Ohio. The heating system used in Dallas is direct resistance heating, while that used in Dayton is an air source heat pump. An air source heat pump can provide three or four times the heat that direct electrical resistance heating unit can provide for every unit of input electricity. For Dayton, Ohio the total electricity demand for one year is 224,981 MW-h.

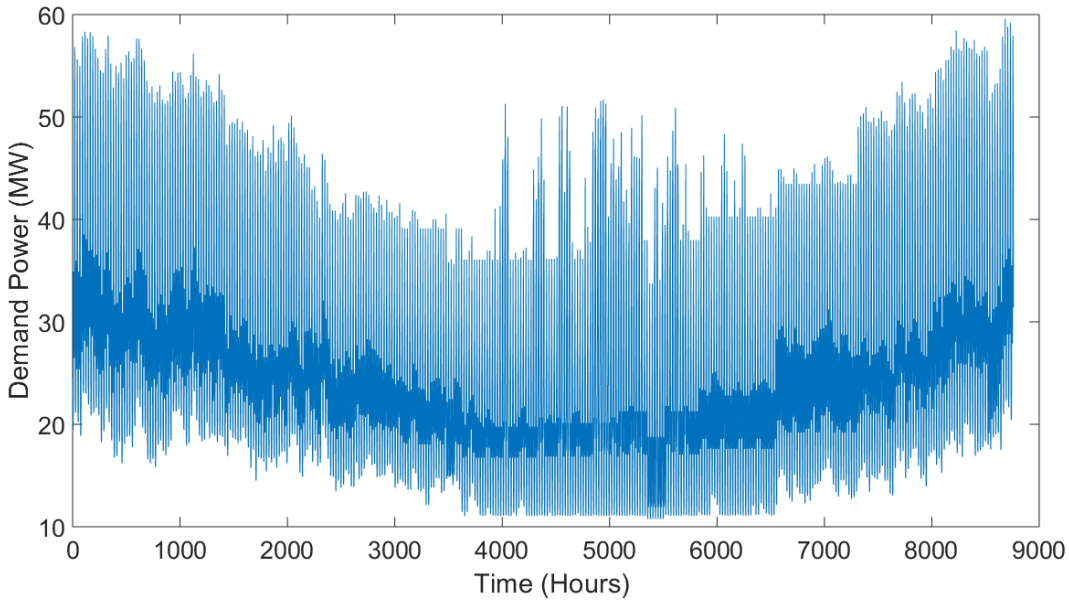

Figure 4.33: Electricity demand for 25000 typical homes located in Dayton, Ohio.

4.4.2. Wind and Solar Resources

The wind, solar, and combined resources for Dayton, Ohio are shown in Figure 4.34. The solar resource is for the power hitting a unit surface tilted at the latitude of Dayton. Of the three

locations studied in this thesis, Dayton has the weakest wind and solar resource. Dayton's combined wind and solar resource is 35% less than that in Rio Vista, California. This has an adverse effect on the economics of wind and solar in Dayton, Ohio. When the wind resource is integrated over one-year a value of 2.43 MW-h/m^2 is obtained. When the solar resource is integrated over one year a value of 1.64 MW-h/m^2 is obtained. The combined resource provides 4.07 MW-h/m^2 for one year.

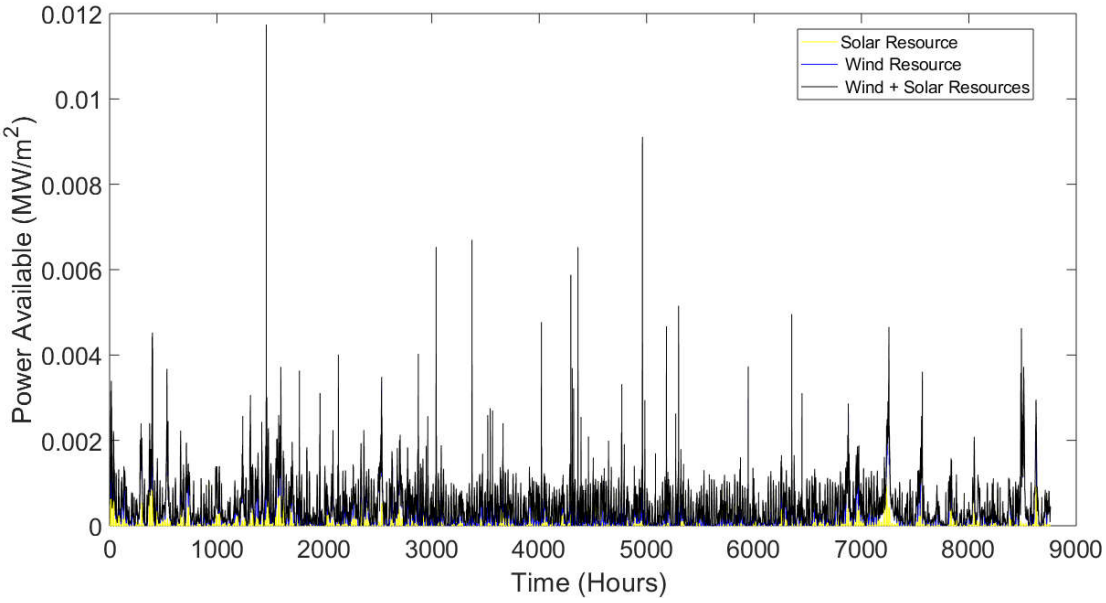

Figure 4.34: Wind and solar resource power density for Dayton, Ohio

4.4.3. Wind-Solar Farm Electricity Production

Energy produced by various configurations of wind-solar farms for an entire year in Dayton, Ohio is shown in Figure 4.35. What is immediately obvious when these plots are comparted to similar plots for Dallas, Texas and Rio Vista, California is the smaller values obtained. Annual total energy generated for various configurations ranges from 0 to 3.9x10^5 MW-h. Annual excess energy generated ranges from -2.2x10^5 MW-h to 1.6x10^5 MW-h.

The yearly excess energy produced by various sizes of wind-solar farms is shown in Figure 4.36. This excess energy plot lies between that of Rio Vista, California (see Figure 4.4) and that for Dallas, Texas (see Figure 4.23). The excess energy plot for Dallas, Texas has most wind-solar farm sizes unable to meet the demands of 25,000 homes in Dallas, Texas. Dayton's plot shows the larger capacity wind-solar farms simulated delivering positive excess power. Rio Vista shows

more than half of the wind-solar farms modeled showing positive excess power. These differences are due to the wind and solar resource available, as well as the electricity demands of the three locations.

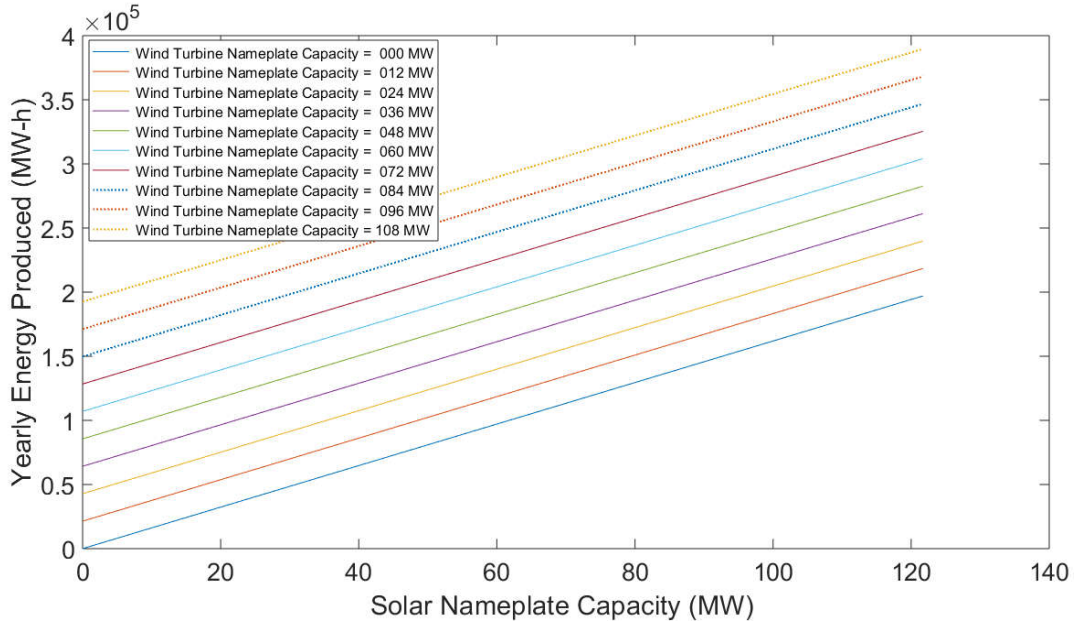

Figure 4.35: Yearly energy produced by different sizes of combined wind and solar installations located in Dayton, Ohio.

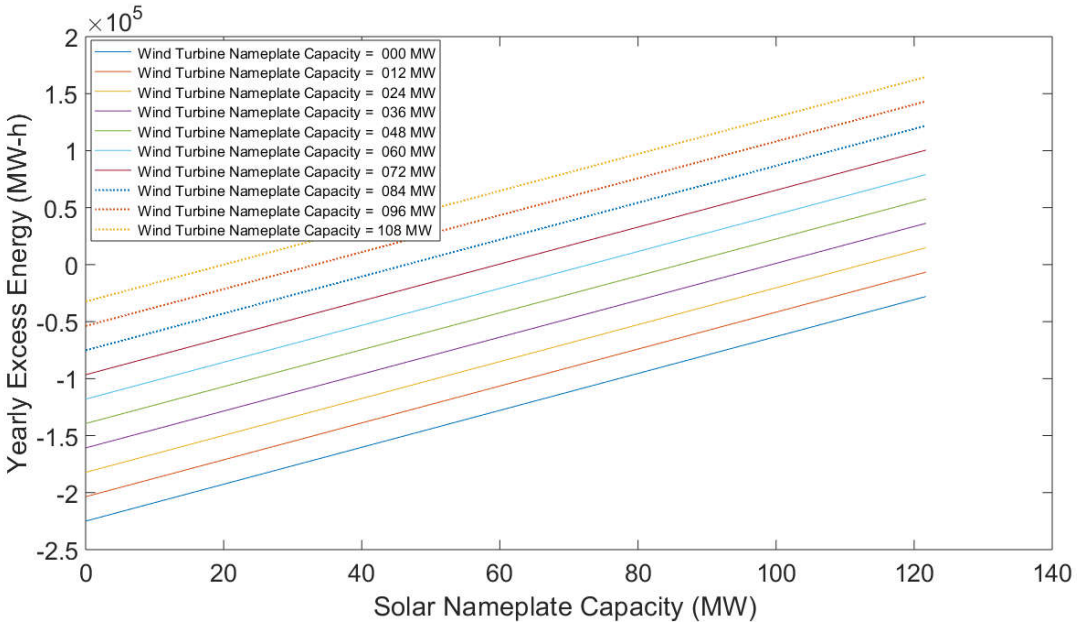

Figure 4.36: Yearly excess energy produced by different sizes of combined wind and solar installations located in Dayton, Ohio.

4.4.4. Wind-Solar Farm Economics

4.4.4.1. Base Case

The present day cost of generating 25 years of electricity with various configurations of wind and solar farms with an industrial electricity price of $0.0196 per kW-h in Dayton, Ohio is plotted in Figure 4.37. No minimum is seen in this plot. In fact, all the curves are fairly linear; more linear than those for the Dallas, Texas base case (see Figure 4.24). At least for Dallas it appeared that a minimum was close, this is not seen in the Dayton results. The question should be asked, why is the Dayton cost analysis is so poor? The big reason is the low cost of grid electricity. No information was found for why an industrial electricity price of $0.0196 per kW-h can be delivered in Dayton. All national production costs for electricity are higher than this number. This leads one to believe that power companies in Dayton are selling power to industrial customers below their costs. It cost just $40 million to deliver electricity to 25,000 homes in Dayton, Ohio for 25 years. This is an incredibly low cost. Because the minimum cost point is at 0 MW of wind capacity and 0 MW of solar capacity no figures are shown for the hourly power produced or the hourly excess power produced.

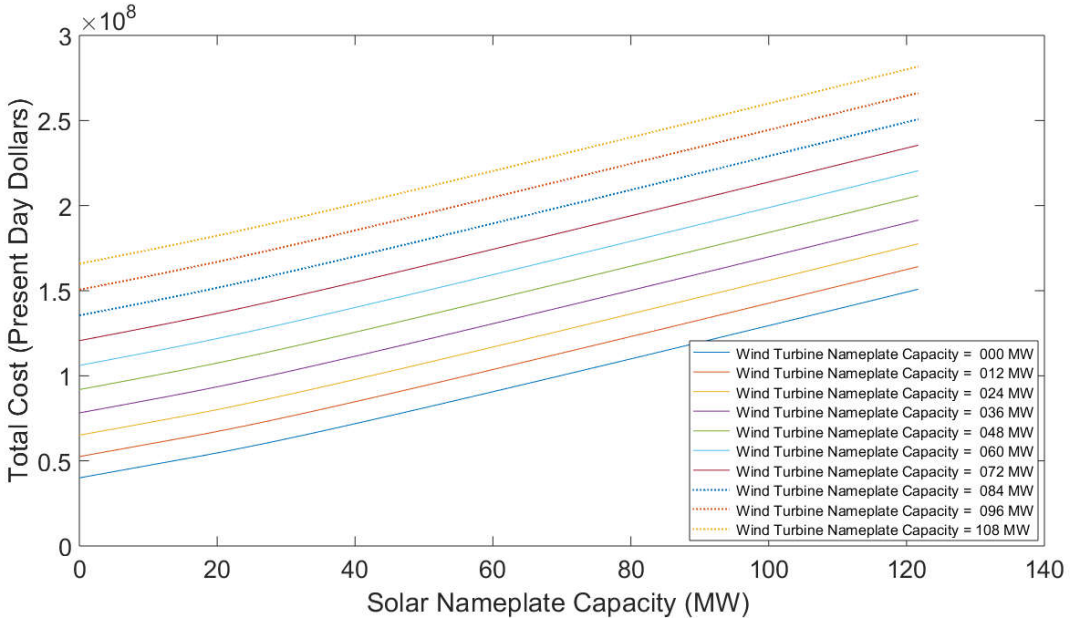

Figure 4.37: Yearly net present cost of energy for different sizes of combined wind and solar installations located in Dayton, Ohio using $1300 per kW nameplate capacity for wind, $1000 per kW nameplate capacity for solar, and an industrial electricity price of $0.0196 per kW-h for purchasing electricity to cover energy deficits.

4.4.4.2. Electricity Sold Back to Grid

Even when electricity is sold back to the grid in Dayton, Ohio, wind-solar farms do not result in a smaller cost of electricity than simply buying all power from the grid. This is shown in Figure 4.38. The selling price of electricity in this case is a measly $0.0098 per kW-h. This does not affect the economics of Dayton wind-solar farms to a noticeable degree. Like the base case there does not even appear to be hope of a minimum occurring if the grid electricity prices are increased. This will be shown in the next section.

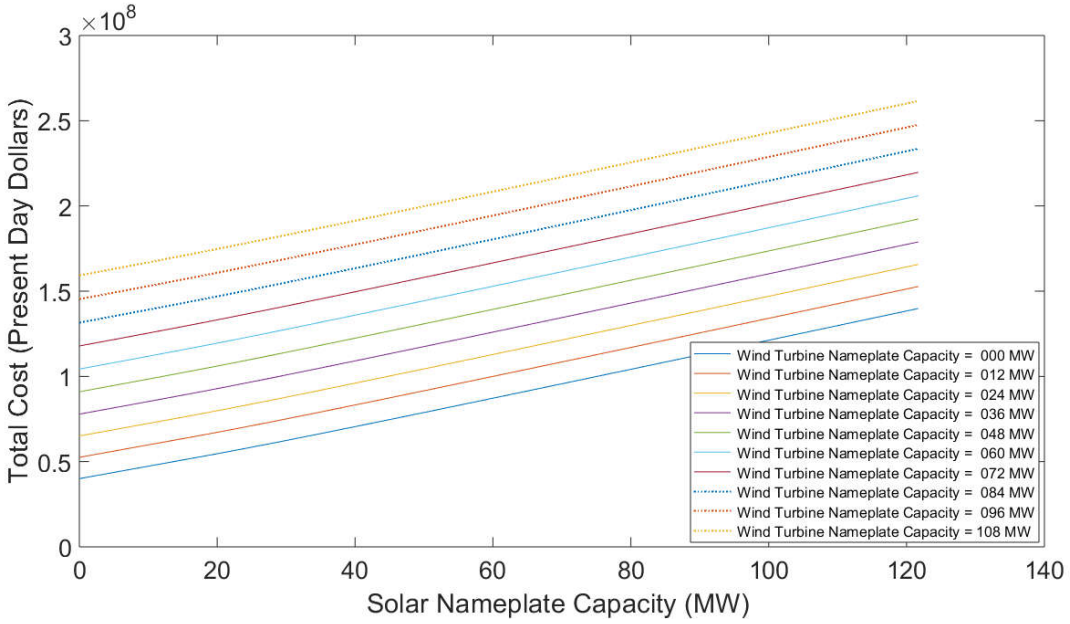

Figure 4.38: Yearly net present cost of energy for different sizes of combined wind and solar installations located in Dayton, Ohio using $1300 per kW nameplate capacity for wind, $1000 per kW nameplate capacity for solar, an industrial electricity price of $0.0196 per kW-h for purchasing electricity to cover energy deficits, and a selling price of $0.0098 per kW-h for excess electricity generated.

4.4.4.3. Commercial Price of Electricity

Even when the price of electricity is increased to the commercial rate of $0.0483 per kW-h, wind-solar farms are not cost competitive against grid purchased electricity. This is shown in Figure 4.39. Figure 4.39 is showing more curvature than the base case and selling cases shown in the prior two sub-subsections, but there still seems to be a way to go to reach an electricity price that would provide a minimum in the curve. It costs $99 million to supply power to the 25,000 home community when power is purchased from the grid at commercial price.

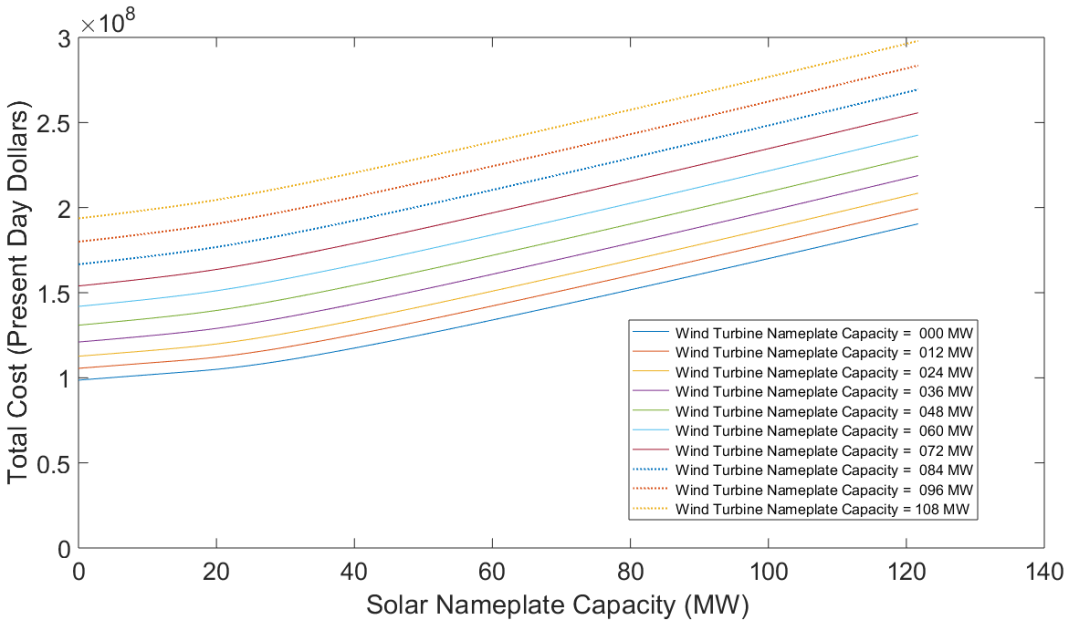

Figure 4.39: Yearly net present cost of energy for different sizes of combined wind and solar installations located in Dayton, Ohio using $1300 per kW nameplate capacity for wind, $1000 per kW nameplate capacity for solar, and a commercial electricity price of $0.0483 per kW-h for purchasing electricity to cover energy deficits.

4.4.4.4. Capital Costs Increased by 50 Percent

Obviously increasing the capital costs for wind and solar will not show a minimum in the yearly cost of energy for any nonzero capacity wind-solar farm. Even though it is obvious this is the case, Figure 4.40 is still shown. This plot is included for completeness sake more than anything else. What can be seen from this plot is the present day costs become more linear and higher than those shown for the base case in Figure 4.37.

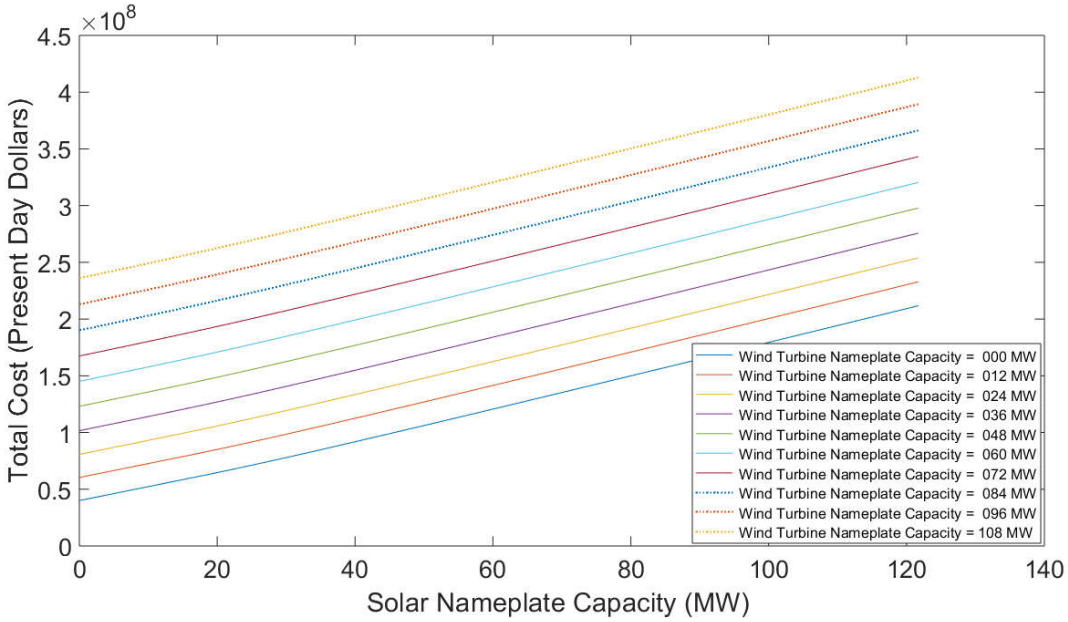

Figure 4.40: Yearly net present cost of energy for different sizes of combined wind and solar installations located in Dayton, Ohio using $1950 per kW nameplate capacity for wind, $1500 per kW nameplate capacity for solar, and an industrial electricity price of $0.0196 per kW-h for purchasing electricity to cover energy deficits.

4.4.4.5. Capital Costs Decreased by 50 Percentage

The present-day cost of generating 25 years of electricity with various configurations of wind and solar farms with an industrial electricity price of $0.0196 per kW-h in Dayton, Ohio and the capital costs reduced by 50% from the base case prices is plotted in Figure 4.41. Again, no minimum is seen. There cost reduces from the base case shown in Figure 4.37, but not enough to overcome the low grid price of $0.0196 per kW-h.

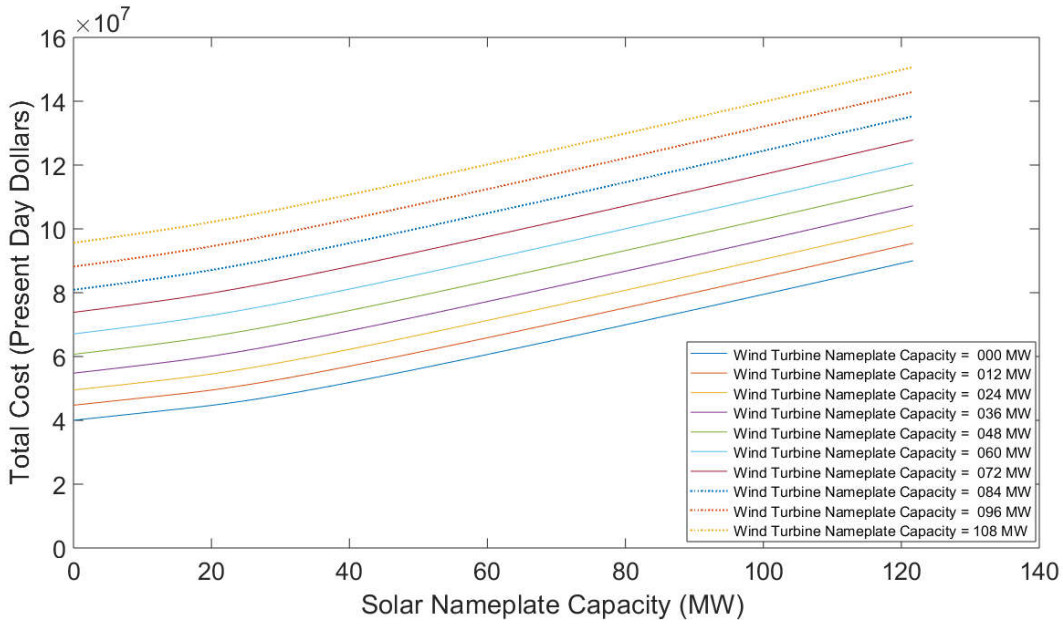

Figure 4.41: Yearly net present cost of energy for different sizes of combined wind and solar installations located in Dayton, Ohio using $650 per kW nameplate capacity for wind, $500 per kW nameplate capacity for solar, and an industrial electricity price of $0.0196 per kW-h for purchasing electricity to cover energy deficits.

4.4.4.6. Capital Costs Decreased by 75 Percent

To see if reducing the capital costs by 75%, to $325 per kW nameplate capacity of wind and $250 per kW nameplate capacity of solar, will produce a minimum in the cost curve, Figure 4.44 was produced. Finally, a minimum is found using 0 MW of wind nameplate capacity and 20 MW of solar nameplate capacity. The minimum cost is $40 million which is a saving of $0.4 million over buying the electricity from the grid. This is not a significant savings for 25 year of electricity for 25,000 homes.

Hourly periodic power generated by the minimum cost configuration of a pure solar farm in Dayton, Ohio when reducing the capital cost of wind and solar equipment by 75% is shown in Figure 4.44. The hourly excess power generated for this case is plotted Figure 4.45. While there are a few peaks in excess power that go above the zero mark, essentially the system is operating in a deficit mode. The hourly excess energy plot and the yearly cost of energy plot indicate that a 75% reduction in capital costs is just barely causing some solar capacity to be less expensive than buying all electrical power from the grid.

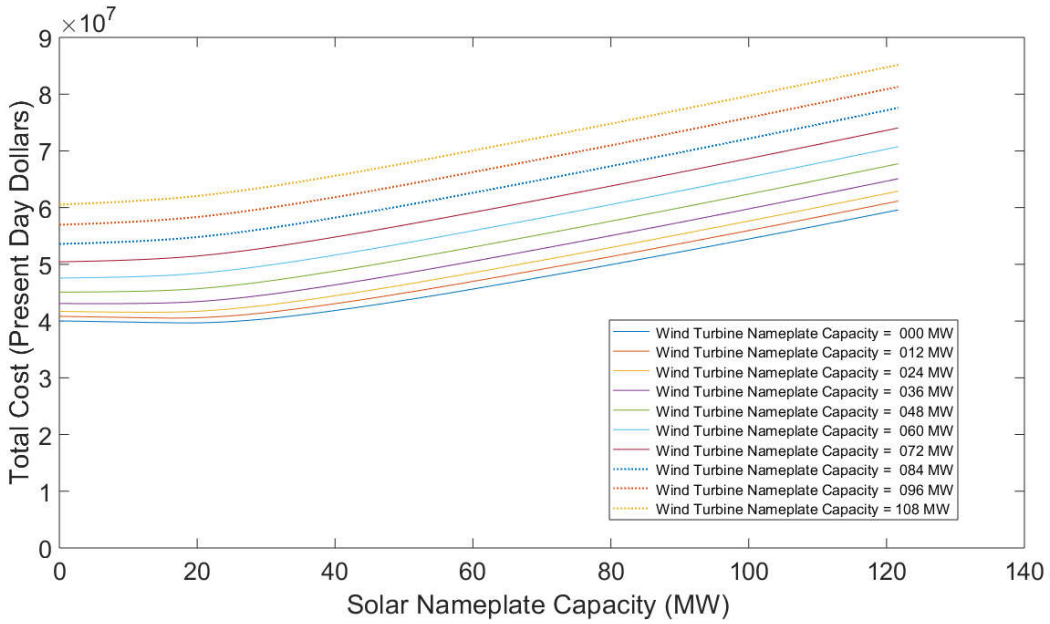

Figure 4.42: Yearly net present cost of energy for different sizes of combined wind and solar installations located in Dayton, Ohio using $325 per kW nameplate capacity for wind, $250 per kW nameplate capacity for solar, and an industrial electricity price of $0.0196 per kW-h for purchasing electricity to cover energy deficits.

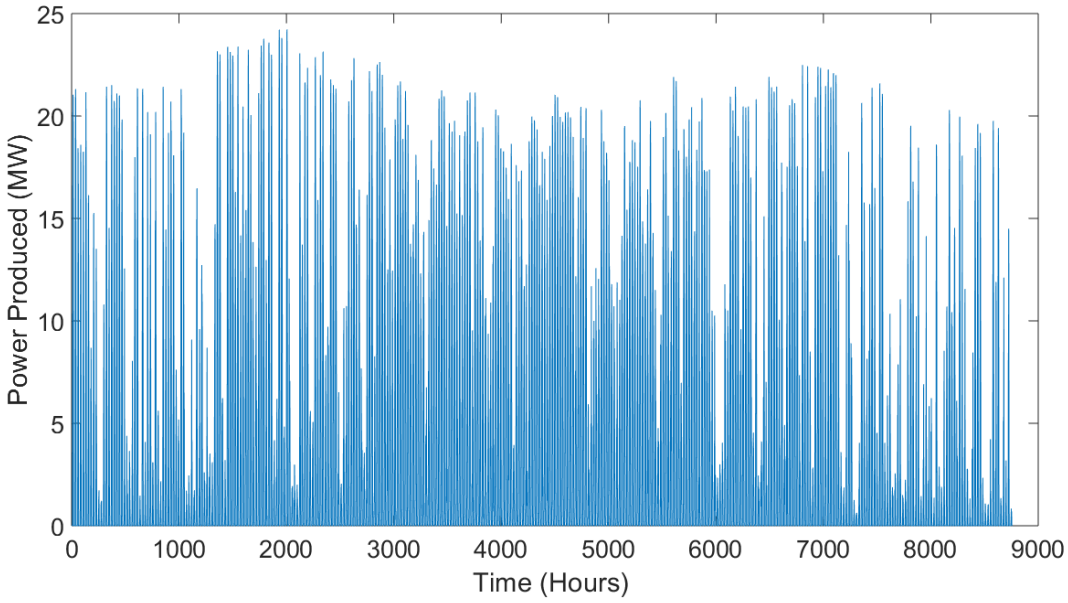

Figure 4.43: Power produced by a 0 MW nameplate capacity wind and 20 MW nameplate capacity solar installation located in Dayton, Ohio. This combined wind and solar installation provides the minimum cost of energy and is the lowest plotted value in Figure 4.42.

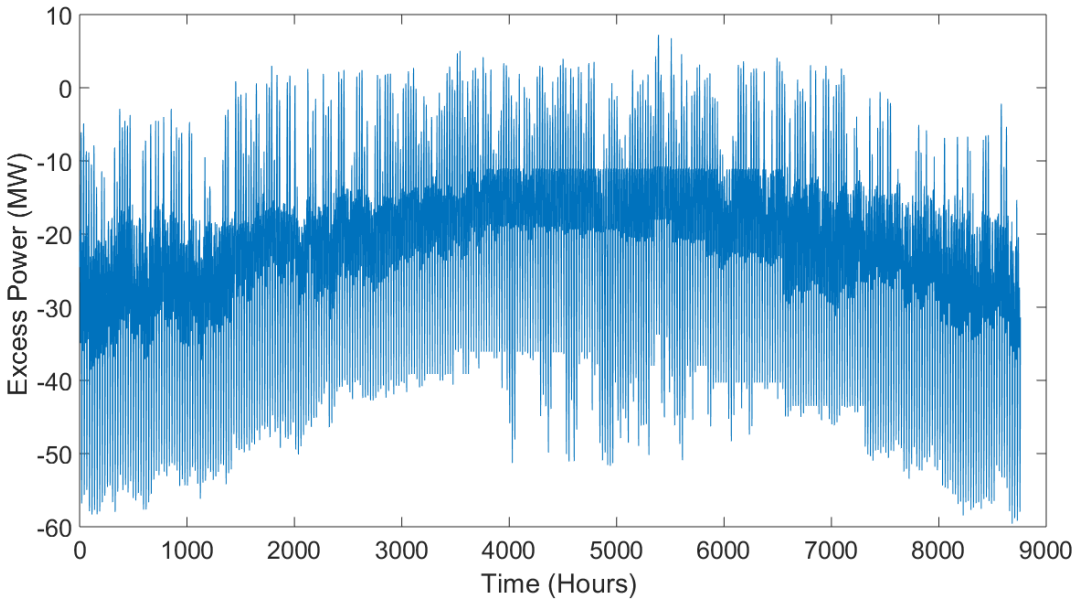

Figure 4.44: Excess power produced by a 0 MW nameplate capacity wind and 20 MW nameplate capacity solar installation located in Dayton, Ohio. This combined wind and solar installation provides the minimum cost of energy and is the lowest plotted value in Figure 4.42.

4.5. Summary of Results

A great deal of results have been presented in this chapter. The results presented are yearly energy values and detailed hourly values. The more important of these quantities are the yearly results connected with the size of the wind-solar farm that provides the minimum cost of electricity for 25,000 homes. These results are summarized in Tables 4.2, 4.3 and 4.4. Table 4.2 shows the results for Rio Vista, California, Table 4.2 shows the results for Dallas, Texas and Table 4.4 shows the results for Dayton, Ohio. These tables show the cost parameter deviated from the base case, the nameplate capacity of the wind turbines at minimum cost, the nameplate capacity of the solar panels at minimum costs, and the minimum cost. These tables clearly show that the best results are obtained for Rio Vista, California and the worst results are obtained for Dayton, Ohio. The results for Dallas, Texas are in between these two. The reasons for these results are the cost of buying electricity from the grid, the capital costs of wind turbines and solar panels, whether electricity is being sold back to the grid, the magnitude of the wind and solar resource available at the site, and how well the demand profile matches the solar resource profile. In this study it seems the most significant of these is the cost of grid electricity at the site.

The results from Rio Vista, California clearly indicate the advantages of using wind turbines combined with solar panels to meet a specified demand. The Dallas, Texas results also indicate this for the case where capital costs are reduced by 50%. For the commercial electricity case for Dallas, Texas only solar provides cost reductions, indicating there are some cases where only using solar is advantageous. It is thought that using only wind can be beneficial under the right conditions. The results from Dayton, Ohio simply indicate that it is very difficult to compete against very low electrical rates. Probably artificially low grid electrical rates.

Table 4.2: Summary of results at minimum cost points for Rio Vista, California.

Rio Vista, California					
Quantity	**Base**	**Electricity Sold Back to Grid**	**Commercial Price of Electricity**	**Capital Costs Increased by 50%**	**Capital Costs Decreased by 50%**
Purchase Price of Electricity ($/kW-h)	$0.0898	$0.0898	$0.1408	$0.0898	$0.0898
Selling Price of Electricity ($/kW-h)	$0.000	$0.0449	$0.000	$0.000	$0.000
Capital Cost of Wind ($/kW of Nameplate Capacity)	$1300	$1300	$1300	$1950	$650
Capital Cost of Solar ($/kW of Nameplate Capacity)	$1000	$1000	$1000	$1500	$500
Nameplate Capacity of Wind (MW)	24	60	36	12	48
Nameplate Capacity of Solar (MW)	25	52	29	20	32
Net Present Cost for 25 Years of Electricity (millions of $)	$149	$134	$194	$171	$113
Savings Compared to Grid Only (millions of $)	$29	$44	$85	$7	$65

Table 4.3: Summary of results at minimum cost points for Dallas, Texas.

Dallas, Texas					
Quantity	**Base**	**Electricity Sold Back to Grid**	**Commercial Price of Electricity**	**Capital Costs Increased by 50%**	**Capital Costs Decreased by 50%**
Purchase Price of Electricity ($/kW-h)	$0.0557	$0.0557	$0.0816	$0.0557	$0.0557
Selling Price of Electricity ($/kW-h)	$0.000	$0.0279	$0.000	$0.000	$0.000
Capital Cost of Wind ($/kW of Nameplate Capacity)	$1300	$1300	$1300	$1950	$650
Capital Cost of Solar ($/kW of Nameplate Capacity)	$1000	$1000	$1000	$1500	$500
Nameplate Capacity of Wind (MW)	0	0	0	0	48
Nameplate Capacity of Solar (MW)	0	0	49	0	59
Net Present Cost for 25 Years of Electricity (millions of $)	$218	$218	$307	$218	$195
Savings Compared to Grid Only (millions of $)	$0	$0	$13	$0	$24

Table 4.4: Summary of results at minimum cost points for Dayton, Ohio.

Dayton, Ohio						
Quantity	**Base**	**Electricity Sold Back to Grid**	**Commercial Price of Electricity**	**Capital Costs Increased by 50%**	**Capital Costs Decreased by 50%**	**Capital Costs Decreased by 75%**
Purchase Price of Electricity ($/kW-h)	$0.0196	$0.0196	$0.0483	$0.0196	$0.0196	$0.0196
Selling Price of Electricity ($/kW-h)	$0.000	$0.0098	$0.000	$0.000	$0.000	$0.000
Capital Cost of Wind ($/kW of Nameplate Capacity)	$1300	$1300	$1300	$1950	$650	$325
Capital Cost of Solar ($/kW of Nameplate Capacity)	$1000	$1000	$1000	$1500	$500	$250
Nameplate Capacity of Wind (kW)	0	0	0	0	0	0
Nameplate Capacity of Solar (kW)	0	0	0	0	0	20
Net Present Cost for 25 Years of Electricity (millions of $)	$40	$40	$99	$40	$40	$39.6
Savings Compared to Grid Only (millions of $)	$0	$0	$0	$0	$0	$0.4

Chapter 5
Conclusions

This work has shown that combining wind turbines with solar panels in a wind-solar farm that uses the local electrical grid as backup to meet a specified demand can reduce costs compared to wind turbines alone, solar panels alone, or grid generated electricity alone. Positive results for wind-solar farms do not always result, but depend on the conditions and costs present at a given location. Three locations were studied in this thesis: Rio Vista, California, Dallas, Texas, and Dayton, Ohio. One base case cost condition along with four alternative cost conditions were studied in Rio Vista, California and Dallas, Texas. The same base case condition with five alternative cost conditions were studied in Dayton, Ohio. All four or five alterations of the base case cost conditions changed one cost in the base cost scenario. Base case cost conditions use local industrial rates for grid generated electricity, capital costs for wind turbines of $1300 per kW of nameplate capacity, capital costs for solar panels of $1000 per kW of nameplate capacity, operation and maintenance costs for the wind turbines of $0.00368 per kW-h of electricity generated, operation and maintenance costs for the solar panels of $0.0012 per kW-h of electricity generated, a lifetime of the wind-solar farm of 25 years, and an interest rate of 10%. For the base case costs the only location where wind-solar farms provided economic benefit over supplying all the demand from the local grid was Rio Vista, California. The minimum cost was for a wind-solar farm that contained approximately equal amounts of wind turbine and solar panel capacity. Thus, combining wind with solar and utilizing grid backup reduced the costs of providing a demand for 25,000 homes, for 25 years in Rio Vista, California. These results demonstrate that a combination of wind

and solar reduces the intermittency problem of wind alone or solar alone under the right conditions. It also shows that when intermittency issues are included in an economic analysis, wind and solar produced electricity can be still be better economically than grid supplied electricity alone.

The first cost alteration from the base case studied was excess electricity generated by the wind-solar farm could be sold to the gird at half the industrial rate. The second alteration from the base case was to use the commercial rate for grid electricity, instead of the industrial rate. This increased the cost of grid electricity by 57% in Rio Vista, California, 46% in Dallas, Texas, and 146% in Dayton, Ohio. The highest jump in electricity rates is seen in Dayton, Ohio but it must be remembered that the industrial rates in Dayton are extremely low. The third and fourth alterations had to do with increasing the capital equipment costs by 50% and decreasing the capital equipment costs by 50%. Finally, for the Dayton, Ohio location capital equipment costs were decreased by 75%. Results show that increasing the grid cost of electricity and decreasing the capital cost of wind turbines and solar panels favors wind-solar farms.

For Rio Vista, California all five cost scenarios resulted in a wind-solar farm with grid backup providing cheaper electricity than grid provided electricity alone. All five of these cost scenarios also had a combination of wind and solar capacity being cheaper than wind or solar alone. It is impressive that a wind-solar farm is still cost advantageous in Rio Vista, California when the capital costs for wind and solar are increased by 50%. The savings over grid only electricity shrunk by 24% when the capital cost were increased by 50% from the base case, but combined wind and solar was still beneficial. The most savings in Rio Vista, is obtained when the capital cost decrease by 50%. The largest wind-solar farm in Rio Vista is utilized to produce the minimum costs for the case where electricity is sold back to the grid.

In Dallas, Texas a combined wind-solar farm is only advantageous when the capital cost of wind turbines and solar panels are decreased by 50%. Larger amounts of wind capacity and solar capacity are utilized in this case than any case studied, but this occurs because of the large electrical demands of 25,000 homes in Dallas, not because of cost benefits. It is interesting that for the commercial electricity price case in Dallas, a pure solar farm helps to reduce the cost of electricity, but wind does not help.

The only case that a wind-solar farm is attractive in Dayton, Ohio is when the cost of capital is decreased by 75% and this just barely is cost advantageous. The major reason why wind-solar

farms do not fair well in Dayton, Ohio is the low cost of grid electricity. A lesser, but contributing factor, is the smaller wind and solar resources in Dayton, Ohio.

Besides providing cost information which allowed for the direct comparisons of wind-solar farms, pure wind farms, pure solar farms, and purchasing all electricity from the grid, it was also an objective of this work to present the electrical production of different sized wind-solar farms. This was done for all three locations, for all combinations of wind nameplate capacities that ranged from 0 to 108 MW and solar capacities that ranged from 0 to 120 MW. These were sufficient ranges to isolate minimum cost points for the electrical demands for all cases studied. Calculated electricity production rates were compared to electricity demands on an hourly basis, summed, and excess yearly energy production plots produced. Some values in these excess energy plots are negative and some are positive. The most severe demands were put forth by a community in Dallas, Texas. Even though yearly excess energy plots are positive, this does not mean electricity is not purchased from the grid. Purchasing decisions are made on an hour by hour basis. Hourly energy production plots and hourly excess energy plots for all the minimum cost points are presented in this thesis. Both the yearly and hourly excess energy plots indicate that it is not cost efficient to generate all demand with a wind-solar farm, but only a fraction of the demand. This fraction is a function of the cost of electricity, the capital costs of wind turbines and solar panels, the wind and solar resources present at a location and how the wind and solar resource hourly profiles match the hourly demand profiles.

Detailed mathematical models were used to predict the wind and solar resource present at a given location. Energy in the wind is calculated by obtaining actual wind speeds at 5 minute intervals for a year. Since these are given at a certain height above the ground that is different than the hub height of the wind turbines, these wind speeds are scaled to the hub height with a logarithmic scaling equation. Wind turbine power curves are then used to predict how much of the energy in the wind is converted into electricity. Energy in the solar radiation is calculated by obtaining actual total horizontal incident radiation in one hour intervals for a year. These measured total, incident values are converted to beam and diffuse components using a clearness index. The diffuse component is separated into circumsolar and isotropic diffuse portions using an anisotropic index. The ground reflected component is obtained by using a ground reflectivity. All these solar quantities for a horizontal surface are properly altered for a tilted surface. Solar panels facing due south, titled at an angle from the horizontal equal to the latitude were used to provide maximum

solar energy collection with fixed panels over the course of a year. Shadowing of solar panels by the panels in front of them is included in this analysis. The electricity produced by the solar panels is determined by using a solar panel conversion efficiency. The economic model used in this work accurately includes the time value of money.

References

1. ETV 2 NITTTRCHD. (2018, November 23). “Integration of Renewable Energy sources with Grid Module 9 session 2” [Online video clip]. YouTube. https://www.youtube.com/watch?v=MocCm-3mA7c.

2. A. Walker, J. Scheib, C. Turchi, R. Robichaud, G. Tomberlin, K. Burman, M. Hillesheim, B. Kroposki and M. Qu. “*Integration of Renewable Energy Systems”,* ASME Press, 2016.

3. *“CO2 emissions from fuel combustion highlights,”* International Energy Agency, IEA Statistics, 2011 Edition, p. 10.

4. Bent Sorensen, *Renewable Energy-Its Physics, Engineering, Use, Environmental Impacts, Economy and Planning Aspects,* Third Edition, Elsevier Academic Press.

5. Rajesh Kumar, R. A. Gupta, and Ajay Kumar Bansal, “Economic analysis and power management of a standalone wind/photovoltaic hybrid energy system using biogeography-based optimization algorithm,” *Swarm and Evolutionary Computation,* Elsevier Publications, Volume 8, Pages 33-43, February 2013.

6. Alternative Energy, “Alternative Energy Solutions for the 21st Century,” [Online] Available: http://www.altenergy.org/renewables/renewables.html.

7. Hongxing Yang, Wei Zhou, Lin Lu, and Zhaohong Fang, “Optimal sizing method for stand-alone hybrid solar wind system with LPSP technology by using genetic algorithm,” *Solar Energy,* Elsevier Publications, Volume 82, Issue 4, Pages 354-367, April 2008.

8. R. Ramakumar, I. Abouzahr, K. Krishnan and K. Ashenayi, "Design scenarios for integrated renewable energy systems," *Transactions on Energy Conversion,* IEEE Publications, Volume 10, Issue 4, Pages 736-746, December 1995.

9. B. S. Borowy and Z. M. Salameh, "Methodology for optimally sizing the combination of a battery bank and PV array in a wind/PV hybrid system," *Transactions on Energy Conversion,* IEEE Publications, Volume 11, Issue 2, Page 367-375, June 1996.

10. A. Kashefi Kaviani, G. H. Riahy, and SH.M.Kouhsari,“Optimal design of a reliable hydrogen-based standalone wind/PV generating system, considering component outages,” *Renewable Energy,* Elsevier Publications, Volume 34, Issue 11, Pages 2380-2390, November 2009.

11. John A. Duffie and William A. Beckman, *Solar Engineering of Thermal Processes,* Fourth Edition, Chapters 1-3, John Wiley & Sons, Inc., 2013.

12. M. Iqbal, *An Introduction to Solar Radiation,* Elsevier Academic Press, September 1983.

13. Global Climate Change, “Solar Energy,” last updated on 5/9/2017 [Online] Available: https://archive.epa.gov/climatechange/kids/solutions/technologies/solar.html.

14. EEWeb, “Solar Thermal Energy,” posted on 8/10/2015 [Online] Available: https://www.eeweb.com/quizzes/solar-thermal-energy.

15. LEONICS, “Basics of a Solar Cell,” last updated on 5/12/2020 [Online] Available: http://www.leonics.com/support/article2_13j/articles2_13j_en.php.

16. American Wind Energy Association, “Basics of Wind Energy,” last updated on 5/12/2020 [Online] Available: https://www.awea.org/wind-101/basics-of-wind-energy.

17. Office of Energy Efficiency & Renewable Energy, “Utility scale wind,” last updated on 5/12/2020 [Online] Available: https://windexchange.energy.gov/markets/utility-scale.

18. Office of Energy Efficiency & Renewable Energy, “Land based wind,” last updated on 5/12/2020 [Online] Available: https://windexchange.energy.gov/markets/land-based.

19. Office of Energy Efficiency & Renewable Energy, “Offshore wind,” last updated on 5/12/2020 [Online] Available: https://windexchange.energy.gov/markets/offshore.

20. Anurag Chauhan and R. P. Saini, *“A review on Integrated Renewable Energy System based power generation for stand-alone applications: Configurations, storage options, sizing methodologies and control,” Renewable and Sustainable Energy Review*, Elsevier Publication, Volume 38, Pages 99-120, October 2014.

21. A. Mellit, M. Benghanem, A. Arab Hadj and A. Guessoum, “An adaptative artificial neural network model for sizing stand-alone photovoltaic systems: application for isolated sites in Algeria,” *Renewable Energy,* Elsevier Publications, Volume 30, Issue 10, Pages 1501-1524, August 2005.

22. Alireza Askarzadeh, “A discrete chaotic harmony search based simulated annealing algorithm for optimum design of PV/wind hybrid system” *Solar Energy*, Elsevier Publications, Volume 97, Pages 93-101, November 2013.

23. I. Abouzahr and R. Ramakumar, “An approach to assess the performance of utility-interactive wind electric conversion systems,” *Transactions on Energy Conversion*, IEEE Publications, Volume 6, Issue 4, Pages 627-638, December 1991.

24. Richard Perez, Robert Seals, Pierre Ineichen, Ronald Stewart, David Menicucci. “A new simplified version of the Perez diffuse irradiance model for tilted surfaces” *Solar Energy*, Elsevier Publications, Volume 39, Issue 3, Pages 221-231, 1987.

25. Office of Energy Efficiency & Renewable Energy, “U.S. Installed and Potential Wind Power Capacity and Generation,” last updated on 5/12/2020 [Online] Available: https://windexchange.energy.gov/maps-data/321.

26. K. G. T. Hollands and R. G. Huget, “A probability density function for the clearness index, with applications,” *Solar Energy*, Elsevier Publications, Volume 30, Issue 3, Pages 195-209, 1983.

27. A. Chauhan and R. P. Saini "A review on Integrated Renewable Energy System based power generation for stand-alone applications: Configurations, storage options, sizing methodologies and control," *Renewable and Sustainable Energy Reviews*, Elsevier Publications, Volume 38, Pages 99-120, October 2014.

28. B. S. Borowy and Z. M. Salameh, "Methodology for optimally sizing the combination of a battery bank and PV array in a wind/PV hybrid system," *Transactions on Energy Conversion*, IEEE Publications, Volume 11, Issue 2, Pages 367-375, June 1996.

29. J. E. Hay and J. A. Davis, "Calculations of solar radiation incident on an inclined surface" *Proceedings of First Canadian Solar Radiation Data Workshop*, Canadian Atmospheric Environment Service, Canada, Pages 59-72, 1980.

30. Felix A. Farret and M. Godoy Simoes, *Integration of Alternative Sources of Energy*, John Wiley & Sons Publications.

31. J. P. Barton and D. G. Infield, "Energy storage and its use with intermittent renewable energy," *Transactions on Energy Conversion*, IEEE Publications, Volume. 19, Issue 2, Page 441-448, June 2004.

32. Open EI- Residential Load Data, "E-Plus" [Online] Available: https://urldefense.proofpoint.com/v2/url?u=https-3A__openei.org_datasets_files_961_pub_&d=DwIGAg&c=3buyMx9JlH1z22L_G5pM28wz_Ru6WjhVHwo-vpeS0Gk&r=rYwk0SYG8FeZuIYmoyamP3P-NTUrThpO3uSkkxmzlMQ&m=C4esCTzeJH7Eoy-gMuYorcW9-98_H_Vgu3dNPTv54DU&s=kpeKL6gznNKQVm7UMP5orZnwp5TO0Hl539IGyrZEZCk&e=.

33. National Renewable Energy Laboratory, "The Wind Prospector" [Online] Available: https://maps.nrel.gov/wind-prospector/?aL=cNCkEH%255Bv%255D%3Dt%26p7FOkl%255Bv%255D%3Dt%26p7FOkl%255Bd%255D%3D1%26dXykOt%255Bv%255D%3Dt%26dXykOt%255Bd%255D%3D2%26Rh9Ekq%255Bv%255D%3Dt%26Rh9Ekq%255Bd%255D%3D3%26xY_VBM%255Bv%255D%3Dt%26xY_VBM%255Bd%255D%3D4&bL=jMjAyq&cE=0&lR=0&mC=33.60599089750828%2C-112.125051&zL=10.

34. National Renewable Energy Laboratory, "NSRDB Data Viewer," [Online] Available: https://maps.nrel.gov/nsrdb-viewer/?aL=UdPEX9%255Bv%255D%3Dt%26f69KzE%255Bv%255D%3Dt%26f69KzE%255Bd%255D%3D1&bL=clight&cE=0&lR=0&mC=33.60599089750828%2C-112.125051&zL=10.

35. Electricity Local, "Electricity Rates & Usage" [Online] Available: https://www.electricitylocal.com/.

36. Lazard, *"Lazard's Levelized Cost of Energy Analysis – Version 13.0,"* 2019, Accessed on: May 18, 2020, [online] Available: https://www.lazard.com/media/451086/lazards-levelized-cost-of-energy-version-130-vf.pdf.

37. A. Arabali, M. Ghofrani, M. Etezadi-Amoli, M. S. Fadali and Y. Baghzouz. *"*Genetic-Algorithm-Based Optimization Approach for Energy Management,*" Transactions on Power Delivery,* IEEE Publications, Volume 28, Issue 1, Pages 162-170, January 2013.

38. Vikas Khare, Savita Nema and Prashant Baredar. "Optimization of the hybrid renewable energy system by HOMER, PSO and CPSO for the study area," *International Journal of Sustainable Energy,* Taylor & Francis Group Publications, Volume 36, Issue 4, Pages 326-343, March 2015.

39. Getachew Bekele and Björn Palm, "Feasibility study for a standalone solar–wind-based hybrid energy system for application in Ethiopia," *Applied Energy,* Elsevier Publications, Volume 87, Issue 2, Pages 487-495, February 2010.

40. Sanjoy Kumar Nandi and Himangshu Ranjan Ghosh. "Techno-economical analysis of off-grid hybrid systems at Kutubdia Island, Bangladesh," *Energy Policy,* by Elsevier Publications, Volume 38, Issue 2, Pages 976-980, February 2010.

41. Ahmed M. A. Haidar, Priscilla N. John, and Mohd Shawal, "Optimal configuration assessment of renewable energy in Malaysia," *Renewable Energy,* Elsevier Publications, Volume 36, Issue 2, Pages 881-888, February 2011.

42. Dhaker Abbes, André Martinez and Gérard Champenois. "Life cycle cost, embodied energy and loss of power supply probability for the optimal design of hybrid power systems," *Mathematics and Computers in Simulation,* Elsevier Publications, Volume 98, Pages 46-42, April 2014.

43. Ajai Gupta, R. P. Saini, and M. P. Sharma. "Steady-state modelling of hybrid energy system for off grid electrification of cluster of villages," *Renewable Energy,* Elsevier Publications, Volume 35, 1ssue 2, Pages 520-535, February 2010.

44. Hongxing Yang, Lin Lu and Wei Zhou. "A novel optimization sizing model for hybrid solar-wind power generation system," *Solar Energy,* Elsevier Publications, Volume 81, Issue 1, Pages 76-84, January 2007.

45. Dheeraj Jumar Khatod, Vinay Pant and Jaydev Sharma. "Analytical approach for well-being assessment of small autonomous power systems with solar and wind energy sources," *Transactions on Energy Conversion,* IEEE Publications, Volume 25, Issue 2, Pages 535-545, June 2010.

46. G. Tina, S. Gagliano, and S. Raiti. *"*Hybrid solar/wind power system probabilistic modelling for long-term performance assessment,*" Solar Energy,* Elsevier Publications, Volume 80, Issue 5, Pages 578-588, May 2006.

47. A. Zidan and E. F. El-Saadany, "Network reconfiguration in balanced distribution systems with variable load demand and variable renewable resources generation," *2012, IEEE Power and Energy Society General Meeting,* IEEE Publications, pages 1-8, July 2012.

48. Kamal Anoune, Mohsine Bouya, Abdelali Astito and Abdellatif Ben Abdellah, “Sizing methods and optimization techniques for PV-wind based hybrid renewable energy system: A review,” *Renewable and Sustainable Energy Reviews*, Elsevier Publications, Volume 93, Pages 652-673, October 2018.